



DELIVERABLE REPORT

Deliverable:	D 6.1: Potencies of a list of prioritised MNMs on test organisms
Work Package:	WP6: MNM bioavailability & biological affects in vitro/in vivo (ecotoxicology)
Lead Beneficiary:	The University of Exeter (UNEXE)
Nature of Deliverable:	Report
Dissemination Level:	Public (PU)
Delivery Date:	28/02/2015
Submitted By:	Charles Tyler (UNEXE)
Revised By:	Wim de Jong (RIVM), Håkan Wallin (NRCWE)
Approved By:	Eva Valsami-Jones (UoB)

Project full title: "Engineered nanomaterial mechanisms of interactions with living systems and the environment: a universal framework for safe nanotechnology"

Grant agreement no: NMP4-LA-2013-310451



Table of contents

1. Executive Summary	Page 2
2. Introduction	Page 3
3. Test Organisms	Page 3
4. Selected Particles	Page 7
5. Experimental approaches, Results and Discussion for Test Organisms	Page 7
6. Conclusions and recommendations	Page 64
7. References	Page 66
8. Appendix	Page 73

1. Executive Summary

A range of test and sentinel organisms was studied to investigate the relative toxicity and the organisms' sensitivity to selected nanoparticles (NPs) that are currently suspected to have biological effects (e.g. nano silver). The test organisms included a freshwater algae (*Clamdomonas reinhardtii*), a freshwater fish (*Danio rerio*), and a range of terrestrial invertebrates including roundworms (*Caenorhabditis elegans*), earthworms (*Eisenia fetida*) springtails (*Folsomia candida*), soil mites (*Hypoaspis aculeifer*) and isopods (*Porcellio scaber*). Some of the tests conducted followed standardised OECD test guidelines but we also developed new protocols better suited for studies on NPs for those specific test organisms. Effects analyses were focused on apical endpoints, spanning mortality, to development, growth, reproduction, neurological function (e.g. behaviour assays) and photosynthetic yield (algae). Of the NPs studied only AgNPs were found to show toxicity at concentration modelled for surface waters and surface soils in Europe, and they did so across the wide range of study organisms we tested. Our results, together with the existing literature indicate that the release of Ag⁺ and its uptake into the cell is the main cause of AgNP toxicity. For ZnO NP dissolution in the aquatic exposure medium was rapid and the predominant mode of toxicity of ZnO NP is likely to be due to zinc ions. However, we found no adverse effects for environmentally relevant concentrations of ZnONP in the terrestrial and aquatic organisms tested. We found no effects of CeO₂ or for TiO₂ on apical endpoints for any dosing level tested in the animals studied. In our adopted methodologies for this work we show that microscopy-based analysis of embryogenesis in zebrafish offers the potential for medium throughput screening for toxicity assessments of NPs. This approach, in combination with measuring particle uptake, distribution and localization through imaging and/or use of isotopically labelled materials would provide a highly integrative and informative approach for analysis on NP effects. We show too that harnessing of the 'seizure assay' in a semi-automated analysis system in zebrafish early life stages could readily be adopted for *in vivo* nanoparticle toxicity screening based on behaviour effects. Terrestrial isopods offer an excellent model for assessing NP accumulation from soil and this is likely to be a key factor in any effects associated with NP exposure. We show that *C. elegans* provides an excellent system for assessing chronic exposure effects of NPs (in a life span model) and also offers significant potential for the development of a medium throughput method to screen NPs in a liquid media. *C. elegans* could also be adopted to assess for neuromuscular effects of NPs via observation of processes such of egg-laying and for studies on neural behaviour phenotypes.



2. Introduction

In this work package we have conducted a series of studies on a range of test and sentinel organisms to identify the relative toxicity and the organisms' sensitivity to selected nanoparticles (NPs). Studies have been conducted through dose-response analysis for a selection of NPs that are currently expected to have biological effects (e.g. nano silver). The tests conducted include those following standardised OECD test guidelines but also newly developed protocols that are better suited for studies on NPs for the specific test organisms. Exposures have been conducted via environmental media (water or soil) and effects analysis have focused on apical endpoints, spanning mortality to development, growth, reproduction, neurological function (e.g. behaviour assays) and photosynthetic yield (algae). In addition, for some organisms we have measured a suite of biomarkers of stress. The test organisms include aquatic algae (*Chlamydomonas reinhardtii*, [EAWAG]) and fish (*Danio rerio*, [UoE and KIT] and terrestrial invertebrate organisms, including roundworms (*Caenorhabditis elegans*, [IUF]), earthworms (*Eisenia fetida*, [Eurofins]) springtails (*Folsomia candida* [Eurofins]) and soil mites (*Hypoaspis aculeifer*, [Eurofins]), and the isopod (*Porcellio scaber*, [UNI-LJ]).

We have structured the report in a manner that is best suited to illustrate the experiments undertaken and effects identified for each of the test species. Thus, after an introduction to the test species and the NPs tested, the report details the experiments conducted and results obtained for the different test species separately. For continuity and cohesion the results are discussed separately also for each study organism. In the final conclusions section we illustrate the commonalities and differences in the effects analyses for each species and particle types tested and provide further critical insights to the findings and their implications.

3. Test organisms

We used a range of organisms, listed above, that include both aquatic and terrestrial species.

Aquatic Test Species:

Chlamydomonas reinhardtii: The wild type (CC-125) of the freshwater algae *Chlamydomonas reinhardtii* was used as the model algae species. *Chlamydomonas* is a genus of the unicellular green algae *Chlorophyta*. The cells show a polar structure with a basal chloroplast and two anterior flagella, which are used for locomotion. A cell wall that is closely appressed to the plasma surrounds the cell and protects the inner organelles including the nucleus, the contractile vacuole and a light perceiving eye spot.

The algae can photosynthetically assimilate CO₂ as the only carbon source (photoautotrophic). *C. reinhardtii* is also capable of using light and organic carbon sources at the same time (mixotrophic) or even growing in total darkness by utilizing organic carbon sources present in the culture medium (heterotrophic). Strains of *C. reinhardtii* can reproduce sexually as well as asexually. *Chlamydomonas* is widely used as a model organism for genetic and biochemical studies. It can be easily cultured and its short generation time enables fast analysis of multiple generations. The genome of *C. reinhardtii* is sequenced and multiple tools are available for the study of physiological and molecular endpoints.

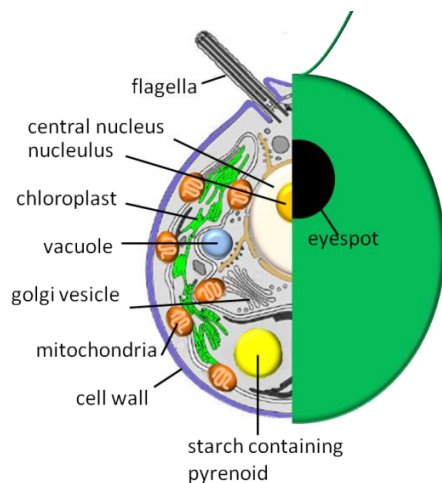


Figure 1: Cell structure of *Chlamydomonas reinhardtii*. Modified from (Harris et al. 2009).

Zebrafish, *Danio rerio*: Zebrafish (*Danio rerio*) are an excellent model vertebrate organism for investigations into nanotoxicology. With a highly researched developmental process and a plethora of supporting literature, zebrafish embryos offer a wide range of experimental conveniences, including the ease for observing developmental effects through a transparent chorion and body up until 24 hours post fertilisation (hpf). Additionally the ease of culture and number of replicates available using embryos facilitates a research set up that not only can be regarded as high-throughput but also can be used to provide toxicity testing to organisms for the entirety of their early life stages, incorporating exposures via their natural environment. Many studies have been centred on the zebrafish and predominantly zebrafish embryos. There are a series of new OECD guidelines for fish embryo toxicity tests (OECD (2013), e.g. *Test No. 236: Fish Embryo Acute Toxicity (FET) Test* that define testing conditions and endpoints which can be applied to NPs. Recently, the zebrafish embryo has thus emerged as a vertebrate model organism for *in vivo* nanotoxicity tests. Automated microscopy combined with automated image analysis has facilitated quantification of phenotypes upon NP exposure (e.g. lethality, hatching, malformations) (Alshut et al., 2010, Mikut et al., 2013).

The chorion of the zebrafish embryo however presents a (debatable) barrier to NP entry into embryos. Some studies showing uptake of single particles across the chorion membrane (Lee *et al.*, 2007, Browning *et al.*, 2009) and others provide evidence that exposure scenarios to some NPs results in aggregation on the outside of the chorion membrane with no uptake detectable (Osborne *et al.*, 2013). It is known that the embryo chorion is a dynamic layer which undergoes changes to its permeability (as does the embryo itself) and its structure during the early stages of its development, potentially as a result of protease activities (Hagerdorn *et al.*, 1998; 1997 and Kim *et al.*, 2005). This places great importance upon the stage at which the embryo is exposed for uptake and effects analyses of NPs. As a consequence of this, the suitability of the zebrafish embryo can be questioned with regards to its sensitivity due to the unknown bioavailability of NPs to the developing embryo.

Adult zebrafish have also been exposed to a range of NPs to assess lethality, tissue loading, cellular responses such as oxidative stress and changes in gene expression (Bilberg *et al.*, 2012; Choi *et al.*, 2010; van Aerle *et al.*, 2013), using the adult stage of the model eliminates the uptake assessment difficulties but it is potentially more robust and adaptive to a chemical challenge as well as being less sensitive than developing stages (when more of the genome is being transcribed). Early larval stage zebrafish that are newly hatched could potentially provide a sympathetic model for nanotoxicity studies. We (UJEXE)



investigated the use of behaviour in zebrafish early life stage fry to assess the toxicity of selected NPs and compared effects/potency with those developing embryos (morphological aberrations at 0-48 hpf).

Studies on zebrafish embryos conducted at KIT used strain: AB ZIRC KA and studies were conducted for up to day 5 of development (120 hours post fertilization). Wild Indian Karyotype zebrafish were used at UEXE.

Terrestrial species:

***Eisenia fetida* (Savigny):** Although *Eisenia fetida* is not a typical agricultural soil species, it occurs in soil rich in organic matter, e.g. in highly organic forest soils. It is rarely found in non-anthropogenic biotopes (Dunger 1964; Lee 1985; Ponge and Delhaye 1995; Ronde 1960; Satchell 1983; Wilcke 1953; Zicsi 1968). It mainly occurs in man-made accumulations of rich organic material such as compost heaps, manure piles, and sewage sludge, giving *E. fetida* the common name “compost worm”. Its susceptibility to chemicals is considered to be representative of soil earthworm species.

The earthworms used for the test were obtained from a healthy laboratory rearing stock culture maintained in the testing facility at Eurofins. They were at least two months old, but not older than a year with a clitellum and a body weight between 300 and 600 mg. The age of the worms used between the different exposures did not differ more than four weeks.

***Folsomia candida* (Willem):** *Folsomia candida* (springtails) are distributed worldwide. Although it is not common in most natural soils, it often occurs in very high numbers in humus rich sites. It has been recorded in agricultural soils all over Europe (Hopkin, 1997). It has an omnivorous feeding habit, and food sources include fungal hyphae, bacteria, protozoa and detritus. It interacts through grazing with infectious plant pathogenic fungi (Ulber 1983) and may influence mycorrhiza. It is an eyeless, unpigmented collembolan, which reproduces parthenogenetically. *F.candida* has proven to be the best collembolan species for ecotoxicological testing. Soil dwelling springtails represent arthropod species with both a different route and rate of exposure compared to earthworms and enchytraeids. Their role as potential regulators of soil processes through microbivory and microfauna predation places them among the most important soil invertebrates.

The springtails used for the test were obtained from a healthy laboratory rearing stock culture. Juvenile springtails were 9 to 11 days old at the start of exposure.

***Hypoaspis (Geolaelaps) aculeifer* Canestrini (Acari: Laelapidae):** The gamasid mite *Hypoaspis (Geolaelaps) aculeifer* is considered to be a relevant representative of soil fauna and predatory mites in particular. It has a worldwide distribution and feeds on enchytraeids, springtails, mites and nematodes, and has a potential for regulating plant parasitic nematodes and bulb mites. It is encountered frequently in agricultural sites and can easily be reared in the laboratory (Karg, 1993; Ruf, 1991; 1995; 1996).

The mites were obtained from a healthy laboratory rearing stock culture maintained at the testing facility at Eurofins. Adult females were introduced into the test 28-35 days after the start of the egg laying period in the synchronisation, as the females can then be considered as already mated and having passed the pre-oviposition stage.

***Porcellio scaber*:** Terrestrial isopods are a good choice for toxicity studies since oral uptake is the main route for contaminant intake and their accumulation in the body is attributed almost exclusively to



dietary exposure (Drobne 1997). The digestive gland (hepatopancreas) cells are a major entity in the handling and processing of toxicants. They have an ability to assimilate high amounts of metals from the lumen of the gland (Hames & Hopkin 1989). Exposure of terrestrial isopods (prominently for *P. scaber*) to contaminant-treated food has been established as a standard toxicity testing protocol by Drobne and Hopkin (1994, 1995). Feeding exposure of *P. scaber* enables assessment of an exact exposure dose (Drobne 1997).

***Caenorhabditis elegans*:** The free-living soil nematode *Caenorhabditis elegans* (*C. elegans*) has evolved as an invaluable model species for biomedical research. This animal model has contributed to fundamental insights in neuroscience, development, signal transduction, cell death and organismal aging. The worms rising usage as a model organism in toxicology is in part due to the fact that the adult worm lives for only 2 – 3 weeks which enables chronic exposure studies and respective life span and progeny analyses relatively easily (Meyer and Williams, 2014). The genome of *C. elegans* has been sequenced showing that approximately 20.000 genes encode for the nematode's proteins and the majority of human genes (60 - 80%) including disease genes have a counterpart / homologue in the worm (Kaletta and Hengartner, 2006). Models for human disorders such as the neurodegenerative disorder Parkinson's disease (PD) can be developed in *C. elegans*. For example, worms with mutations in certain disease genes feature locomotory defects such as motor switching that exactly mimic neurological symptoms of the human condition. In contrast with humans, *C. elegans* with defect locomotory behaviours can be observed in high throughput analyses – i.e. multiwell-plate assays, and are thus used for pre-screening of potential PD drugs (Vidal-Gadea et al., 2011).

Through confocal microscopy of silica or polystyrene NPs in living *C. elegans*, two major entry portals of nanomaterial uptake have been identified. Uptake occurs via the pharynx to the intestinal system and via the vulva to the reproductive system including spermatheca (Scharf et al., 2013). On the subcellular level, NPs become located throughout the cytoplasm and the cell nucleus in single intestinal and vulval worm cells. Notably, intracellular localization of certain NPs in distinct *C. elegans* tissues has been correlated with a reduction in respective organ function that in turn are observable and quantifiable as behavioural phenotypes. In *C. elegans* silica NPs induce premature reproductive senescence, feeding defects and amyloid protein aggregation that all normally represent age-related phenotypes (Pluskota et al., 2009; Scharf et al., 2013). While acceleration of organismal aging in *C. elegans* might represent a nanoparticle-bio-interaction specifically induced by silica NPs other toxicity assessments mainly address life span and reproduction. Ag, CeO₂, CdTe, Al₂O₃ and ZnO NPs were identified as reducing life span and/or reproduction, while Pt nanoparticles in contrast prolonged life span (Sakaue et al., 2010). Notably, these nanotoxicological studies in *C. elegans* applied a considerable variety of nanomaterials, methodology and nematode strains, e.g. mutants.

In these studies the wild type *C. elegans* strain N2 was used for the investigation of interactions between NanoMILE NPs and a soil organism in chronic exposure studies. *C. elegans* is a transparent roundworm of 1 mm length with a simple anatomy consisting of an invariable number of 959 cells (in the adult hermaphrodite) of which 302 cells are neurons. Despite of the small cell number *C. elegans* exhibits complex tissues such as intestine, muscle, hypodermis, gonad, and a fully differentiated nervous system. A hermaphrodite adult stage, lasting 2 to 3 weeks, is preceded by four larval stages (L1 to L4) that are completed in approximately 2 days under typical growth conditions. The fact that many basic physiological processes and stress responses are conserved between *C. elegans* and humans enables comparison of molecular mechanisms. 12 out of 17 known signal transduction pathways as well



as specific epigenetic marks are conserved in *C. elegans* and humans. The relative ease of cultivation and its transparency allow for observation of organismal end points such as life span and progeny production. A well-defined nervous system that comprises virtually all important neurotransmitters can be analysed by live imaging. Simple serotonergic, dopaminergic, cholinergic or glutamatergic neuronal circuits control complex behaviours such as movement, chemotaxis, feeding, and reproduction (Schafer, 2005).

C. elegans is abundant in soil ecosystems where it lives in the solid to liquid phase. As part of the soil food web it plays a key role in nutrient cycling. Accordingly, the nematode (strain N2) was isolated from a compost site near Bristol in the 1960s by Sidney Brenner who was looking for a simple, amenable, but relevant model organism. Notably, the wild type worms that are currently used in laboratories share a virtually identical genetic background with freshly isolated specimen from contemporary soil environments which makes *C. elegans* a real life model organism (Kiontke and Sudhaus, 2006) with intrinsic relevance for (nano)ecotoxicological studies.

4. Selected particles

Various metal and metal oxide based particles were applied in the ecotoxicity testing. They included the core focus particles for work package 6: Ag NM300K, ZnO NM110, CeO₂ NM212 or CeO₂ NM211 NPs as well as other specific particles designated for study under NanoMILE, as either produced or sourced and characterised by work package (WP) 2. These particles were obtained from the European Commission Joint Research Centre (JRC) and characterized by various methods (see WP2 for details). Details on the specific particle exposures for the different test organisms are given under the subsequent experiment sections.

5. Experimental approaches, Results and Discussion for Test Organisms

Exposures with the freshwater green algae *Chlamydomonas reinhardtii* (zinc oxide and silver nanomaterials)

Brief background on toxicity of zinc oxide and silver nanoparticles in algae

Studies conducted with the model organism *C. reinhardtii* have shown a growth inhibition (8 days EC₅₀=10 µg L⁻¹) attributed to zinc ions dissolved from the particles surface (Gunawan et al. 2013). However, the bioavailability and internalization of the zinc ions in that study was strongly influenced by the stabilizers used for particle dispersion. In the case of uncoated particles and particles stabilized by polyacrylic acid, zinc bioaccumulation could be predicted almost completely on the basis of particle dissolution. In contrast, sodium hexametaphosphate-stabilizer stimulated the zinc accumulation within algae exposed to ZnO NP and induced its own biological effects (Merdzan et al. 2014).

Silver nanoparticles have been shown to reduce growth rate in freshwater and marine algae at concentrations in microgram per liter range. However, in all studies dealing with silver nanoparticles it has been questioned whether the adverse effects observed in exposure experiments are induced by nanoparticles, the dissolved silver ions or a combination of both. Several studies report that AgNP toxicity is primary mediated by free silver ions, which are released from the surface of nanoparticles (Miao et al. 2009; Navarro et al. 2008; Piccapietra et al. 2012). Other studies suggest that the toxicity of

nanoparticles cannot be explained by metal dissolution alone and the adverse effects induced by AgNP and Ag⁺ result from different pathways (Burchardt et al. 2012; Miao et al. 2010; Ribeiro et al. 2014; Wang et al. 2012). However, in both cases the role of Ag⁺ ions in the interaction of silver nanoparticles with aquatic organisms should not be neglected. In this respect the determination of bioavailability of silver and its bioconcentration within the algae cell is essential for a better understanding of the mechanisms involved in nanoparticle toxicity. No proof of internalization of nanoparticles into *C. reinhardtii* cells has been reported as of date. It can therefore be presumed that silver is taken up in form of free silver ions. As Ag(I) and Cu(I) are isoelectric and share further chemical properties, it is likely that the ions can be taken up by the same transport system that cannot discriminate between silver and copper ions (Benetti et al. 2014; Fortin and Campbell 2000; Howe and Merchant 1992).

Materials & Methods

Exposure particles

Nanoparticles	NanoMILE code	Mean particle size [nm]	Specific surface area [m ² g ⁻¹]	Content
Zinc oxide, JRC NM-110 (uncoated)	JRC-ZnOun-NM110-0960a	150	12	
Zinc oxide, JRC NM-111 (coated with Triethoxycaprylyl-silane)	JRC-ZnOTECS-NM111-2800b	140	15	
Silver nanoparticles JRC NM-300K	JRC-Ag<20nm-NM300k-0798g	15		10% (w/w)

Nanoparticle Suspension Preparation: The ZnO nanoparticles were suspended in nanopure H₂O and ModTalaCa²⁺ F20 medium at nominal concentration of 100 mg L⁻¹. The stock suspension was sonicated for 10 min at 20 kHz and 90% amplitude. The JRC NM-111 particles were first dispersed in 0.5% v/v EtOH (final concentration) and then added to the medium for characterization. The AgNM300K nanomaterials stock suspensions with the nominal concentration of 93 μM were freshly prepared in nanopure H₂O and ModTalaCa²⁺ F20.

	ModTalaCa ²⁺ F20 medium
Compound	Final concentration [M]
Salts	
CaNO ₃	0.25 x 10 ⁻⁴
MgSO ₄ x 7 H ₂ O	1.50 x 10 ⁻⁴
NaHCO ₃	1.20 x 10 ⁻³
Nutrients	
K ₂ HPO ₄ x 3H ₂ O	5.00 x 10 ⁻⁵
NH ₄ NO ₃	1.00 x 10 ⁻³
Trace elements	
CoCl ₂ x 6 H ₂ O	5.00 x 10 ⁻⁸
H ₂ BO ₃	5.00 x 10 ⁻⁵
Na ₂ MoO ₄ x 2 H ₂ O	8.00 x 10 ⁻⁸
CuSO ₄	1.63 x 10 ⁻⁷
MnCl ₂ x 4 H ₂ O	1.22 x 10 ⁻⁶
ZnSO ₄ x 7 H ₂ O	1.58 x 10 ⁻⁷
FeCl ₃ x 6 H ₂ O	9.00 x 10 ⁻⁷
Metal ligand	
Na ₂ EDTA	2.00 x 10 ⁻⁵
Buffer	
MOPS, pH 7.5	1.00 x 10 ⁻²

Size and Zeta Potential Determination: The size and the surface charge of nanoparticles were determined with the use of a Zetasizer Nano (Zetasizer Nano ZS ZEN 3600, Malvern Instruments, UK) in nanopure water, as well as in the exposure medium. However, since this technique tends to bias towards larger agglomerates, the NanoSight LM10 (NanoSight, UK) was chosen as a second technique for samples containing particles of different sizes.



Dissolution: To estimate the dissolution of free metal ions from the nanoparticle surface and its dependence on time, the free ion concentration of the metal of interest was determined by Inductive Coupled Plasma Optical Emission Spectrometry in case of ZnO NP (ICP-OES, Ciro, Spectro Analytical Instruments, Germany) and High Resolution Inductive Coupled Plasma Mass Spectrometry in case of AgNM300K (Element 2 High Resolution Sector Field ICP-MS, Thermo Finnigan, Germany). Prior to ICP-OES and HR-ICP-MS measurements, the separation of the free ion fraction was performed by centrifugal ultrafiltration. The nanoparticle suspensions were incubated at 90 x rpm, 23 °C, 276 $\mu\text{E m}^{-2} \text{s}^{-1}$ under continuous illumination in an incubation shaker for 0.5, 3, 6 and 24 h.

Modelling of the Chemical Equilibrium: The zinc and silver ions released from the nanoparticles may undergo further reactions with the elements present in exposure media. To predict the equilibrium speciation of ions in the exposure medium the software Visual MINTEQ 3.0 (vminteq.lwr.kth.se) was used.

Growth Conditions: The algal cells were grown in ModTalaCa²⁺ F20 medium in Erlenmeyer flasks under controlled axenic conditions (90 x rpm, 23 °C, 276 $\mu\text{E m}^{-2} \text{s}^{-1}$, continuous illumination) in an incubation shaker.

Long Term Exposure: The exposure was performed in ModTalaCa²⁺ F20 medium with exponentially growing cells at a final concentration of 2×10^5 cells ml^{-1} to different nanoparticle concentrations. After 0.5, 3, 6 and 24 h of exposure samples were taken for the analysis of different physiological and molecular endpoints. After 24 h of incubation, the pH of the control and exposure media was measured.

Bioaccumulation: To ensure no contamination of metals, all experimental materials were soaked in HNO₃ (0.03 M, suprapure) over night. In addition, the cellulose nitrate filters were boiled in HNO₃ and dried at 50 °C. The cultures exposed to nanoparticles were harvested (3000 rpm, 5 min, RT) and washed in fresh ModTalaCa²⁺ F20 medium three times to remove nanoparticles adsorbed on the surface of the algae. To complex and remove particles as well as free metal ions adsorbed to the cell surface, the samples were washed with 1 mM cysteine for 10 min. Subsequently 10 ml of each culture were collected on cellulose nitrate filters (pore size 0.45 μm , Sartorius, Germany) in triplicates. The filters were dried and digested with 4 ml HNO₃ (65% suprapure) in a High Performance Microwave Reactor (UltraCLAVE, MLS, Germany).

Physiological Endpoints: The effects of nanoparticles on *C. reinhardtii* were estimated on different physiological endpoints (cell growth and cell volume, photosynthesis, intracellular ATP content and exopolymeric substance (EPS) production).

Cell Growth and Cell Volume: The cell number and cell volume were detected by a cell counter (CASY Model TT, Roche Innovatis, Germany). Nonlinear regression and exponential growth equation was performed to calculate the growth rate.

Photosynthesis: The photosynthetic yield of the algae cultures were measured with a pulse-amplitude modulated chlorophyll fluorometer (Phyto-PAM, Heinz Walz, Germany) using the formula:

$$Yield = \frac{(F_m - F_t)}{F_m} = \frac{dF}{F_m}$$

where *Yield* is the photosynthetic yield of the PSII (this value is used to estimate the efficiency of electron transport through PSII) F_m the maximum fluorescence and F_t the fluorescence at ambient light conditions.

Intracellular ATP Content: To investigate the cell viability and the metabolic activity, the intracellular ATP content was measured using the BacTiter-Glo Microbial Cell Viability Assay (PROMEGA, USA). 100 μ l of the cell culture were mixed with 50 μ l BacTiter-Glo reaction agent in opaque white 96 micro well plates (Greiner Bio-One, Austria). The luminescence signal was recorded immediately using an Infinite M200 plate reader (TECAN, Switzerland).

Staining of Extracellular Polymeric Substances (EPS): EPS consists of a complex matrix of polysaccharides, glycoproteins, proteins and other biomolecules. Lectins are a group of proteins, which bind specific carbohydrate structures and thus can be used to identify and trace carbohydrates in complex matrices. For the analysis of extracellular polymeric substances, the lectin HPA form *Helix pomatia* was used, which binds to terminal N-glycosylamine residues present in EPS.

The samples were fixed with formaldehyde (3.7% final concentration) and with the fluorescein (FITC) labeled lectin HPA. The FITC label was then visualized by confocal microscopy (Leica DMI 600B epifluorescence microscope, Leica Microsystems, Germany) with an excitation laser of 488 nm and the emission was measured at 520 nm.

Statistical analysis: Statistical analysis was performed using one-way ANOVA combined with the Dunnett's Multiple Comparison Test. The data collected at one time point were compared to the respective control.

Results

Zinc Oxide Nanoparticles

Size and Zeta Potential: The size and zeta potential of JRC NM-110 and JRC NM-111 in nanopure water and in the exposure medium ModTalaCa²⁺ F20, measured by DLS, is shown in Figure 2. JRC NM-110 dispersed in nanopure water has a zeta average size of 284.45 \pm 7.6 nm. The zeta potential was 29.1 μ V and decreased to 16.5 μ V after 6 h. In ModTalaCa²⁺ F20 medium the initial size was 361.9 \pm 4.91 nm. After 6 h, the particles agglomerated to an average size of 646.8 \pm 5.26 nm. However, within 24 h the large agglomerates underwent sedimentation, which lead to a decrease in the measured zeta average size to 385.5 \pm 6.5 nm. The zeta potential in the exposure medium was not time dependent (-27.15 \pm 0.58 μ V). In contrast to JRC NM-110 it was not possible to achieve a stable suspension of coated particles JRC NM-111 in nanopure water. In ModTalaCa²⁺ F20 the zeta average size as well as the

zeta potential stayed stable over a period of 24 h with values of 225.01 ± 16.78 nm and -35.6 ± 1.83 μ V respectively.

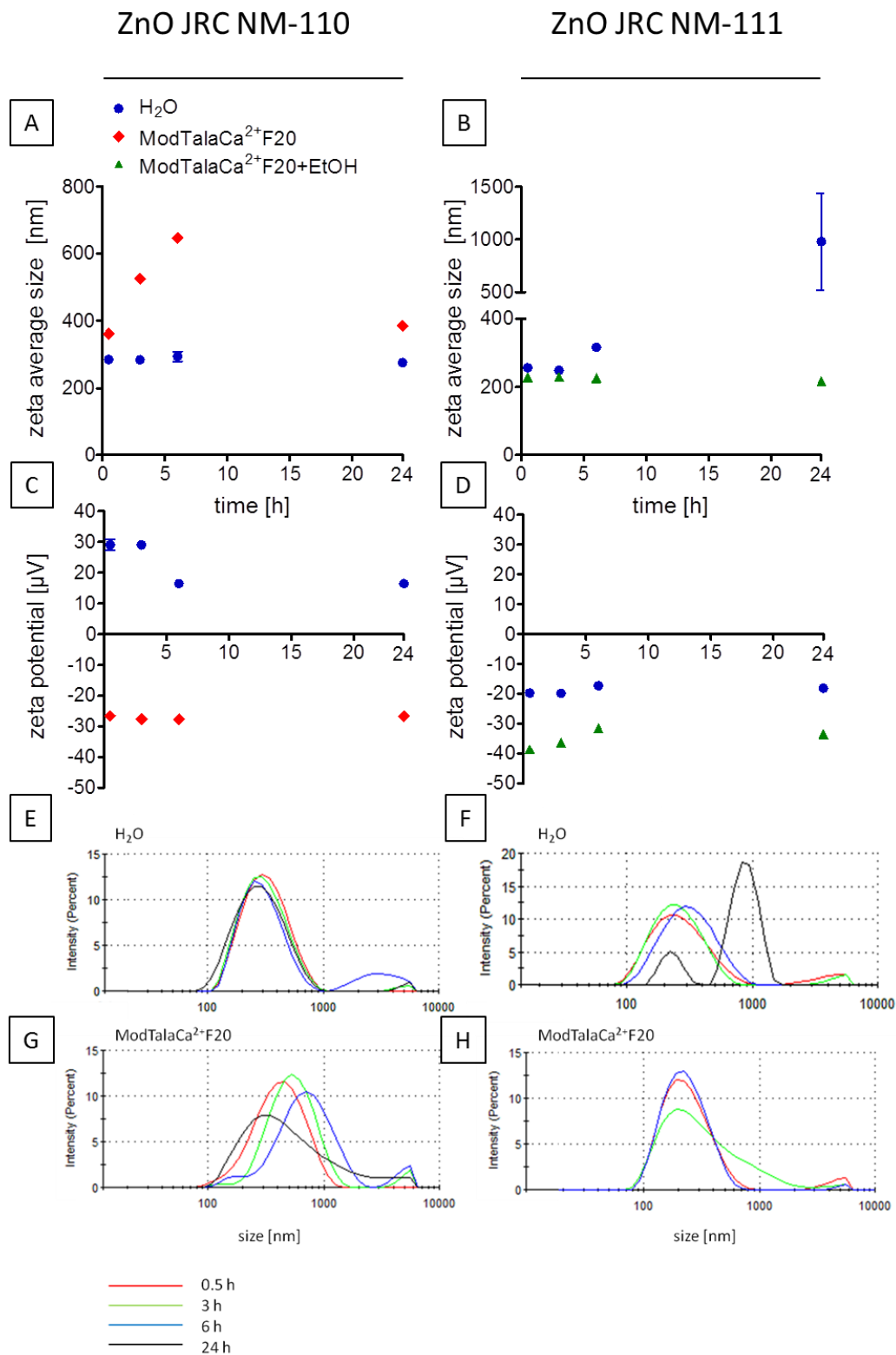


Figure 2: ZnO NP size and zeta potential as estimated by Zetasizer Nano (DLS). A and C: ZnO JRC NM-110 (uncoated) and B and D: ZnO JRC NM-111 (coated). The results are given as average of three subsequent measurements of the same sample with standard deviation. E and G, F and H show the size distribution of ZnO JRC NM-110 and ZnO JRC NM-111 respectively in

nanopure water and the exposure medium measured at 0.5, 3, 6 and 24 h. The results are shown as mean of 3 technical replicates with standard deviations.

Dissolution: The zinc concentration in ZnO JRC NM-110 (uncoated) and ZnO JRC NM-111 (coated) stock suspensions were determined by ICP-OES and they were 1.022 mM and 0.658 mM, respectively. The difference of 64% in between the two types of nanoparticles can be explained by the coating, which contributed to the total weight of the ZnO JRC NM-111.

The dissolution of ZnO JRC NM-110 (uncoated) and ZnO JRC NM-111 (coated) as percentage of the added nanoparticle concentration was measured after 0.5, 3, and 6 h (Figure 3). For both types of nanoparticles, the dissolution was not time dependent. With increasing ZnO NP concentration a higher percentage of nanoparticles dissolved. However, at nanoparticle concentrations higher than 26.75 μM , the percentage of dissolved particles decreased. By considering the total measured Zn^{2+} (Table 1) it can be seen that no further dissolution occurs after the concentration of around 30 μM Zn^{2+} is reached. This results in lower percentage of dissolved nanoparticles at higher concentrations, as estimated from Visual MINTEQ.

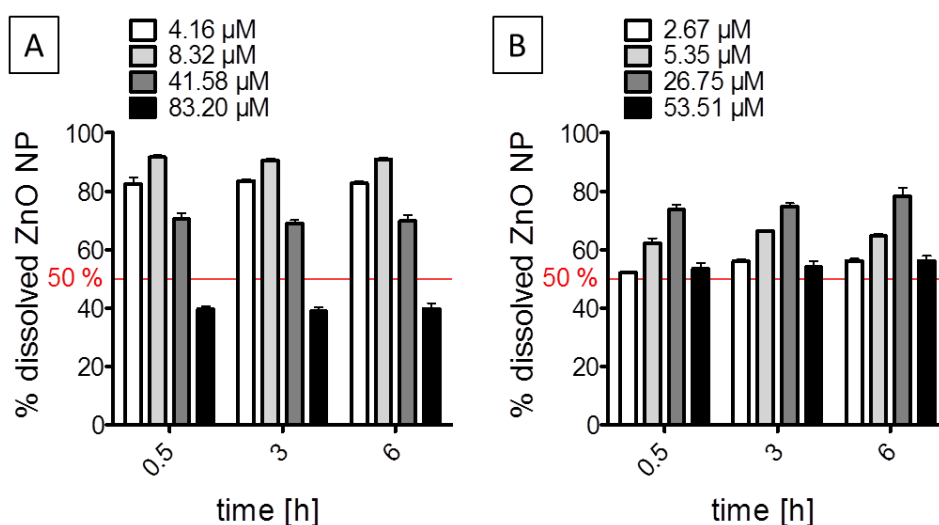


Figure 3: Dissolution of ZnO NP. A: ZnO JRC NM-110 (uncoated) and B: ZnO JRC NM-111 (coated) as % of the added nanoparticle concentration measured after 0.5, 3, and 6 h via centrifugal ultrafiltration. The results are shown as mean of 3 technical replicates with standard deviations.

Table 1: Dissolution of ZnO NP. Data are shown as total Zn²⁺ [μM] measured after 0.5, 3, and 6 h via centrifugal ultrafiltration.

ZnO JRC NM-110 (uncoated)				
time [h]	4.16 μM	8.32 μM	41.58 μM	83.2 μM
0.5	3.43 ±0.08	7.62 ±0.05	29.27 ±0.55	32.90 ±0.38
3	3.47 ±0.02	7.53 ±0.04	28.68 ±0.35	32.35 ±0.49
6	3.44 ±0.02	7.56 ±0.05	28.99 ±0.63	33.02 ±0.66
ZnO JRC NM-111 (coated)				
	2.67 μM	5.35 μM	26.75 μM	53.51 μM
0.5	1.39 ±0.01	3.32 ±0.06	19.70 ±0.35	28.58 ±0.59
3	1.50 ±0.01	3.55 ±0.00	19.97 ±0.26	28.94 ±0.56
6	1.50 ±0.01	3.46 ±0.02	20.91 ±0.63	30.03 ±0.50

Modelling of Chemical Equilibrium: The percentage of dissolved compounds Zn²⁺, CO₃²⁻ and PO₄³⁻ are shown as a function of total added Zn²⁺ concentration in Figure 4. At a concentration of 30 μM Zn²⁺, Zn²⁺ is expected to precipitate with PO₄³⁻. At higher Zn²⁺ concentrations (>100 μM), the free zinc ions are also expected to precipitate with CO₃²⁻. However, at Zn²⁺ total concentrations below 20 μM the zinc is 100% present in the dissolved fraction as a complex with EDTA⁴⁻. The measured and modeled free zinc ion concentrations as a function of the total added Zn²⁺ in form of nanoparticles or as free ions respectively is shown in Figure 5. There is a clear correlation between the free zinc concentrations measured in the dissolution experiments and the total dissolved modeled Zn²⁺ concentration. The results indicate that at the higher applied ZnO NPs concentrations the dissolution is underestimated due to zinc precipitation.

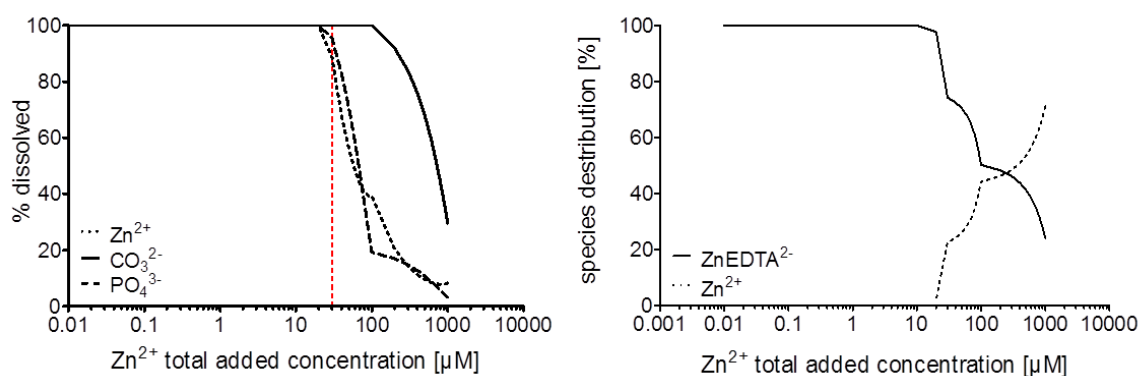


Figure 4: Modeling of chemical speciation of Zn⁺ A: percentage of Zn²⁺, CO₃²⁻ and PO₄³⁻ present in the dissolved fraction at equilibrium as a function of total added Zn²⁺ concentration, the red dotted line represents the concentration of 30 μM. B: species distribution of the dissolved fraction of Zn²⁺ in ModTalaCa²⁺F20 medium at equilibrium as percentage of total concentration.

Silver Nanoparticles: The stock suspensions of AgNM300K and AgNO₃ were freshly prepared in ModTalaCa²⁺ F20 medium with nominal concentrations of 93 μM and 20 μM respectively. The mean values of measured stock concentrations were 63 μM and 18 μM for AgNP and AgNO₃ respectively. In case of AgNM300K silver recovery of 88% (lowest recovery reported by Navarro et al., 2008) was assumed. From the mean of three measured stock suspensions the applied concentrations of 0.3, 1.3, 3.1, 6.3 μM for AgNP and 0.009, 0.09, 0.18, 0.27 μM for AgNO₃ were calculated.

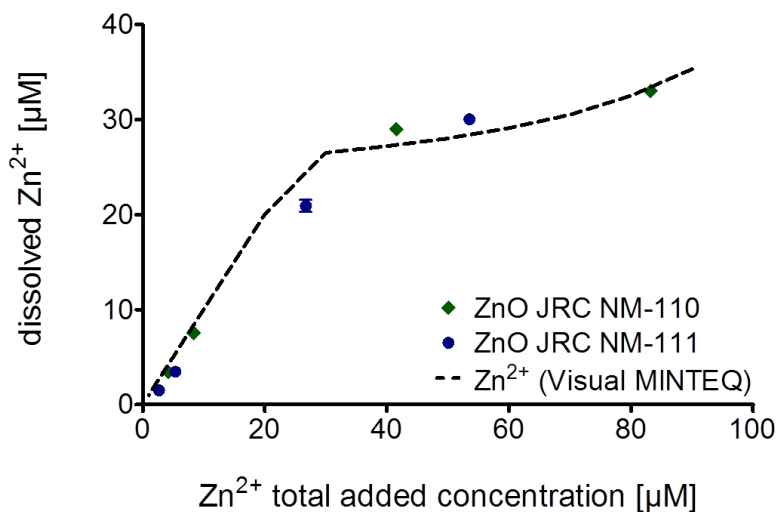


Figure 5: Correlation of measured and modeled free zinc ion concentrations. Data are shown as a function of the total added Zn^{2+} in nanoparticulate form measured in the dissolution experiments with ZnO JRC NM-110 (green \diamond) and ZnO JRC NM-111 (blue \circ) and dissolved zinc ion concentrations as a function of the total added Zn^{2+} modeled (dashed line).

Size and Zeta Potential: The size distribution indicated the presence of two particle populations (Figure 6, C, D): a peak at 50 nm and a second peak of small particles of about 5 nm. The PDI of the measurements was around 0.5 indicating that the suspension was polydispersed and the size of particles cannot be estimated from the zeta average size given by DLS measurements. However, the polydispersity of the suspension did not interfere with the estimation of the zeta potential. The measured zeta potential in nanopure water and in the exposure medium was $-7.3 \pm 1.2 \mu V$ and $-2.9 \pm 0.4 \mu V$, respectively (Figure 6B). The particle size estimated by NTA (Figure 6A) had a mean particle size of $47.2 \pm 2.2 \text{ nm}$ and $46.6 \pm 3 \text{ nm}$ in nanopure water and in the exposure medium, respectively.

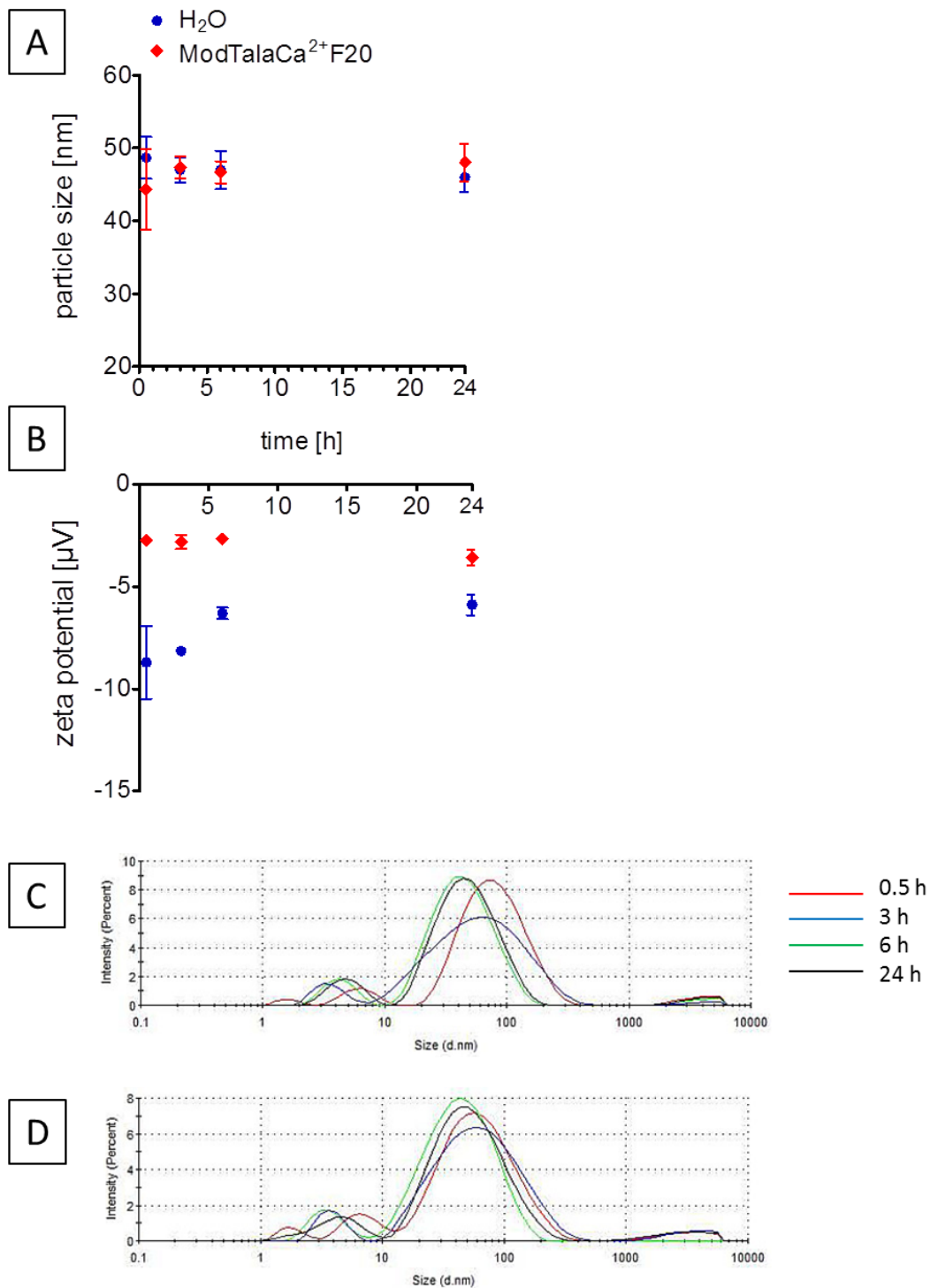


Figure 6: Size and zeta potential determination of AgNP. A: Size determination of AgNP NM-300K nanoparticles with the use of Nanosight (NTA). B: zeta potential determination of AgNP NM-300K by Zetasizer Nano (DLS). C and D show the size distribution determined by Zetasizer Nano (DLS) of AgNP NM-300K in nanopure water and the exposure medium, respectively measured at 0.5, 3, 6 and 24 h.

Dissolution: The dissolution of AgNM300K is shown in Figure 7 as percentage of the added nanoparticle concentration measured after 0 (stock), 0.5, 3, 6 and 24 h. The free silver ion concentration measured in the stock suspension indicated a nanoparticle dissolution of 1.55%. At the concentrations chosen for the

exposure experiments a trend towards lower particle dissolution with decreasing applied particle concentration could be observed.

After one hour incubation 0.1, 0.8, 1.5 and 1.9% of nanoparticles dissolved at the applied AgNP concentrations of 0.3, 1.3, 3.1, 6.3 μM , respectively. However, with time the Ag^+ concentration in the suspensions decreased at all applied concentrations.

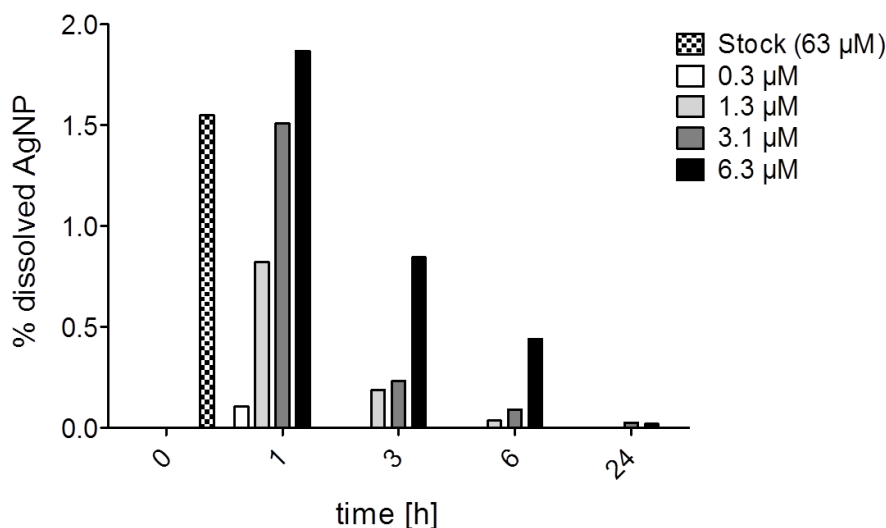


Figure 7: Dissolution of AgNM-300K. Data are shown as percentage of the added nanoparticle concentration measured after 0.5, 3, 6 and 24 h via centrifugal ultrafiltration.

Modelling of Chemical Equilibrium: Species distribution of the dissolved fraction of Ag^+ in ModTalaCa²⁺ F20 medium is depicted in Figure 8. In the exposure medium, the chloride concentration was reduced to 5.24 μM so that $\text{AgCl}_{(\text{aq})}$ species accounts only for 0.8% whereas 95% of the total silver is present as free ions (Figure 8).

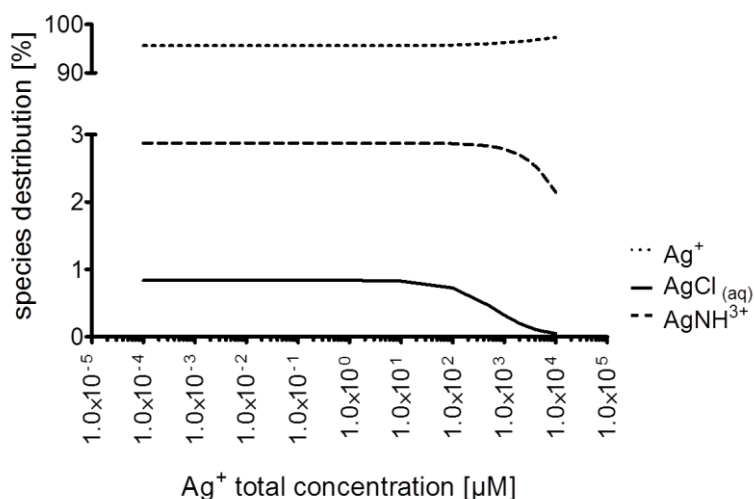


Figure 8: Modeling of chemical speciation of Ag^+ . Species distribution of the dissolved fraction of Ag^+ in ModTalaCa²⁺ F20 medium at equilibrium as % of total concentration. Only the three main species are shown.

Bioaccumulation: The silver uptake by *C. reinhardtii* on exposure to AgNP and AgNO_3 was estimated by HR-ICP-MS. Between 89-99% and 40-97% of total silver could be removed by cysteine wash in cultures

exposed to AgNP and AgNO₃, respectively. It was assumed that the amount of silver, which could not be removed, was intracellular.

The uptake of silver was rapid and the maximal intracellular silver concentrations were reached already after 30 minutes (Figure 9). In case of silver nanoparticles, the intracellular silver content increased with the applied AgNP concentration and approached a maximum at the intracellular concentration of around $7 \times 10^{-4} \text{ mol L}^{-1} \text{ cell}^{-1}$ (Figure 9A). Upon exposure to increasing concentrations of AgNO₃ the intracellular silver concentration increased linearly ($R^2=0.99$, **Error! Reference source not found.** Figure 9 B, C). In contrast to AgNP exposure, no plateau in bioaccumulation at high concentrations was observed.

Interestingly, the intracellular silver concentration in cells exposed to AgNP decreased over time by 85 to >99% at all applied particle concentrations, except the highest exposure. Also for AgNO₃, a decrease in intracellular silver concentration was observed, but only after an exposure duration of 3 h.

The bioaccumulated silver when plotted as a function of the highest percentage of dissolved silver (1.9%) showed a higher bioaccumulation by the algae exposed to AgNP than AgNO₃. The maximal intracellular silver content was reached at an applied Ag⁺ concentration of 0.023 μM with no further increase in silver uptake at higher concentrations. The highest intracellular silver concentration in experiments conducted with AgNO₃ was 1.3 times lower even though the applied Ag⁺ concentration was 10 times higher than in AgNP experiments (Figure 9C).

Physiological Endpoints

Cell Growth and Cell Volume: The effects of AgNP and the dispersant on the growth rate of *C. reinhardtii* are depicted in figure 10. The median effective concentration (EC₅₀) was reached at a concentration of 3 μM. The EC₅₀ for AgNO₃ was 0.16 μM. The growth rate inhibition by AgNP, when plotted as a function of the dissolved Ag⁺ content (1.9%) showed that the particles induced a stronger inhibition as compared to AgNO₃. The EC₅₀ values calculated based on the AgNP exposures were 2.7 times lower than for AgNO₃ (0.06 and 0.16 μM respectively, figure 10 B). The AgNP and AgNO₃ exposure concentrations that affected the growth rate also had an effect on the cell volume (Figure 10 C, D). However, in presence of 0.5 μM of cysteine no effects of AgNP on the growth and cell volume of *C. reinhardtii* could be observed (Figure 10 E, F).

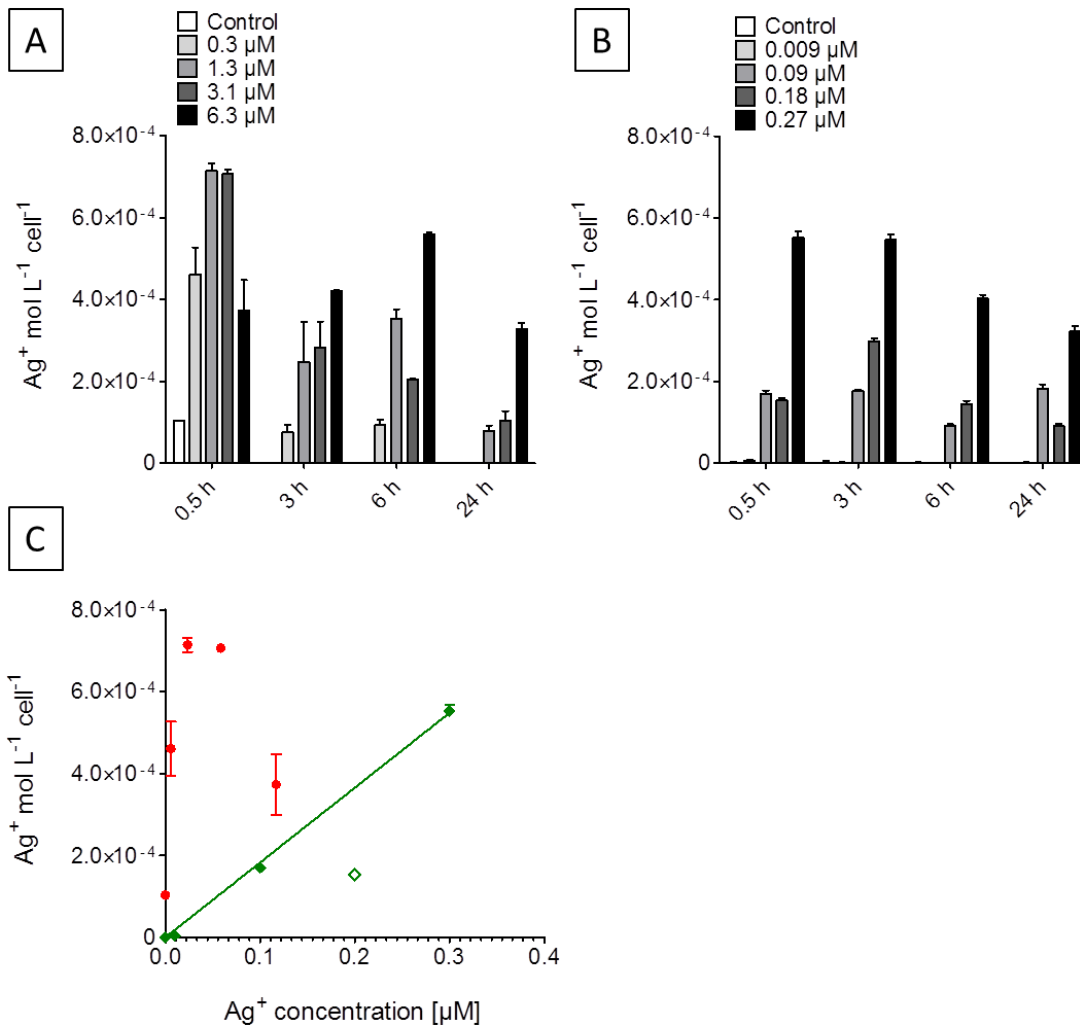


Figure 9: Intracellular silver content in cells exposed to silver compounds. Intracellular silver upon exposure to AgNP (A) and AgNO₃ (B) measured after 0.5, 3, 6 and 24 h. C: Intracellular silver content as a function of AgNO₃ concentration (green) and Ag⁺ dissolved from the particles by assuming a dissolution of 1.9% (red) measured after 0.5 h. Empty symbol shows an outlier. The measured silver content was normalized to the cell number and volume. The results are shown as mean of 3 technical replicates with standard deviations.

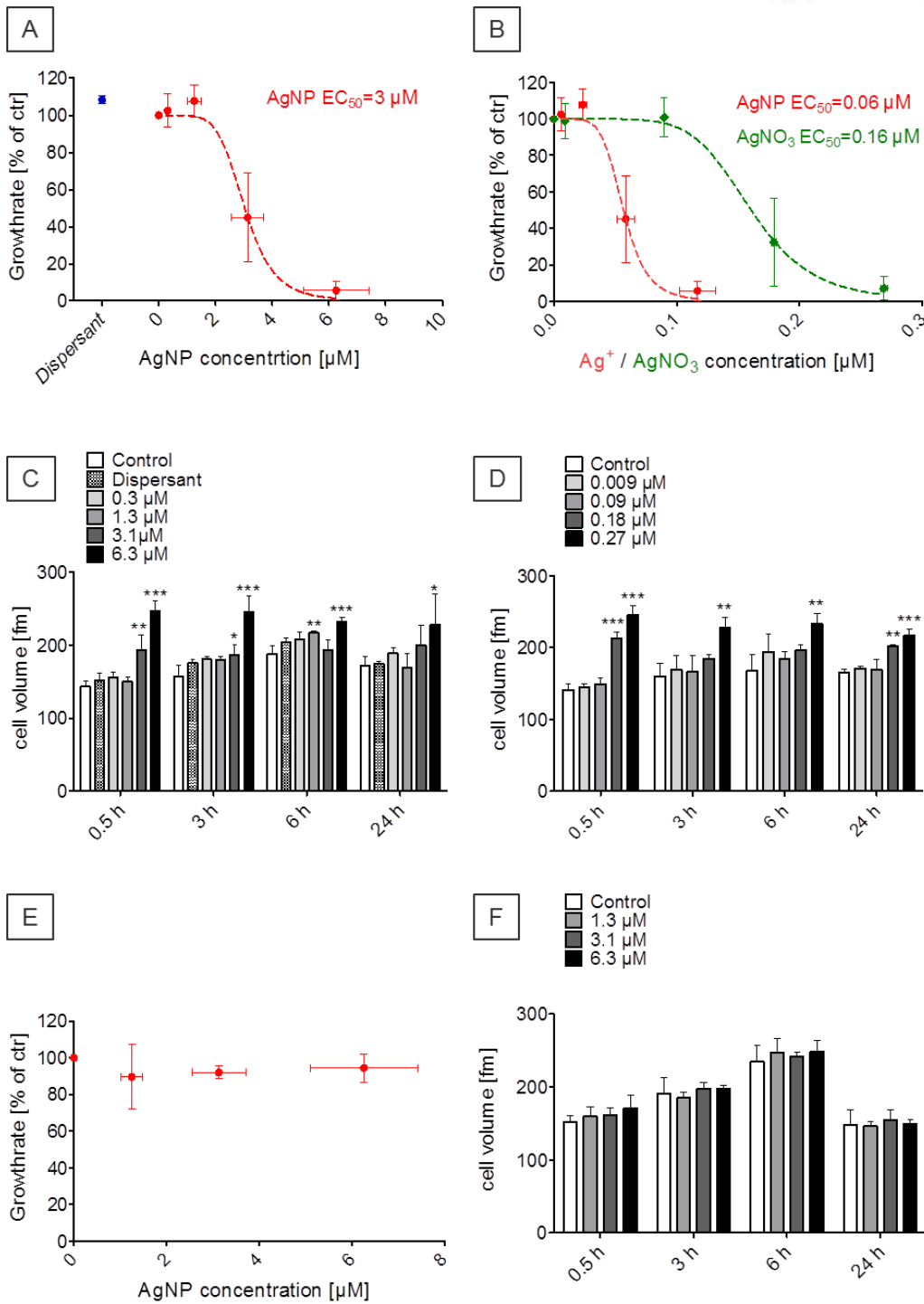


Figure 10: Effects of silver on cell growth and cell volume A: growth rate as a function of concentration of AgNP. The growth rate of cells exposed to the dispersant (blue). B: growth rate as a function of concentration of AgNO_3 (green) and the Ag^+ dissolved from the particle surface (red). Volume of cells exposed to AgNP (C) and AgNO_3 (D) measured over 24 h. E: growth rate as a function of AgNP concentration in presence of cysteine. F: Volume of cells exposed to AgNP in presence of cysteine.

The photosynthetic yield of the cultures exposed to 0.09 and 0.18 μM AgNO_3 reduced significantly. Comparable with AgNP, an almost complete recovery was observed after 3 and 24 h (Figure 11). The strongest effect on photosynthetic yield was measured at a concentration of 0.27 μM AgNO_3 with no recovery. As already observed in experiments conducted with AgNP, the EC_{50} values increased with time.

The effect of AgNP on photosynthetic yield when plotted as a function of the dissolved Ag^+ content showed that the particles induced a stronger inhibition as compared to that by AgNO_3 . The EC_{50} values calculated based on the AgNP experiments were more than 2 times lower than for AgNO_3 . No effects of silver nanoparticles on the photosynthetic yield could be observed in presence of 0.5 μM cysteine.

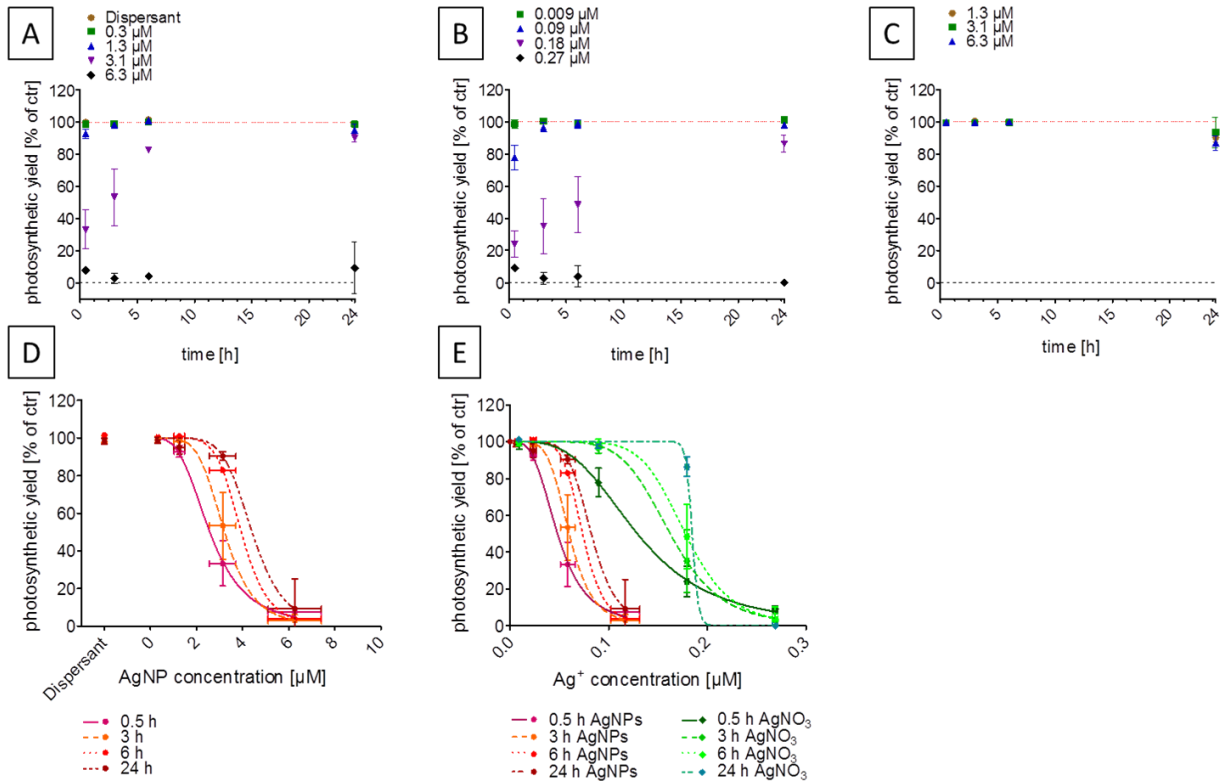


Figure 11: Photosynthetic yield of cultures exposed to silver compounds. Photosynthetic yield upon exposure to AgNP (A), AgNO_3 (B) and AgNP in presence of cysteine (C) over the duration of 24 h. Photosynthetic yield as a function of increasing concentration of AgNP (D), AgNO_3 (E green) and Ag^+ dissolved from the particle surface by assuming a dissolution of 1.9% (E red) as % of control measured over the duration of 24 h.

Table 2: EC_{50} values calculated based on the measurement of the photosynthetic yield of cultures exposed to AgNP and AgNO_3 .

Time	0.5 h	3 h	6 h	24 h
A: AgNP				
EC_{50} [μM]	2.58	3.21	3.94	4.41
B: AgNO_3				
EC_{50} [μM]	0.129	0.162	0.178	~0.184
C: AgNP (normalized to dissolved Ag^+)				
EC_{50} [μM]	0.048	0.06	0.074	0.082

Intracellular ATP Content: The effects of AgNP and AgNO_3 on the ATP content is shown in figure 12. A significant adverse effect on the ATP concentration could only be detected in cultures exposed to the highest AgNP. No recovery could be observed algae exposed to any concentration of AgNP (Figure

12 A). Similar to cultures exposed to AgNP, a significant ($P \leq 0.001$) decrease in ATP content could be observed only at the two highest concentrations.

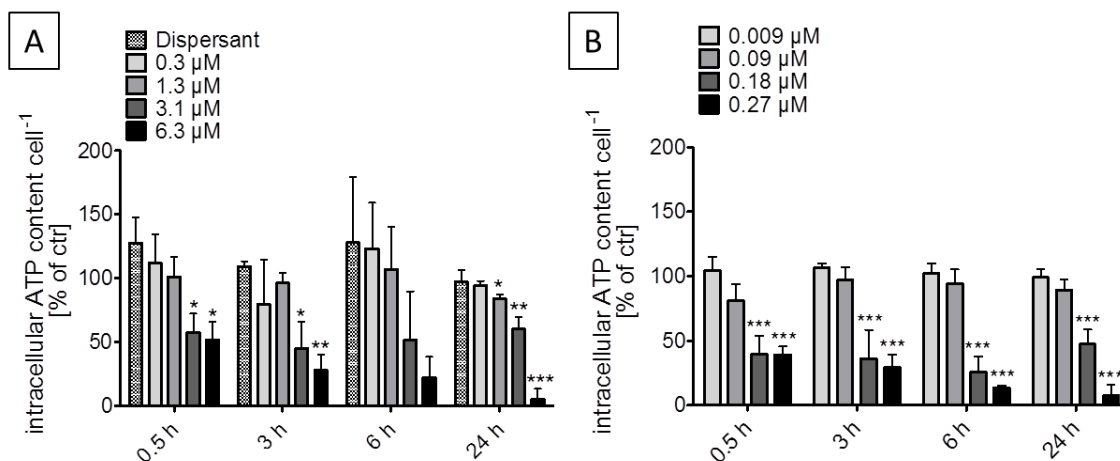


Figure 12: Intracellular ATP content of cells exposed to silver compounds. ATP concentration upon exposure to AgNP (A) and AgNO₃ (B).

Data on the effects on ZnO NP are not included in this report for D6.1 because the ZnO nanoparticles dissolved to ions (nearly 100%).

Discussion

Zinc Oxide Nanoparticles Dissolve Under the Exposure Conditions: The dispersion and behaviour of the zinc oxide nanoparticles, JRC NM-110 and JRC NM-111, were characterized in suspension under experimental conditions. The surface properties of the particles and their interactions with ions in suspension had a higher influence on the mean particle size, by reducing or inducing agglomeration, than the primary particle size measured by the provider. Strong agglomeration of zinc nanoparticles in suspension has also been observed in previous studies (Domingos et al. 2013; Franklin et al. 2007; Merdzan et al. 2014).

Both the particles dissolved in the exposure medium in a concentration dependent manner. The dissolution of the particles was not time dependent and the maximal free ionic zinc concentration could already be reached after 30 minutes in suspension. In contrast to previous studies (Merdzan et al. 2014; Waalewijn-Kool et al. 2013) no effect of the coating on the dissolution of the particles could be detected.

Increasing phosphate concentrations have been shown to reduce the amount of free zinc ions in solution and to change the particle morphology towards material containing ZnO phases and zinc phosphate (Li et al. 2013; Lv et al. 2012). The reduced amount of ionic zinc resulted in a strong decrease in toxicity of ZnO NP towards bacteria (Li et al. 2013). Runoff from agricultural lands and facilities as well as wastewaters and industrial effluents cause an increased phosphate concentration in surface waters. Under this aspect the interaction of zinc oxide nanoparticles with phosphate in natural waters is inevitable and need to be carefully investigated in studies dealing with nanoparticle fate and toxicity (Lv et al. 2012).



At all tested concentrations more than 50% of the nanoparticles rapidly dissolved after introduction into the exposure medium. With decreasing initial concentration from 100 to 1 mg L⁻¹ an increase in dissolution from 2 to 70% could be observed (Gunawan et al. 2013). Heinlaan et al. (2008) suggested that at initial concentrations below 1 mg L⁻¹ over 69% of ZnO NP dissolve (Heinlaan et al. 2008). This is in good agreement with other studies reporting a substantial dissolution of particles of up to 100% at low concentrations (Adam et al. 2014; Miller et al. 2010). At lower concentrations, where the difference between the actual and the equilibrium concentration is high, the particles have a tendency to dissolve faster due to high dissolution rate (Adam et al. 2014).

Due to the rapid, time independent dissolution it is likely that a major fraction (up to 100%) had already dissolved in the stock suspension. Therefore, under exposure conditions the test organism would be exposed predominantly to ionic zinc from the onset. Although zinc is an essential nutrient, high concentrations can disturb the metal homeostasis and lead to adverse effects. For two freshwater algae EC₅₀ values as low as 40 µg L⁻¹ zinc have been reported (Franklin et al. 2001; Franklin et al. 2007; Muysen and Janssen 2001). Under these circumstances, it is very challenging to differentiate between the effects caused by ionic zinc and possible nanospecific effects like photoinduced ZnO NP toxicity. As a consequence it was not deemed useful to assess the toxicological effects on algae for these exposures to ZnONPs.

Silver Nanoparticles Form a Stable Suspension in the Exposure Medium: The physicochemical properties of nanoparticles, including the large surface area and surface reactivity, are attributed to their small size, which distinguishes them from the bulk materials. However, depending on the chemical composition of the exposure medium increase of the particle size due to flocculation and agglomeration may occur. In order to link the physico-chemical properties of the particles with their toxicity potential, an accurate characterization of the particles within the exposure medium under exposure conditions was of utmost importance in the present study. Indeed, the zeta potential of AgNP was dependent on the ionic strength of the medium. In nanopure water the particles showed a negative zeta potential whereas in ModTalaCa²⁺F20 the zeta potential was close to zero. Nevertheless, in nanopure water as well as in the medium the size of the particles was comparable and both suspensions stayed stable over the duration of 24 h. This indicates a rather sterical stabilization of the particles provided by the dispersants (polyoxyethylene glycerol trioleate and Tween 20) than stabilization by charge as being reported earlier (Thio et al. 2012; Wang et al. 2012).

The mean particle size of AgNP determined by NTA was ~ 47 nm. The DLS measurements indicated the presence of a small fraction of particles with the size below 10 nm. Two size peaks measured for AgNP NM-300K by DLS were also reported in a previous study and confirmed by TEM measurements (Klein et al. 2011; Sorensen and Baun 2014). This fact makes the investigation of the toxicity potential of AgNP NM-300K and the connection between the particle size and the effects more challenging as the differently size particles may cause toxic effects of different magnitudes. Ivask et al. (2014b) showed an enhanced bioavailability and toxicity of particles with the size <10 nm as compared to 20–80 nm AgNP (Ivask et al. 2014b). Furthermore, it is likely that the presence of algae and algal exudates in the exposure medium influences the agglomeration of AgNP. However, accurate determination of particle size in the presence of algae was not possible.

Dissolution of Silver Nanoparticles is Concentration and Time Dependant: Oxidation of Ag(0) to Ag(I) in the presence of oxygen and other oxidizing agents leads to the release of free Ag⁺ from silver nanoparticles (Behra et al. 2013; Wang et al. 2012). Various studies report that Ag⁺ contribute

considerably to the toxic effects induced by AgNP (Ivask et al. 2014b; Leclerc and Wilkinson 2014; Navarro et al. 2008), which makes the measurement of particle dissolution an essential part of toxicity tests. In the present study 1.55% of the particles dissolved already during the stock preparation, which indicates that a fraction of particles quickly dissolves upon contact with the exposure medium. However, the possibility cannot be excluded that silver ions are already present in the source suspension provided by the University of Birmingham, UK. Nevertheless, the particle dissolution was below 2%, which is in agreement with previous studies (Burchardt et al. 2012; Ivask et al. 2014b; McTeer et al. 2014; Navarro et al. 2008).

At concentrations chosen for the toxicity assays a higher percentage of particles dissolved at higher concentrations. Contrary to the present study, higher particle dissolution at lower concentrations was reported by various authors (Laban et al. 2010; Miao et al. 2010). However, the particle dissolution is always dependent on the medium as well as the AgNP used. The particles used in the present study are polydispersed. The higher specific surface area of <10 nm particles is likely to result in faster dissolution, similar to earlier studies, which report a higher dissolution of smaller nanoparticles (Ivask et al. 2014a; Ivask et al. 2014b; Ma et al. 2012). The application of a higher particle concentration would logically result in a larger amount of <10 nm particles in suspensions, which may lead to higher percentage of Ag⁺ with increasing AgNP concentrations.

The highest amounts of Ag⁺ were measured after 0.5 h and interestingly, the amount of free Ag⁺ decreased at later time points. The decrease of Ag⁺ over time may be caused by formation of insoluble Ag precipitates. Furthermore, the media were incubated at continuous illumination during the dissolution experiments. Therefore photochemical reduction of Ag(I) to Ag(0) under the exposure conditions can possibly result in Ag⁺ depletion over time. In addition, sorption of Ag⁺ to the beaker walls could also lead to the silver ion decrease in the media.

As the AgNP dissolution is surface area limited, the Ag⁺ depleted in the media cannot be replenished right away and decreased with time for this reason. This effect is more severe at lower concentrations because at higher AgNP concentrations Ag⁺ depletion could be faster replenished. The decrease of free Ag⁺ in solution with time was also observed in previous studies, although to a different extend (Miao et al. 2010; Turner et al. 2012). In presence of algae the chemistry of the exposure medium may change due to excretion of ligands and other algal exudates. These additional factors, which cannot be analysed in the scope of the present study, may influence the particle dissolution.

Silver Nanoparticles Inhibit Growth of *C. reinhardtii*: Silver nanoparticles decreased the growth rate of *C. reinhardtii* in a concentration dependent manner. Based on the total amount of silver added, the nanoparticles seem to induce a lower toxicity as compared to AgNO₃. Several studies report effects of AgNP on growth of different algae species in micromolar range whereas AgNO₃ seems to induce toxicity already at nanomolar to low micromolar concentrations (Burchardt et al. 2012; Miao et al. 2010). However, a comparison of the studies among each other is not possible due to different experimental parameters, including the test organisms, exposure conditions (seawater and freshwater) and test duration.

The growth inhibition is probably due to effects on the metaphase of the cell division by regulation of proteins involved in the algae cell cycle, including cyclin-dependent kinase and anaphase promoting complex, as shown in an earlier study (Pillai et al. 2014). Upon exposure to high AgNP and AgNO₃ concentrations, the cell volume significantly increased as compared to the control. Changes in the cell

size are a common effect of stressors such as UV radiation, nutrient deficiency and heavy metals on green algae (Bacelo and Poschenrieder 2004; Hessen et al. 1997; Vandonk and Hessen 1995).

Photosynthetic Yield is a Sensitive Physiological Endpoint to Detect Early Effects and Recovery of Cells Exposed to Silver Nanoparticles: Silver nanoparticles decreased the photosynthetic yield of *C. reinhardtii* in a concentration dependent manner. A deterioration of the photosystem II reaction centre and adverse effects on the oxygen evolving complex and electron transport activity were shown for *C. reinhardtii* exposed to 5 and 10 μM AgNP, with stronger inhibition induced under light as compared to dark conditions (Dewez and Oukarroum 2012). The inhibition of electron transport and effect on the photosynthetic activity at AgNP and AgNO_3 concentrations of 1 to 10 μM were also demonstrated by Matorin et al. (2013).

The inhibition of the photosynthetic yield can be caused by binding of Ag^+ to thiol groups of proteins involved in photosynthetic processes. Especially in enzymes, which require Cu^+ to function, such as plastocyanin and cytochrome oxidase, the displacement of Cu^+ by Ag^+ can lead to alteration or loss of their function. Indeed, a regulation of plastocyanin and cytochrome oxidase upon exposure to AgNO_3 has been shown at the transcriptome and proteome level (Pillai et al. 2014). In addition, an altered regulation of light harvesting complex proteins and serine-threonine protein kinases involved in their phosphorylation has been demonstrated (Pillai et al. 2014). For this reason it was suggested that interactions of Ag^+ with proteins involved in the photosynthetic machinery leads to the disturbance of the photosynthetic electron transport and to reduction in the photosynthetic yield (Pillai et al. 2014).

In agreement with the previous study (Pillai et al. 2014) a recovery of photosynthetic yield to control algae levels over time could be observed for all AgNP and AgNO_3 concentrations except the highest one adopted. The decrease of intracellular Ag^+ concentration in cultures exposed to AgNO_3 over time suggests the ability of cells to induce detoxifying reactions, such as Ag^+ efflux, and to adapt to the stressor (Pillai et al. 2014). The intracellular Ag^+ concentration also decreased in cells exposed to AgNP over time, indicating similar defense mechanism as observed for AgNO_3 . Furthermore, in case of AgNP the recovery of photosynthetic yield can be explained by the depletion of free silver ions in the exposure medium with time. Stevenson et al. (2013) reported that silver nanoparticles induce a higher toxicity in earlier stages of algal cultures as compared to cultures in the stationary growth phase. It was hypothesized that dissolved organic carbon (DOC) produced by the algae is capable of mitigating AgNP toxicity. However, this could not be shown for AgNO_3 (Stevenson et al. 2013). Nevertheless, the change in the external environment due to algal exudates can lead to a decreased bioavailability of silver by complexation with ligands and thus to recovery.

At the highest concentrations no recovery could be observed. It is possible that at high silver concentrations the damage of the cells was so severe that they could not respond to the stressor. Furthermore, the excretion of dissolved organic carbon is dependent on cell viability and growth. As no growth could be observed at the highest concentration, no mitigating effect of algal ligands can be expected.

Silver Nanoparticles Induce Changes on the Energy Status of *C. reinhardtii*: As a primary source of chemical energy, ATP is essential for metabolic processes within the cell. The ATP content in *C. reinhardtii* cells decreased significantly at AgNO_3 concentrations greater than 0.1 μM whereas a significant decrease of ATP in cells exposed to AgNP occurred only at concentrations greater than 1.3 μM . Comparable to the results obtained by growth rate and photosynthetic yield measurements AgNO_3



induced a stronger effect on the energy content of cells as compared to AgNP based on total silver concentration. A decrease in the ATP concentration can probably directly be linked to a damage or inhibition of enzymes in the chloroplasts and mitochondria, which are the primary organelles for ATP synthesis. It has been shown that upon exposure to AgNO₃ enzymes involved in mitochondrial ATP production, including cytochrome oxidases and subunits of ATP-synthase, were regulated (Pillai et al. 2014), which indicates an interaction between internalized Ag⁺ with energy generation. In addition, the active efflux of silver ions and other detoxifying processes can lead to an increased metabolic demand for ATP and consequently to energy depletion (Pillai et al. 2014).

In contrast to the measurements of photosynthetic yield, no recovery over time could be observed over the period of 24 h. This indicates that the cells need more time to balance the intracellular energy flow.

No Increase in EPS Production upon Exposure to Silver Nanoparticles: Previous studies report a correlation between the ability of various bacterial strains to produce extracellular polymeric substances (EPS) and their higher tolerance towards AgNP. Induction of EPS production as a feedback response to nanoparticles and its role in metal detoxification has also reported for algae (Miao et al. 2009; Pletikapic et al. 2012; Quigg et al. 2013).

In our previous study conducted with *C. reinhardtii* it was shown that the algae cells responded to the presence of cerium oxide nanoparticles by a fast release of EPS. It was hypothesized that the presence of EPS at the cell surface may be the first defense mechanism against nanoparticle toxicity as it creates a physical barrier and increases the distance between the particles and the cell surface (Tierbach 2014). However, in case of AgNP and AgNO₃ exposures no clear trend towards an increase in EPS production with increasing silver concentration could be observed. In contrast to silver nanoparticles, cerium oxide NP's formed agglomerates which adsorbed to the cell surface. It is most likely that the presence of agglomerates induced the EPS release. Moreover, it cannot be excluded, that the chemical composition of EPS changes according to the stressor. HPA binds to α -glycosidically linked N-acetylgalactosamine and N-acetylglucosamine residues (Brooks and Carter 2001). Due to possible differences in the residues composition, the EPS induced by silver could not be stained with the used technique in contrast to cerium oxide. In order to evaluate the role of EPS in nanoparticle toxicity towards *C. reinhardtii* the induced effects need to be compared between the wild type and an EPS lacking mutant. However, up to date no EPS *C. reinhardtii* mutants are available.

The Adverse Effects of Silver Nanoparticles are Induced by Free Silver Ions: The similarities in the dose-response curves obtained for AgNP and AgNO₃ indicate a similar mode of action, which might be via solubilized silver (Ivask et al. 2014b; Miao et al. 2010; Navarro et al. 2008). To take into consideration the role Ag⁺ play in the toxicity of AgNP the results obtained in the toxicity studies were normalized to dissolved Ag⁺. The resulting EC₅₀ values for AgNP were 1.8 to 2.7 times lower compared to AgNO₃. However, in presence of cysteine, a strong ligand for Ag⁺, all effects induced by AgNP on the photosynthesis and growth rate of *C. reinhardtii* were reversed. Therefore, it is possible that measurement of nanoparticle dissolution under abiotic conditions leads to underestimation of silver ions in exposure cultures. In the presence of algae, interaction of AgNP with cell surface and secreted algal substances are likely to result in additional Ag⁺ dissolution. Navarro et al. (2008) suggested that algal metabolic products, such as H₂O₂ might accelerate AgNP oxidation and increase the amount of Ag⁺ in algae cultures as compared to cell free medium. Furthermore, sorption of particles to the cell surface may induce local production of silver ions and facilitate their uptake (Leclerc and Wilkinson 2014). Ivask et al. (2014b) showed by using an *E. coli* biosensor that direct contact between AgNP and cells increases



the bioavailability of the metal, which lead to import higher concentrations of metal ions than could be estimated from particle dissolution in abiotic conditions.

Although it can be assumed that the toxicity of AgNP NM-300K is driven by Ag^+ , the dynamic processes between the cells and AgNP influences the nanoparticle dissolution and may enhance Ag^+ uptake by a local increase of silver concentration on the cell surface.

Silver Bioaccumulation of AgNP Differ from that of AgNO_3 : The bioaccumulation of silver within *C. reinhardtii* cells was investigated upon exposure to AgNP and AgNO_3 . The cells exposed to AgNP accumulated silver very quickly and the highest intracellular concentration was reached already after 0.5 h. This indicates that the steady-state equilibrium was reached very fast. The intracellular silver concentration increased with increasing AgNP in the medium. In experiments conducted with 0.5 μM AgNO_3 a twofold higher internal silver concentration was reported in *C. reinhardtii* ($1.7 \times 10^{-3} \text{ mol L}_{\text{cell}}^{-1}$, Pillai et al., 2014). At the AgNP concentration of 6.3 μM , a lower intracellular silver content was measured as compared to lower AgNP exposure concentrations. It was suggested that at high silver concentrations an increased production of ROS causes lipid peroxidation (Pillai et al. 2014). This may lead to membrane disruption and leakage of silver out of the damaged cells.

Upon exposure to AgNO_3 the intracellular silver content increased proportionally to the applied total silver concentration, confirming the data reported by Piccapietra et al. (2012). These findings indicate a linear relationship between the silver concentration in the exposure medium and within the cells. In agreement with data reported by Piccapietra et al. (2012), no increase in the intracellular concentration of cells exposed to silver for more than 30 min could be observed, suggesting that the silver uptake was rapid and the steady-state equilibrium was reached already at the earliest time point. The bioconcentration factor calculated on the basis of the bioaccumulation data was high and lay in the range of 909 to 1820 $\text{L}_{\text{cell}}^{-1}$. Comparable values can be derived from the data reported by Piccapietra et al. (2012) (803-2246 $\text{L}_{\text{cell}}^{-1}$) and Pillai et al. (2014) (~ 300 -1550 $\text{L}_{\text{cell}}^{-1}$) for AgNO_3 concentrations between 0.01 μM and 0.5 μM . The bioaccumulated silver among these studies were however different because different cell densities and media were used. Especially the cell density has a considerable influence on the intracellular silver concentration under the same exposure conditions, with a trend towards higher internal metal concentration at lower cell densities (Piccapietra et al. 2012).

In cells treated with AgNP as well as with AgNO_3 a decrease in the intracellular concentration over time could be observed. In case of AgNP, the intracellular silver concentration decreased continuously almost in all cultures after the exposure duration of 0.5 h. This can be explained with the decrease in measured Ag^+ concentration in the exposure medium over time. However, at a concentration of 6.3 μM AgNP no decrease in intracellular silver content was detectable, confirming the hypothesis that the cells were damaged.

At the two highest AgNO_3 exposure concentrations, a decrease in the intracellular metal concentration could be detected after an exposure period of 3 h. In the previous study, a decrease in the internal metal concentration was reported only after the exposure duration of 5 h. However, the bioaccumulation after 3 h was not measured (Pillai et al. 2014). Based on transcriptome studies, which showed an up-regulation of a P-type ATPase similar to CopATPase in *Enterococcus hirae* (Solioz and Odermatt 1995) it was hypothesized that efflux of Ag^+ from the algae is mediated by a Cu-efflux system. Furthermore, algae are known to release ligands, such as DOC and proteins which accumulate in the



culture medium over time. Proteins with their thiolic functional groups and DOC can bind free metal ions in solution and thus lower their bioavailability (Miao et al. 2009; Stevenson et al. 2013). The comparison between the bioaccumulation experiments showed that based on the total added silver amount, a much higher intracellular silver concentration was measured upon exposure to AgNO_3 . This confirms the observation that Ag^+ is more bioavailable than silver in form of AgNP (Piccapietra et al. 2012). However, when normalized to the dissolved free silver ion concentration AgNP show a much higher and faster silver uptake into the cells. On the one hand, this effect can originate from an incomplete removal of nanoparticles, which agglomerate to sizes above $0.45 \mu\text{m}$ in presence of algae and can be adsorbed on the filter. However, on the other hand an enhanced uptake of silver ions resulting from the sorption of particles to the cell surface and a local increase in Ag^+ concentration cannot be ruled out.

Exposures with zebrafish embryos and early life stage zebrafish

Background on the Toxicity of Metal and Metal Oxide Nanoparticles in Zebrafish

Various metal and metal oxide NPs have been tested in zebrafish (see review by (Shaw and Handy, 2011)) and their chemical composition and size play important roles for their toxicity. Silver NPs show definite toxicity in zebrafish, but few toxic effects have been observed for gold (Au) (see review by (Shaw and Handy, 2011)). More recent studies have demonstrated that a suitable coating markedly increases the bioavailability of gold-NPs, resulting in toxic effects (Harper et al., 2011). CeO_2 has not been found to be non-toxic to zebrafish embryos in several studies (Van Hoecke et al., 2009, Jemec et al., 2012, Jemec et al., 2015). The coating also influences the solubility/dispersal of e.g. Ag-NPs, and can thereby either suppress or enhance toxicity (Cunningham et al., 2013). Effects observed in zebrafish embryos exposed to nanomaterials include mortality, hatching delays and various developmental malformations [metal-NPs (Asharani et al. 2011), metal oxide-NPs (Zhu et al. 2008) and carbon-NPs (Zhu et al. 2007)]. ZnO NPs have been shown to block the hatching of zebrafish embryos from their chorion and this was due to Zn^{2+} ions inhibiting the activity of the zebrafish hatching enzyme ZHE1 (Lin et al., 2013).

Exposures of zebrafish to a series of selected NPs were conducted on embryos (KIT) and both embryos and early life stage fish (UEXE). Automated microscopy was combined with automated image analysis to facilitate quantification of phenotypes upon NP exposure (e.g. lethality, hatching, malformations) (Alshut et al., 2010, Mikut et al., 2013). In addition assays capturing swimming behaviour in early life stage zebrafish were employed captured using an automated systems (see below).

Exposures of zebrafish embryos (KIT)

Materials & Methods

Selected particles

Table 3: List of selected nanomaterials

Name	Material	Size in nm	Coating
CeO ₂ -un (PROM)	CeO ₂	20	—
CeO ₂ -un (JRC NM-212)	CeO ₂	33	—
ZnO-uncoated (JRC NM-110)	ZnO	42	—
ZnO-TECS (JRC NM-111)	ZnO	34	TECS (triethoxycaprylyl silane)
Ag (JRC NM-300K)	Ag	15	Dispersant
Ag dispersant (JRC NM-300Kdis)	—	—	—

Particle preparation: see WP4 SOP “Preparation of NP dispersions for exposure of cells” for a detailed description of particle handling and preparation. Particle dispersions were prepared shortly before exposure. Briefly, dispersed particles were diluted to 5mg/ml in ddH₂O and sonicated for 5min (water bath). Powdered nanomaterials were weighed in to 5mg/ml in ddH₂O and sonicated for 15min (water bath). Due to hydrophobicity of ZnO Nm111 both ZnO particles were prepared according to the NanoGenotox protocol (15.6mg were pre-wetted with 96% Ethanol and then dispersed in ddH₂O 0.05% BSA before sonification with a tip sonifier for 2x 1min). From there all dispersions were diluted in Holtfreter’s medium to 2x of the exposure concentration. Before each dilution step, the dispersions were mixed by pipetting or vortexing. All particles were tested at least twice for toxicity by screening experiments at 1 and 125 µg/ml in embryo medium (5 days of exposure). For those materials showing adverse effects (ZnO, Ag), additional concentrations were tested to obtain dose response curves.

Zebrafish and imaging: Zebrafish husbandry and crossing was performed as described previously (Kimmel et al., 1995, Westerfield, 1995). Adult wild-type zebrafish (strain: AB ZIRC KA; 1 female, 2 male) were allowed to spawn in facility water. High quality clutches were collected 1 hour after spawning and kept separately in petri dishes in facility water. Only clutches with a fertilization rate of > 80% were processed further. Low quality eggs or unfertilized were discarded and the embryos were washed 2x with clean facility water and 1x with Holtfreter’s medium (15 mM NaCl, 0.17 mM KCl, 0.23 mM CaCl₂, and 0.6 mM NaHCO₃, pH 7.0) thereby removing any debris. From this point embryos were kept in Holtfreter’s medium. At sphere stage 2-3 clutches high quality clutches were selected and a sufficient number of healthy embryos were pooled into a single petri dish with help of a stereomicroscope. At 30% epiboly embryos were sorted into round bottom 96 well plates, one embryo per well in a volume of 100µl medium. Completeness and embryo quality were checked by visual inspection and missing or damaged embryos were added or replaced, respectively. At 50% epiboly the particle dispersions (100µl) were added resulting in a total exposure volume of 200µl. Plates were kept in a moist chamber in an incubator at 28°C and brightfield images were acquired by automated microscopy (Olympus IX81, 1.25

or 2.5 objective) at 24hpf, 48hpf, 72hpf, 96hpf and 120hpf. The bright field images were analysed for survival, hatching and morphological defects (see Figure 13).

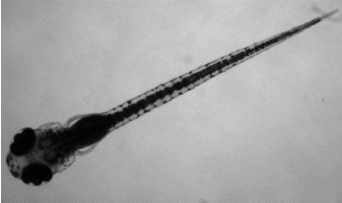
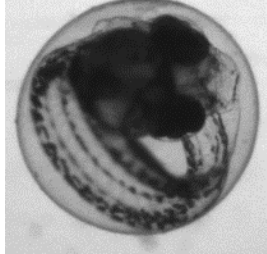
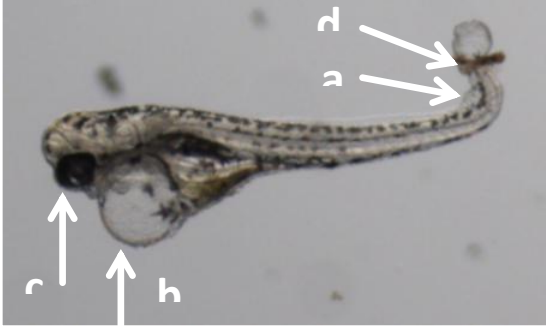
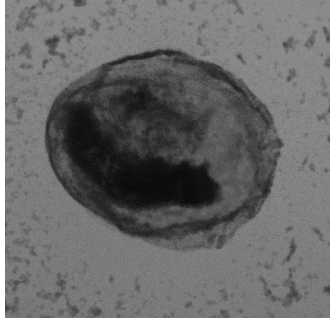
Endpoint	Example image from NP exposure	Description
Normal development		
Hatching		ZnO
Malformation		Ag Examples: a kinked tail; b cardiac edema; c disturbed head morphology; d loss of tissue integrity (lesions, hemorrhage);
Lethality		PS NH ₂

Figure 13: Toxicity endpoints for zebrafish embryos with example images.

Results and Discussion

The selected particles (Table 3) were tested for toxicity by screening experiments with zebrafish embryos at 1 and 125 $\mu\text{g}/\text{ml}$ in embryo medium (5 days of exposure). Table 4 summarizes the results obtained on zebrafish embryo toxicity by KIT for the selected NPs in the highest concentration tested. No obvious adverse effects could be observed for CeO_2 (see Figure 14) whereas ZnO and Ag particles affected development and caused a reduction in embryo survival (see Figure 15 to 20). At high concentrations particles tended to form agglomerates or aggregates in the embryo medium, which settled to the bottom of the wells (for example CeO_2 , see Figure 14) and partially associated with the chorion (especially AgNP, see Figure 17). Automated image analysis was considered but will only work for low particle concentrations as the particle agglomerates frequently obscure the view on the embryo/larvae (Figure 14 and 17). The following figures will describe the effects of the different materials in more detail.

Table 4: Summary table for toxicity on zebrafish early life stages after 5 days of exposure.

Embryos were exposed to particles in embryo medium in the highest concentration used in this study (125 $\mu\text{g}/\text{ml}$) from gastrulation stage (6hpf) onwards. The percentage of normal embryos (alive, hatched and with no obvious malformations) is indicated, based on analysis of microscopic images taken at 120hpf. Results were normalized plate-wise to the negative control (embryo medium) and then the average was calculated from three independent experiments.

Name	Normal embryos (%) 125 $\mu\text{g}/\text{ml}$, 120hpf
CeO_2 -un (PROM)	98
CeO_2 -un (JRC NM-212)	105
ZnO-uncoated (JRC NM-110)	0
ZnO-TECS (JRC NM-111)	0
Ag (JRC NM-300K)	0
Ag dispersant (JRC NM-300Kdis)	106

CeO_2 particles showed no toxicity: The tested CeO_2 particles NM-212 and PROM, had a strong tendency for agglomeration in the higher concentrations and the agglomerates quickly settled on the bottom of the wells where they got in contact with the chorion and the larvae after hatching (Figure 14). The development was undisturbed even at the highest concentration tested 125 $\mu\text{g}/\text{ml}$ with normal hatching, no obvious malformations and no increase in mortality. Thus no adverse effects could be observed for CeO_2 particles in our experimental setup.

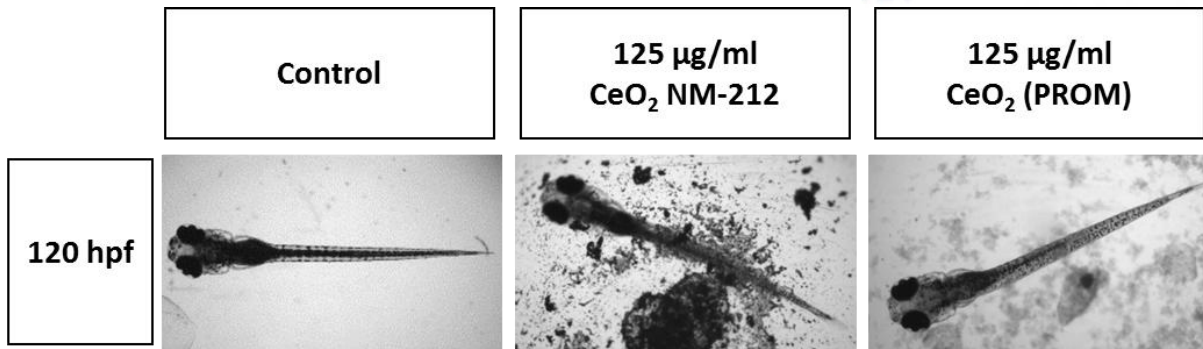


Figure 14: Microscopic images of zebrafish embryos treated with cerium oxide particles (CeO₂ NM-212, CeO₂ PROM) for 5 days. Exposure to cerium oxide particles caused no obvious adverse effects at 125 µg/ml; note the particle agglomerates in the wells surrounding the larvae. Magnification is the same across the panel.

ZnO particles inhibited hatching and reduced larval survival: Both ZnO particles (NM110 and NM111) showed agglomeration in the high concentration and the agglomerates quickly settled on the bottom of the wells where they got in contact with the chorion (Figure 15). Although the embryonic development appeared normal during the first 4 days of exposure, we frequently observed the formation of a whitish precipitate within the chorion fluid together with an increase in mortality at the highest concentration at 120hpf. Unhatched embryos were also observed at 1 µg/ml but with normal morphology and viability. As the ZnO particles showed inhibition of embryo hatching already at 1 µg/ml, additional concentrations were tested to obtain dose response curves (see Figure 16).

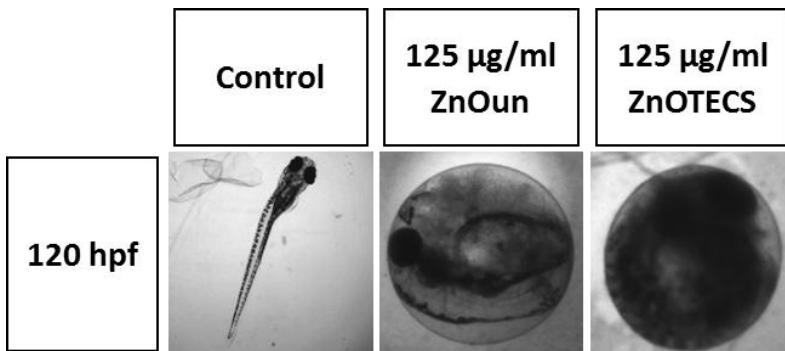


Figure 15: Microscopic images of zebrafish embryos treated with zinc oxide particles (ZnO NM-110, ZnO TECS NM-111) for 5 days. Exposure to both ZnO particles caused complete inhibition of hatching, high mortality and whitish precipitates within the chorion fluid at 125 µg/ml. Note that magnification is lower for the control embryo.

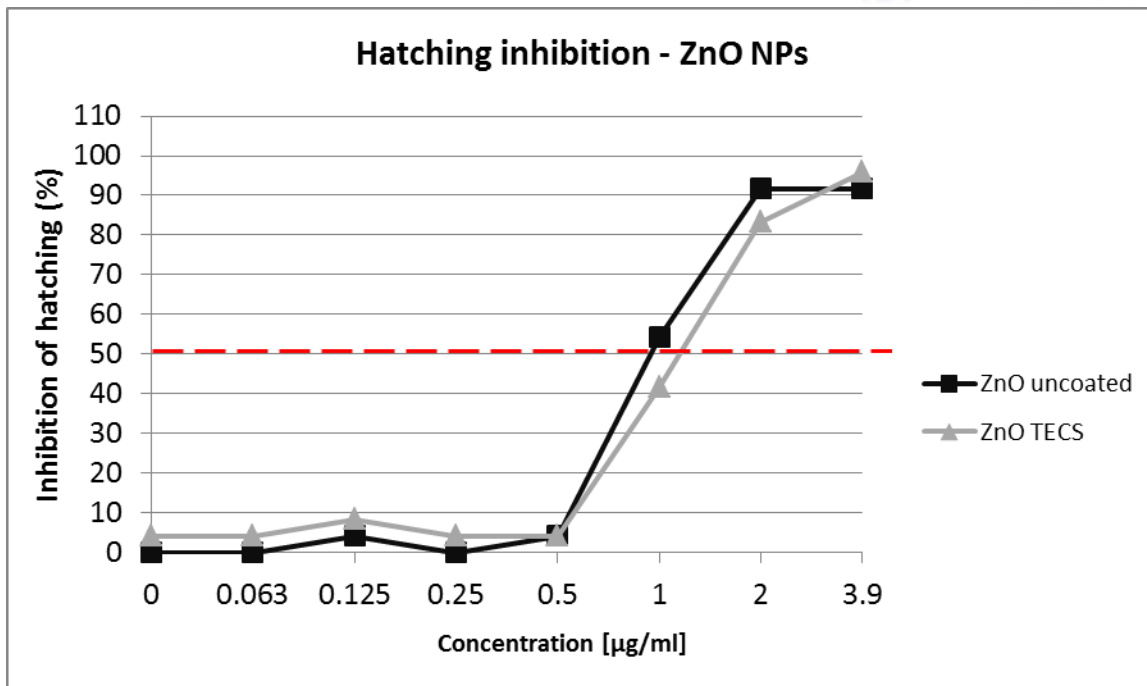


Figure 16: Dose response curves for hatching inhibition at 120hpf of zebrafish embryos treated with zinc oxide particles (ZnO uncoated NM-110, ZnO TECS NM-111). Embryos were exposed to ZnO particles (uncoated NM110 and TECSNM111) in embryo medium in a dilution series ranging from 0.063 to 3.9 µg/ml from gastrulation stage (6hpf) onwards. The percentage of non-hatched embryos is indicated based on analysis of microscopic images taken at 120hpf. The average was calculated from two independent experiments. The EC₅₀ value that can be deduced from the curves is approximately 0.75 for NM110 and 1.0 µg/ml and 1 for NM111.

Silver particles disturbed development and reduced embryo survival: The 20nm Ag 300K NPs showed strong negative effects on hatching rate (Figure 18), morphogenesis (Figure 19) and survival of the zebrafish embryos (Figure 20). The reduced hatching with increasing nanoparticle concentrations could be a consequence of disturbed development or death of the embryos (Figure 17). No adverse effects were observed for the Ag dispersant (JRC NM-300Kdis) when used in the same concentration as in the particle preparation.

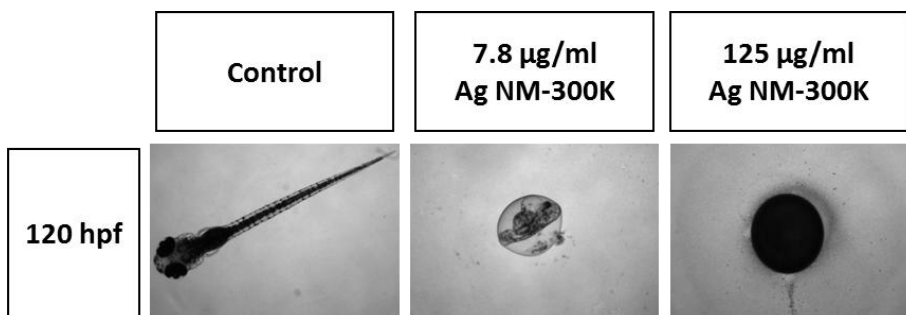


Figure 17: Microscopic images of zebrafish embryos treated with silver particles (Ag NM-300K) for 5 days. Exposure to silver particles caused partial inhibition of hatching, high mortality and malformation rate at 7.8 µg/ml and 100% mortality at 125 µg/ml; note the dark particle agglomerates on the chorion surface at the high concentration. Magnification was the same across the panel.

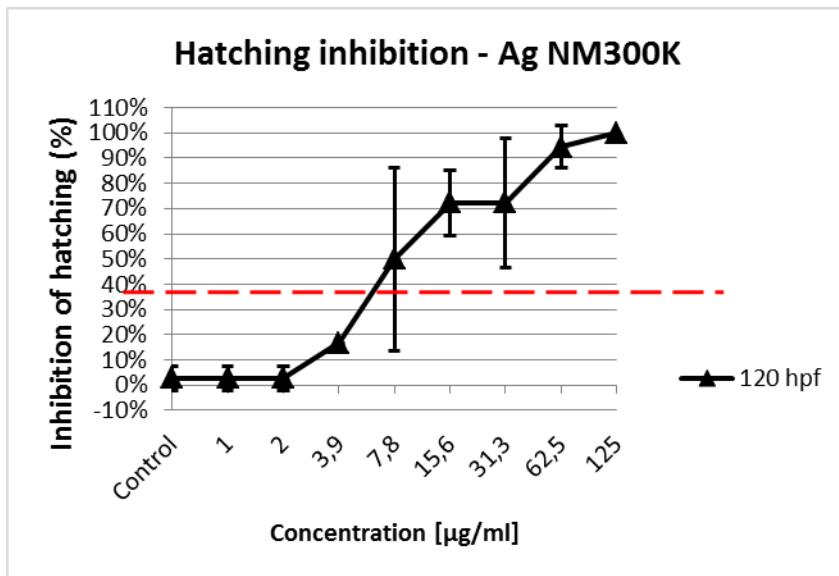


Figure 18: Dose response curves for hatching inhibition at 120hpf of zebrafish embryos treated with silver particles. Embryos were exposed to Ag NM300K particles in embryo medium in a dilution series ranging from 1 to 125 µg/ml from gastrulation stage (6hpf) onwards. The percentage of non-hatched embryos is indicated based on analysis of microscopic images taken at 120hpf. The average was calculated from three independent experiments except that for the concentration 3.9 µg/ml and 125 µg/ml where only one or two experiments were available. The EC₅₀ value (dashed red line) that can be deduced from the curve is approximately 7.8 µg/ml.

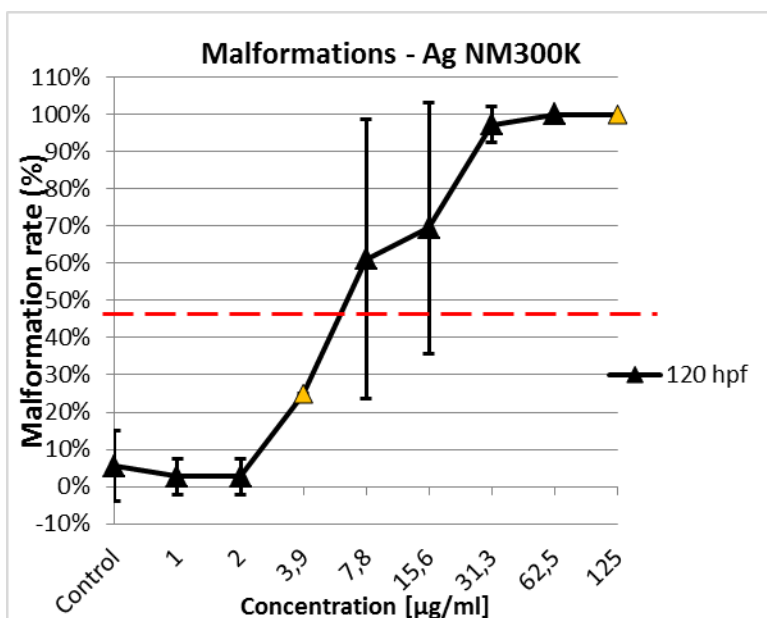


Figure 19: Dose response curve for zebrafish embryo malformation at 120hpf after treatment with silver particles. Embryos were exposed to Ag NM300K in embryo medium in a dilution series ranging from 1 to 125 µg/ml from gastrulation stage (6hpf) onwards. The percentage of malformed embryos is indicated based on analysis of microscopic images taken at 120hpf. The average was calculated from three independent experiments except that for the concentration 3.9 µg/ml and 125 µg/ml where only one or two experiments were available. The EC₅₀ value (dashed red line) that can be deduced from the curve is approximately 7 µg/ml.

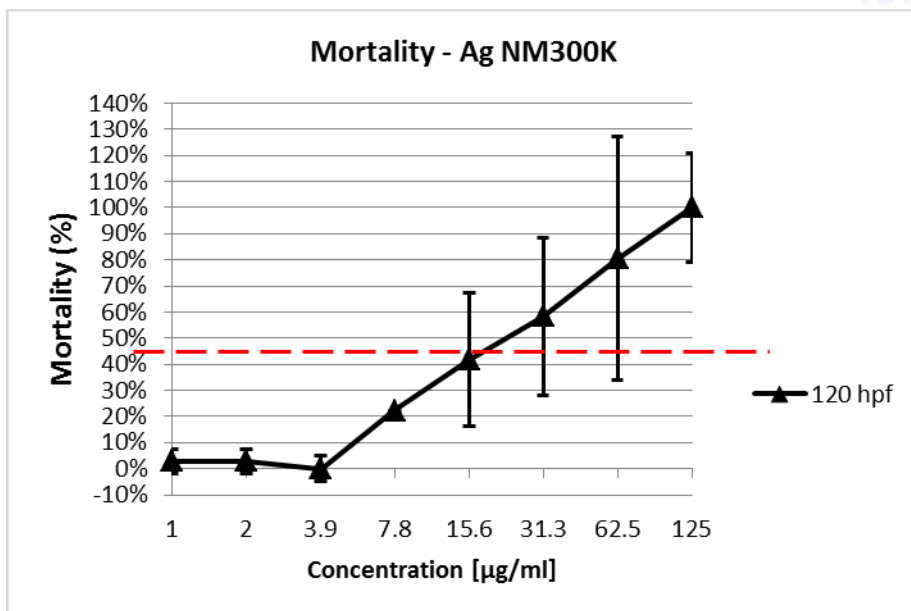


Figure 20: Dose response curve for zebrafish embryo mortality at 120hpf after treatment with silver particles. Embryos were exposed to Ag NM300K in embryo medium in a dilution series ranging from 1 to 125 µg/ml from gastrulation stage (6hpf) onwards. The percentage of dead embryos is indicated based on analysis of microscopic images taken at 120hpf. The average was calculated from three independent experiments except that for the concentration 3.9 µg/ml and 125 µg/ml where only one or two experiments were available. The EC₅₀ value (dashed red line) that can be deduced from the curve is approximately 22 µg/ml.

In summary, for this work on zebrafish, we successfully used nanoparticle exposure and high-content - imaging in a 96 well plate format to obtain quantitative data on several endpoints for zebrafish embryo toxicity. Dose response curves were generated and NOAELs, LOAELs, and EC₅₀ values were deduced for the different endpoints, which are summarized in Table 5. The established exposure conditions and readouts can be applied to other nanomaterials.

Table 5: LOAEL (lowest observed adverse effect level), NOAEL (no observed adverse effect level) and EC₅₀ values for the tested nanomaterials. The concentrations are given in µg/ml. NA - There was no toxicity or the value could not be determined with the tested concentration range.

Name	LOAEL	NOAEL	EC ₅₀ - Hatching inhibition	EC ₅₀ - Malformation	EC ₅₀ - Mortality
CeO ₂ -un (PROM)	NA	NA	NA	NA	NA
CeO ₂ -un (JRC NM-212)	NA	NA	NA	NA	NA
ZnO-uncoated (JRC NM-110)	1	0.5	0.75	NA	NA
ZnO-TECS (JRC NM-111)	1	0.5	1	NA	NA
Ag (JRC NM-300K)	3.9	2	7.8	7	22
Ag dispersant (JRC NM-300Kdis)	NA	NA	NA	NA	NA

Exposures of zebrafish early life stages and embryos (UEXE)

As detailed above zebrafish embryos have a protective outer coating for protection (the chorion), which may reduce and event prevent uptake of nanomaterials from the exposure medium. Early larval stage zebrafish may offer an alternative/additional sensitive life stage for assessing the effects of exposure to nanomaterials. In this part of this work package we investigated the use of sublethal endpoints, specifically features of behaviour (in fish at 5 days post fertilisation) to analyse for effects of the selected nanomaterials. The basis of the behaviour assay is a modified and updated version of the assay published in Winter et al. (2008) and is briefly outlined in the below materials and methods sections. In conjunction with the behavioural assessment we also ran some exposures to zebrafish embryos assessing for morphological aberrations (at 0-48 hpf) for comparison. Exposures were conducted for NP concentrations in the parts per billion (ppb) range.

Materials & Methods

Selected particles

Table 6: Tested Nanomaterials

NanoMILE code	NP type	Size (nm)	Origin
	ZnCl ₂		sigma
NP00282	ZnO Uncoated Hydrophilic (NM-110)	150.0	JRC
NP00214	Silver (NM-300K)	15.0	JRC
NP00221	Ag-citrate coated	7.0	UoB
	Ag-citrate coated	>500	UoB
	Ag-PVP coated	10	UoB
	AgNO ₃		Sigma
	Cerium (IV) Oxide (precipitated, uncoated) NM-211	10.3	JRC
	Cerium (IV) Oxide (precipitated, uncoated) NM-213	> 500	JRC

Experimental approaches - Exposure studies:

Particle preparation: Please see 'WP6 Standard Operation Procedure. Preparation of NP dispersions for exposure to aquatic organisms', for a detailed description of particle handling and preparation. Particle dispersions were prepared freshly shortly before exposure.

Behavioural assay: Adult wild-type zebrafish (strain: WIK) were allowed to spawn in aquarium water. Batches were collected immediately after spawning and transferred to petri dishes where they were washed and kept in 1:5 OECD zebrafish culture media (please refer to WP6 aquatic organism culture media for detailed chemistry). Embryos were checked and cleaned each day, with unfertilised eggs removed at 4 hpf and abnormal or dead embryos removed at 24 hpf. At 5 days post fertilisation, approximately 24 hours prior to assay, the petri dishes of animals to be used in the assay were cleared of debris. The water in the petri dishes must be devoid of as much debris as possible as some particles can be picked up by the videotracking system leading to erroneous data generation.

5 dpf old larvae from a cleaned Petri dish were transferred into the wells of 24 well multiwell plate, in a total of 600 µl of culture water (one larva per well). The standard microplate for use in this assay is a

Corning Costar 24 well plate (Corning NY, 3524, 24 well cell culture cluster, tissue culture treated and sterile), which is prepared by leaching overnight in dechlorinated water to lower the levels of any impurities/plasticizers and then dried before use. To ensure no damage is done to the larvae, the tip of the pipette is removed to allow free passage of larva and water. Typically, 4 x 24 well plates were used for each compound tested. The use of 4 plates allows for an n =12 animals for each of 6 test NP exposure concentrations, a positive control (typically 5 mM pentylenetetrazole (PTZ)) and a negative control (embryo media or solvent control, as appropriate). PTZ is a common convulsant agent which induces a stereotyped and concentration-dependent sequence of behavioural changes culminating in involuntary, rhythmic, muscular contractions and relaxations. It has been shown to chemically-induced seizures in zebrafish generating behavioural and molecular changes that are comparative to equivalent rodent models (Baraban et al., 2005). The methodology and validation for a larval zebrafish convulsant assay, has previously been published (Winter et al., 2008) and the protocol outlined in this methods section is a modified version of the updated assay. Figure 21 depicts a visualisation from typical a dose response assay of PTZ. Placing larvae into microplates the day before assay allows the animal to acclimatise to the test vessels and reduces the amount of fouling of the water (animals are not fed after transfer to the plates), which can be detrimental to the success of the videotracking process.

The test nanomaterial is then suspended in culture water and serial diluted to the appropriate test concentrations, NPs are dosed in the 4x 24 well plates in the manner depicted in Figure 22, via an 80% media change. The positive control is not dosed at this time. The animals are then held under the same culture conditions for 24 hours, food is withheld and the culture water not changed.

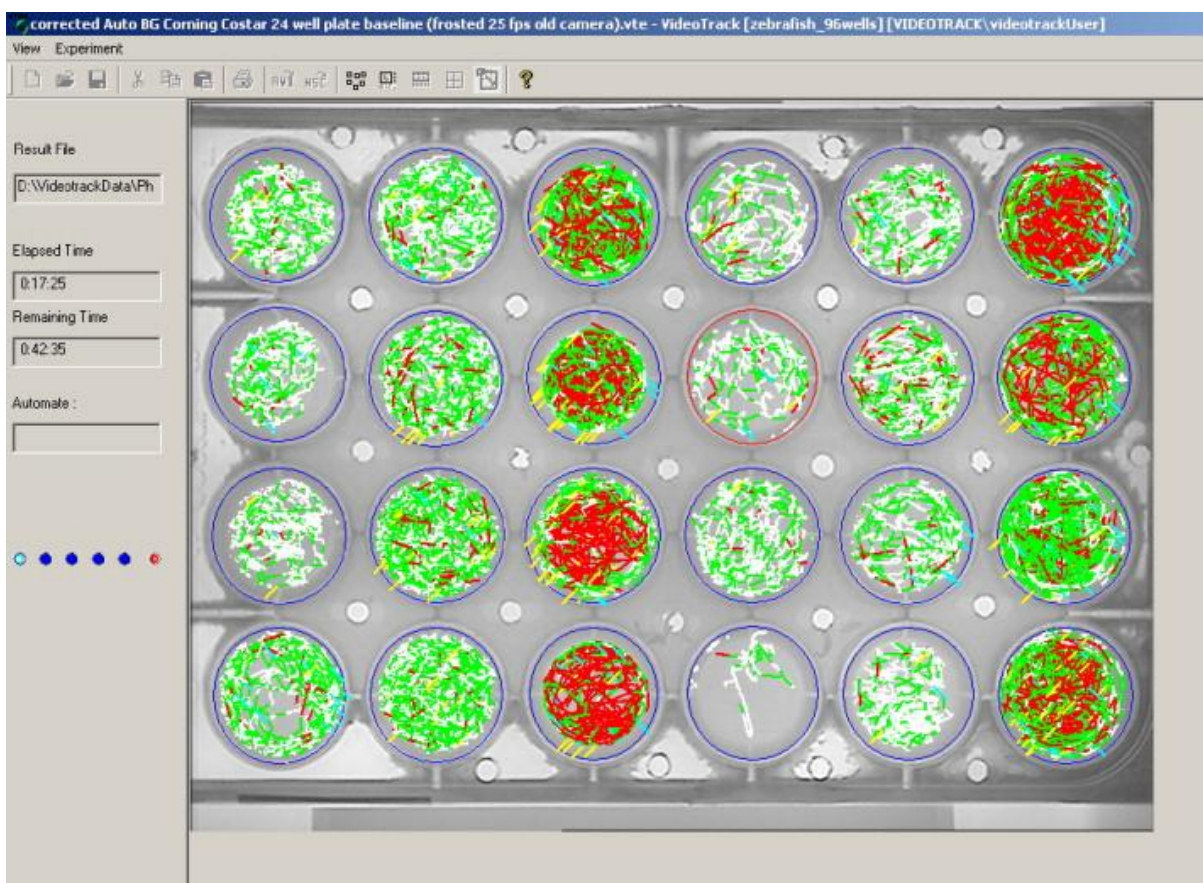




Figure 21. Screen shot from the Viewpoint Videotrack for Zebrafish™ system. A 24 well plate is shown, with the tracking from one 7 dpf larva per well, after 17 min of exposure to PTZ (from left to right, each column shows 4 replicates of PTZ exposed animals at concentrations of 0.625, 1.25, 2.5, 0, 0.3125 and 5 mM). White tracking lines signify low speed movements (< 5 mm/s), light grey (green) lines are medium speed movements (5–20 mm/s) and dark grey (red) lines are high speed movements (> 20 mm/s), according to the thresholds set in the user interface. Images were captured using a 25 frames per second infrared detecting camera. Note the much greater levels of activity at higher concentrations of PTZ, especially in the high speed movement category (> 20 mm/s). Reproduced from Winter et al (2008).

On day 6 (pf), the Viewpoint videotracking system was switched on at least 1-2 hours prior to commencing an experiment, to allow the system to warm up. The Viewpoint zebrafish videotracking system consists of a Controller PC with movement quantification software, and 1 or more attached ZebraBoxes, which contain a chamber with optimal lighting and a high speed video camera for recording activity. The testing was consistent with regards to when the assay is run, as it is possible that the animals will show different locomotory activity at other times.

Prior to assay, all animals in the microplates were checked for mortalities and 5 minutes before the assay commenced, the positive control (5 mM PTZ) is dosed in the same manner as the NPs. Following this check and dosing, each plate was placed on the appropriately numbered Viewpoint ZebraBox (e.g. 1-4) and baseline assessment of locomotor activity is undertaken.

PLATE 1

	1	2	3	4	5	6
A	5th Conc.	DWC/SC	3rd Conc.	2nd Conc.	4th Conc.	Top Conc.
B	5th Conc.	DWC/SC	3rd Conc.	2nd Conc.	4th Conc.	Top Conc.
C	5th Conc.	DWC/SC	3rd Conc.	2nd Conc.	4th Conc.	Top Conc.
D	5th Conc.	DWC/SC	3rd Conc.	2nd Conc.	4th Conc.	Top Conc.

PLATE 2

	1	2	3	4	5	6
A	6th Conc.	PTZ	Top Conc.	5th Conc.	DWC/SC	3rd Conc.
B	6th Conc.	PTZ	Top Conc.	5th Conc.	DWC/SC	3rd Conc.
C	6th Conc.	PTZ	Top Conc.	5th Conc.	DWC/SC	3rd Conc.
D	6th Conc.	PTZ	Top Conc.	5th Conc.	DWC/SC	3rd Conc.

PLATE 3

	1	2	3	4	5	6
A	6th Conc.	2nd Conc.	PTZ	4th Conc.	DWC/SC	3rd Conc.
B	6th Conc.	2nd Conc.	PTZ	4th Conc.	DWC/SC	3rd Conc.
C	6th Conc.	2nd Conc.	PTZ	4th Conc.	DWC/SC	3rd Conc.
D	6th Conc.	2nd Conc.	PTZ	4th Conc.	DWC/SC	3rd Conc.

PLATE 4

	1	2	3	4	5	6
A	6th Conc.	2nd Conc.	4th Conc.	PTZ	5th Conc.	Top Conc.
B	6th Conc.	2nd Conc.	4th Conc.	PTZ	5th Conc.	Top Conc.
C	6th Conc.	2nd Conc.	4th Conc.	PTZ	5th Conc.	Top Conc.
D	6th Conc.	2nd Conc.	4th Conc.	PTZ	5th Conc.	Top Conc.

Figure 22. Standard plate layout for treatments initially randomised by column, for the seizure liability assay. Concentrations run from top, 2, 3, 4, 5, 6 (lowest) to the dilution water or solvent control (DWC/SC). PTZ is the pentylenetetrazole positive control.



Once all plates were loaded onto the Videotracking system and tracking had commenced, visual checks were undertaken regularly and carefully to ensure that for each well the animal was being tracked correctly (e.g. not particles or well edges are being consistently detected instead of the animal).

48 hour developmental assay: Ag NPs were also screened using a 48 hour developmental assay. Endpoints measured included (scored for at 24 and 48 hours):

- Body Shape Subtle Variant
- Body Shape Malformed
- Somites Subtle Variant
- Somites Malformed
- Notochord Subtle Variant
- Notochord Malformed
- Tail Subtle Variant
- Tail Malformed Fins Subtle Variant
- Fins Malformed
- Heart Subtle Variant
- Heart Malformed
- Face Subtle Variant
- Face Malformed
- Neural Tube Subtle Variant
- Neural Tube Malformed Arches/Jaws Subtle Variant
- Arches/Jaws Malformed
- Poor Pigmentation
- Excess Pigmentation
- Abnormal Pigmentation
- Stomach, Not Evident
- Liver -Not Evident
- Liver –Enlarged
- Abdomen distended or yolk sac oedema

Not all parameters are measurable at 24 and 48 hours but are screened for as a precaution. The exposure protocol for the 48 hour assessment replicated the concentrations of the behavioural assay. For all exposures, there were >24 embryos (at the 1–2 cell stage, 1–1.5 hpf) per treatment well. The embryos were incubated at 28 ± 1 °C up to 48 h. After 2 h in culture, the numbers of unfertilised embryos were recorded and these were removed, if the fertilisation success was less than 80% the batch was discarded. At 24 and 48 hpf survival rates and any phenotypic deformities were recorded. Any physical deformities observed were recorded and converted to percentages for each treatment. Embryos were observed and photographed using Nikon SMZ1500 microscope equipped with a digital camera.

Data analysis: Behavioural response data are generated and run through numerous data sorting stages and macros before undergoing an automated probability tree of the likelihood of a positive 'seizure' endpoint (specific arresting behaviour phenotype indicative of an adverse effect) for the test compound, in this case NPs. The information obtained from the statistical analyses which takes into account all of the locomotory end points, and also that from the resultant summary graphs and positive

control data, facilitates the zebrafish “seizure assay” to be used to compute the probability of NP effect on behaviour.

Results

Behavioural assay

Table 7 shows the behavioural responses of zebrafish exposed to NPs at 6 dpf

Table 7. Summary of behavioural assay output.

Nanomaterial	Probability of seizure	p=
Ag NM300k	0.2408	0.988021
Ag PVP	0.011	0.8611
Ag Citrate	0.9652	1
Ag Citrate Bulk	0.4082	1
AgNO ₃	0.9652	1.0
Ce NM 211	0.011	0.1670
Ce NM 213 (Bulk)	0.011	1
ZnO NM 110	0.011	0.000279
ZnCl ₂	0.9652	0.911527

Figures 23-30 give example graphical outputs for behavioural activity from the seizure assay, showing concentration response curves during each time interval, across the 1 hour recording period, for ZnCl₂ (ionic control). Graphs for all tested materials can be found in the appendix (Figures S1-S7).

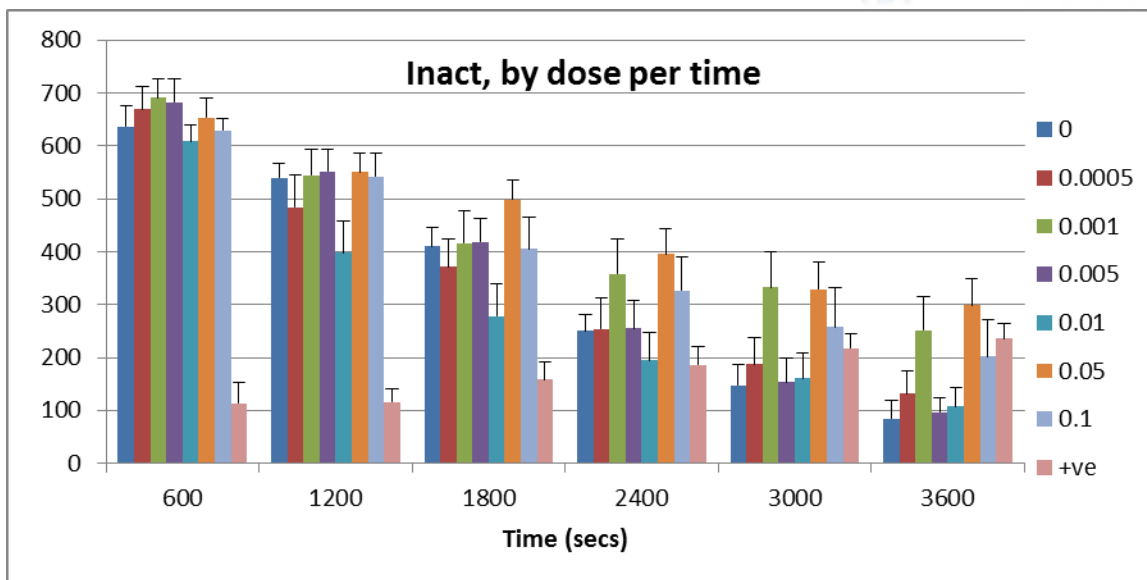


Figure 23. Measurement of inactivity of n=12 zebrafish over 1 hour for various concentrations of ZnCl₂. 0 = negative control, +ve = PTZ positive control, 0.0005 represents 5 μg L⁻¹ with the concentration increasing 10 μg L⁻¹ (0.001), 50 μg L⁻¹ (0.005), 100 μg L⁻¹ (0.01), 500 μg L⁻¹ (0.05) up to 1000 μg L⁻¹ (0.1)

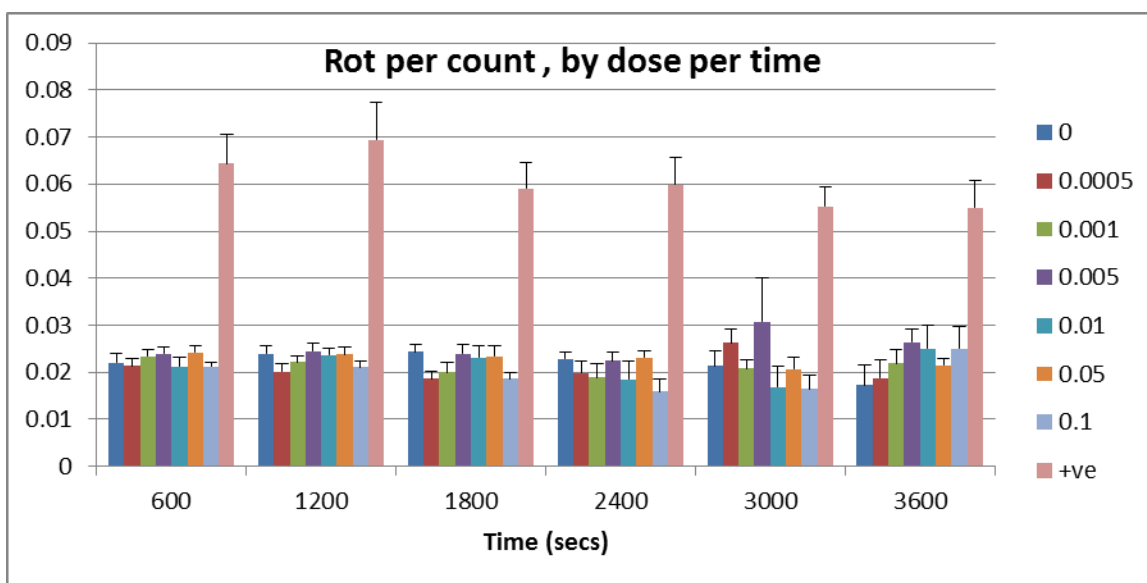


Figure 24. Count of rotations for each ZnCl₂ treatment over the 1 hour assay. 0 = negative control, +ve = PTZ positive control, 0.0005 represents 5 μg L⁻¹ with the concentration increasing 10 μg L⁻¹ (0.001), 50 μg L⁻¹ (0.005), 100 μg L⁻¹ (0.01), 500 μg L⁻¹ (0.05) up to 1000 μg L⁻¹ (0.1)

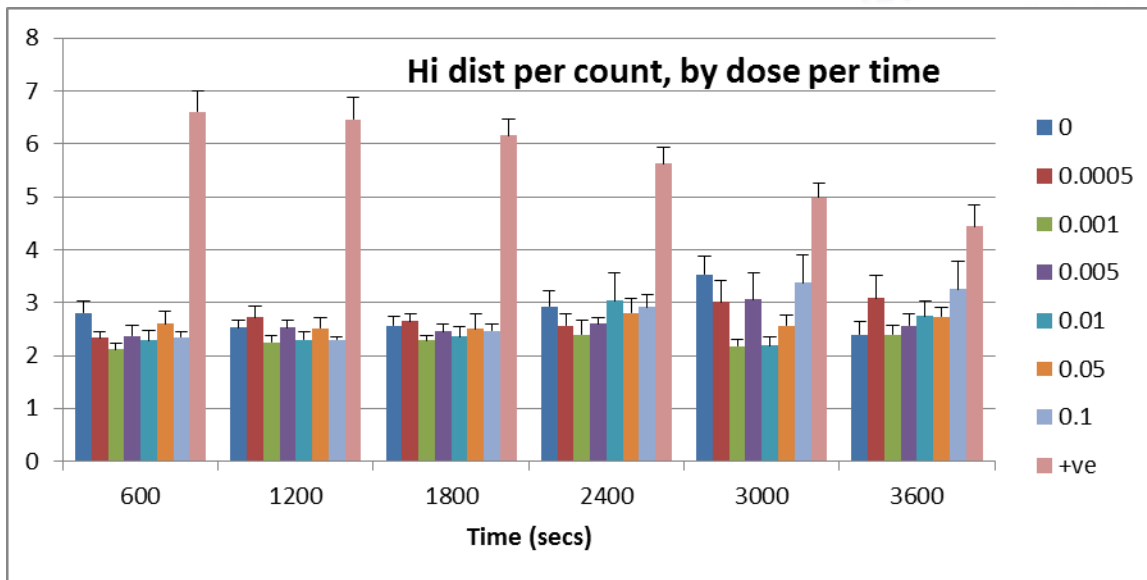


Figure 25. Counts of zebrafish movement distances measured as ‘high’ by the tracking software at time points in the assay for ZnCl₂. 0 = negative control, +ve = PTZ positive control, 0.0005 represents 5 µg L⁻¹ with the concentration increasing 10 µg L⁻¹ (0.001), 50 µg L⁻¹ (0.005), 100 µg L⁻¹ (0.01), 500 µg L⁻¹ (0.05) up to 1000 µg L⁻¹ (0.1)

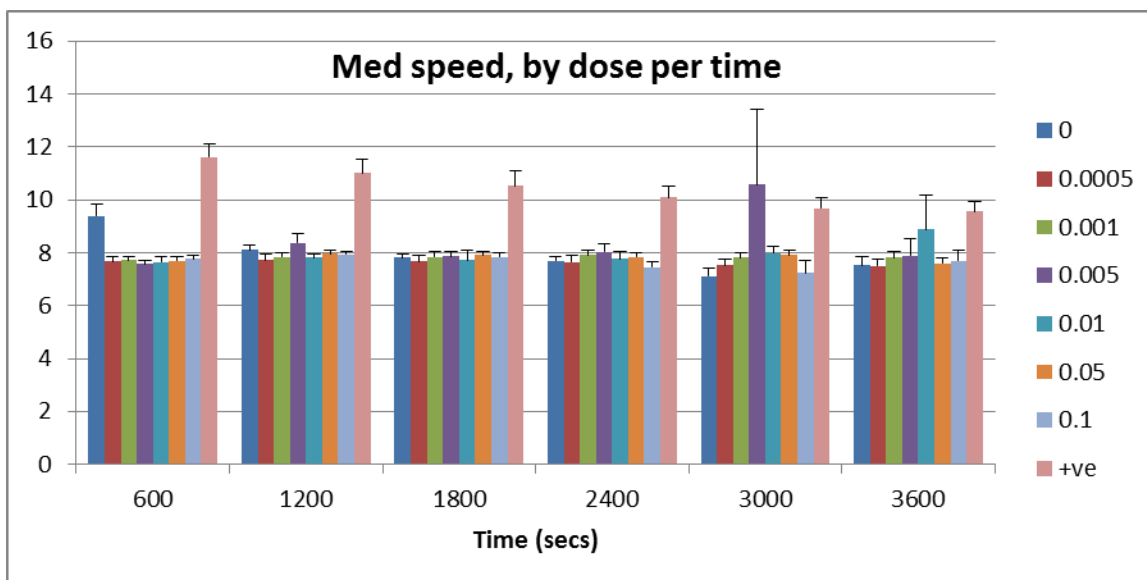


Figure 26. Time spent at a ‘medium speed’ as categorised by the tracking software for the ZnCl₂ treatment. 0 = negative control, +ve = PTZ positive control, 0.0005 represents 5 µg L⁻¹ with the concentration increasing 10 µg L⁻¹ (0.001), 50 µg L⁻¹ (0.005), 100 µg L⁻¹ (0.01), 500 µg L⁻¹ (0.05) up to 1000 µg L⁻¹ (0.1)

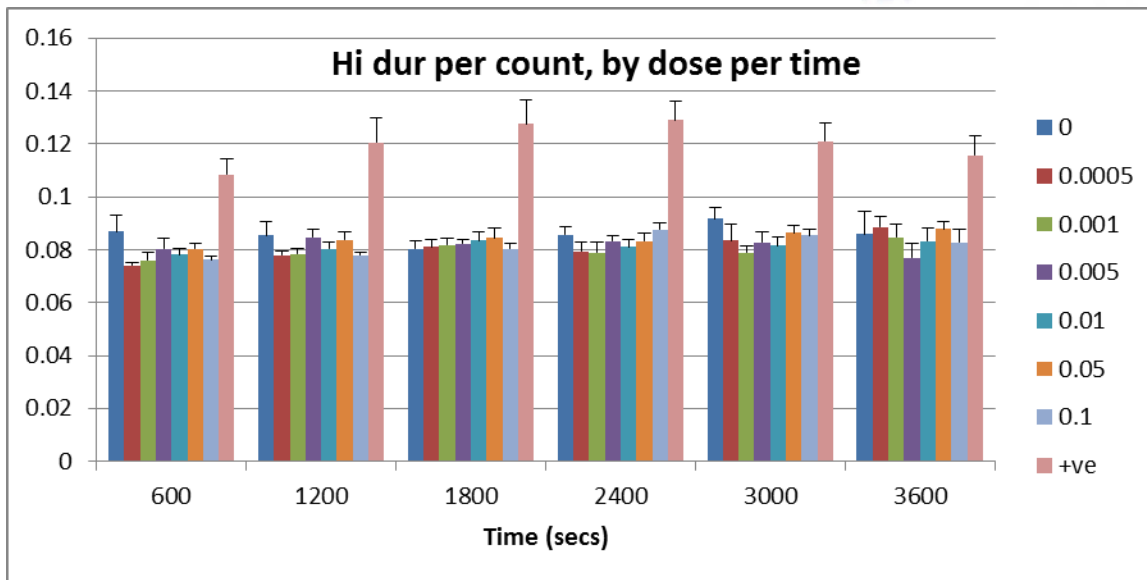


Figure 27. Counts of ‘high duration activities’ as categorised by the video tracking software at set time points for the $ZnCl_2$ treatment. 0 = negative control, +ve = PTZ positive control, 0.0005 represents $5 \mu g L^{-1}$ with the concentration increasing $10 \mu g L^{-1}$ (0.001), $50 \mu g L^{-1}$ (0.005), $100 \mu g L^{-1}$ (0.01), $500 \mu g L^{-1}$ (0.05) up to $1000 \mu g L^{-1}$ (0.1)

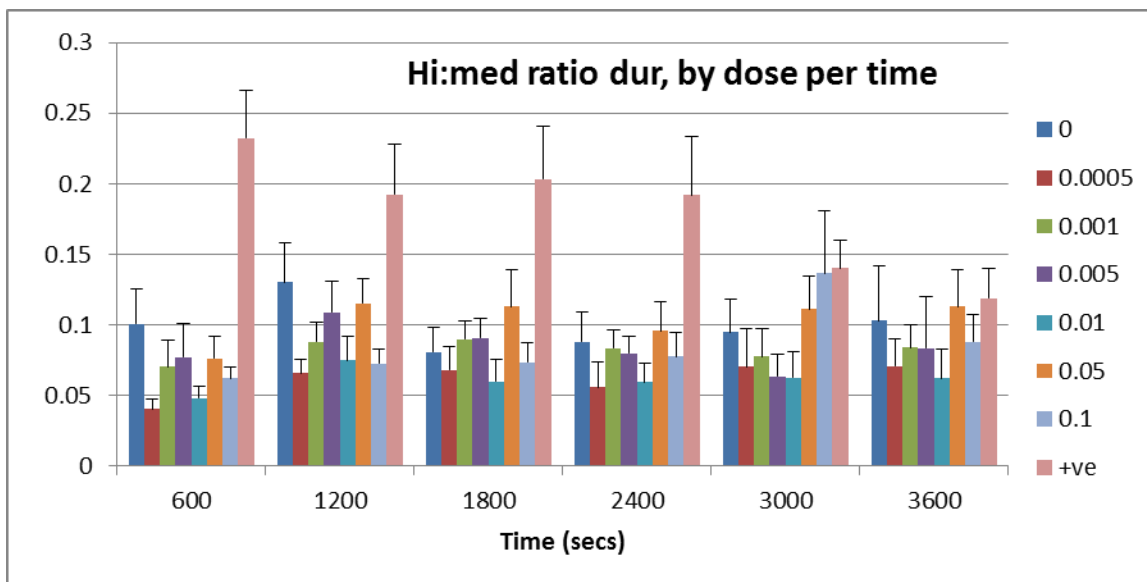


Figure 28. Ratio of high to medium activity durations as categorised by the video tracking software at set time points for the $ZnCl_2$ treatment. 0 = negative control, +ve = PTZ positive control, 0.0005 represents $5 \mu g L^{-1}$ with the concentration increasing $10 \mu g L^{-1}$ (0.001), $50 \mu g L^{-1}$ (0.005), $100 \mu g L^{-1}$ (0.01), $500 \mu g L^{-1}$ (0.05) up to $1000 \mu g L^{-1}$ (0.1)

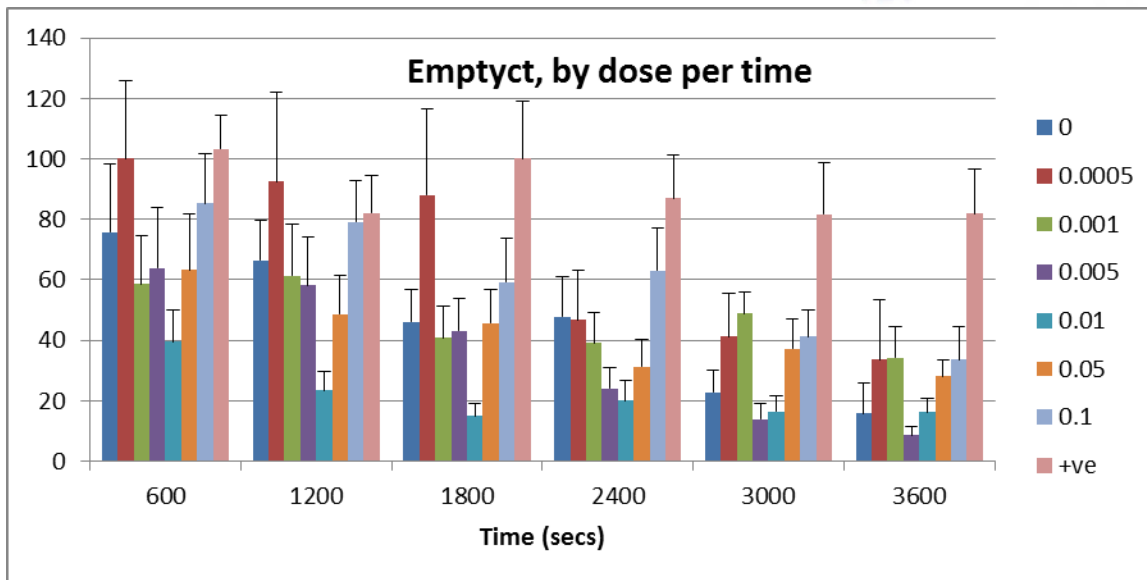


Figure 29. Number of times during which no object/animal is detected in the screening location by the video capture program software at set time points for the ZnCl₂ treatment. 0 = negative control, +ve = PTZ positive control, 0.0005 represents 5 µg L⁻¹ with the concentration increasing 10 µg L⁻¹ (0.001), 50 µg L⁻¹ (0.005), 100 µg L⁻¹ (0.01), 500 µg L⁻¹ (0.05) up to 1000 µg L⁻¹ (0.1)

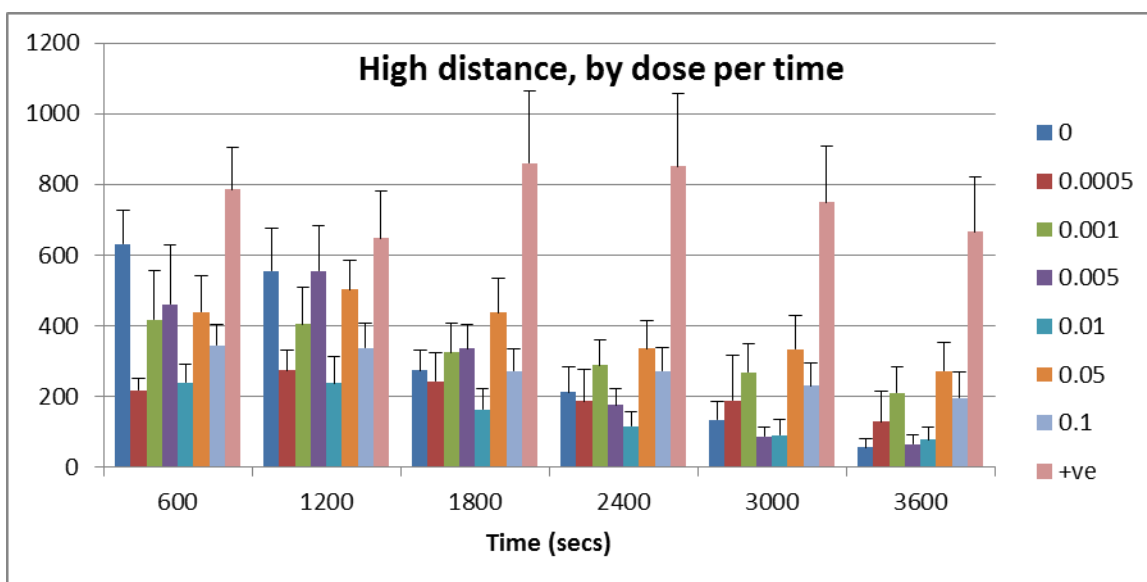


Figure 30. 'High distance' events as categorised by the video tracking software at set time points for the ZnCl₂ treatment. 0 = negative control, +ve = PTZ positive control, 0.0005 represents 5 µg L⁻¹ with the concentration increasing 10 µg L⁻¹ (0.001), 50 µg L⁻¹ (0.005), 100 µg L⁻¹ (0.01), 500 µg L⁻¹ (0.05) up to 1000 µg L⁻¹ (0.1)

Figures 31-38 give an example graphical output showing concentration response curves averaged across all time points by animal for AgNM300k NPs

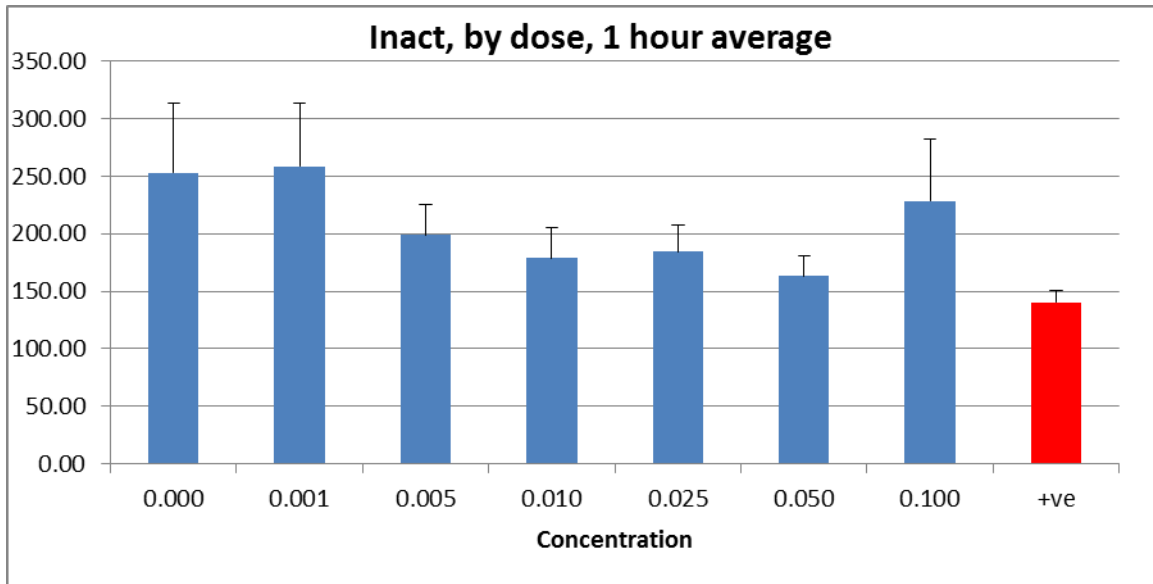


Figure 31. Average inactivity of n=12 zebrafish over 1 hour for increasing concentrations of Ag NM 300k. 0 = negative control, +ve = PTZ positive control, 0.001 represents $10 \mu\text{g L}^{-1}$ with the concentration increasing $50 \mu\text{g L}^{-1}$ (0.005), $100 \mu\text{g L}^{-1}$ (0.01), $250 \mu\text{g L}^{-1}$ (0.025), $500 \mu\text{g L}^{-1}$ (0.05) up to $1000 \mu\text{g L}^{-1}$ (0.1)

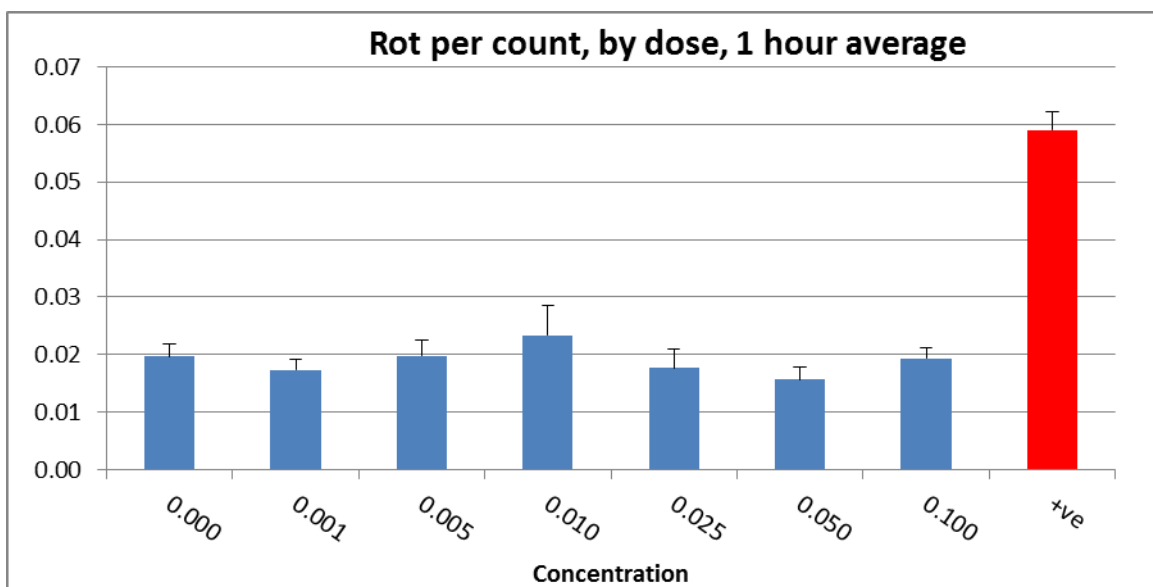


Figure 32. Average counts of 'rotation events' as categorised by the video tracking software of n=12 zebrafish over 1 hour for increasing concentrations of Ag NM 300k. 0 = negative control, +ve = PTZ positive control, 0.001 represents $10 \mu\text{g L}^{-1}$ with the concentration increasing $50 \mu\text{g L}^{-1}$ (0.005), $100 \mu\text{g L}^{-1}$ (0.01), $250 \mu\text{g L}^{-1}$ (0.025), $500 \mu\text{g L}^{-1}$ (0.05) up to $1000 \mu\text{g L}^{-1}$ (0.1)

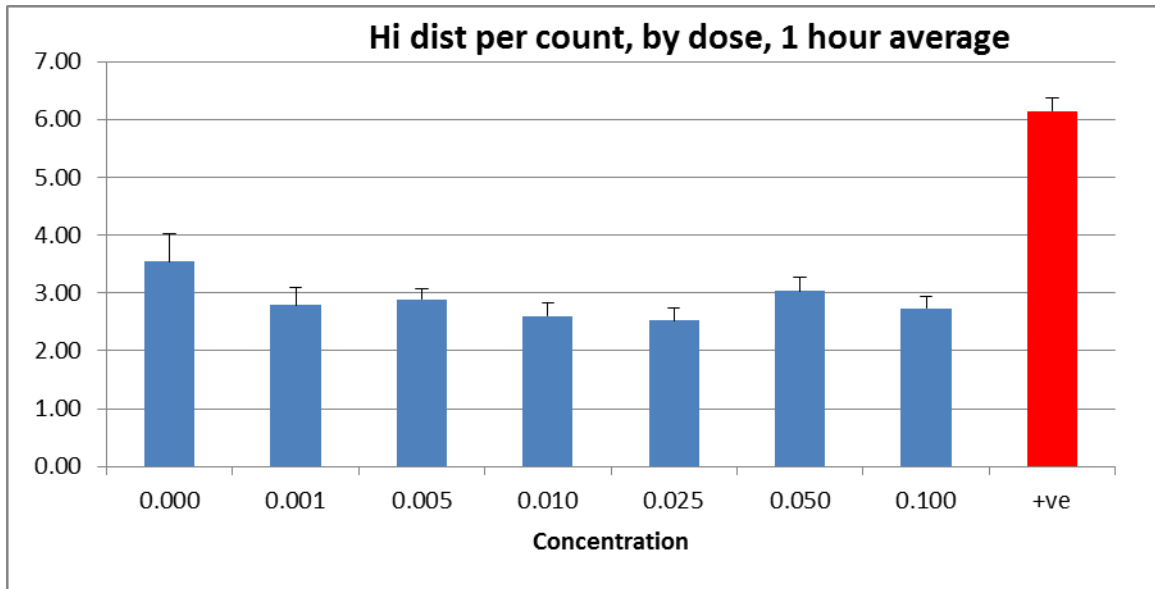


Figure 33. Average counts of zebrafish movement distances categorised as ‘high’ by the tracking software of n=12 zebrafish over 1 hour for increasing concentrations of Ag NM 300k 0 = negative control, +ve = PTZ positive control, 0.001 represents $10 \mu\text{g L}^{-1}$ with the concentration increasing $50 \mu\text{g L}^{-1}$ (0.005), $100 \mu\text{g L}^{-1}$ (0.01), $250 \mu\text{g L}^{-1}$ (0.025), $500 \mu\text{g L}^{-1}$ (0.05) up to $1000 \mu\text{g L}^{-1}$ (0.1)

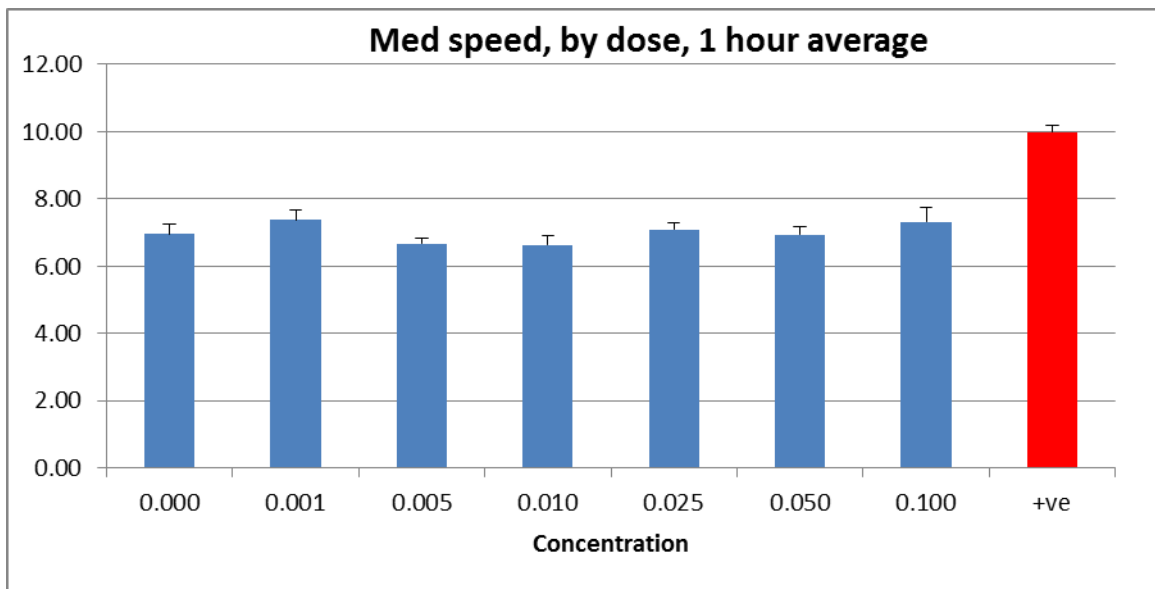


Figure 34. Average counts of zebrafish movement speeds categorised as ‘medium’ by the tracking software of n=12 zebrafish over 1 hour for increasing concentrations of Ag NM 300k 0 = negative control, +ve = PTZ positive control, 0.001 represents $10 \mu\text{g L}^{-1}$ with the concentration increasing $50 \mu\text{g L}^{-1}$ (0.005), $100 \mu\text{g L}^{-1}$ (0.01), $250 \mu\text{g L}^{-1}$ (0.025), $500 \mu\text{g L}^{-1}$ (0.05) up to $1000 \mu\text{g L}^{-1}$ (0.1)

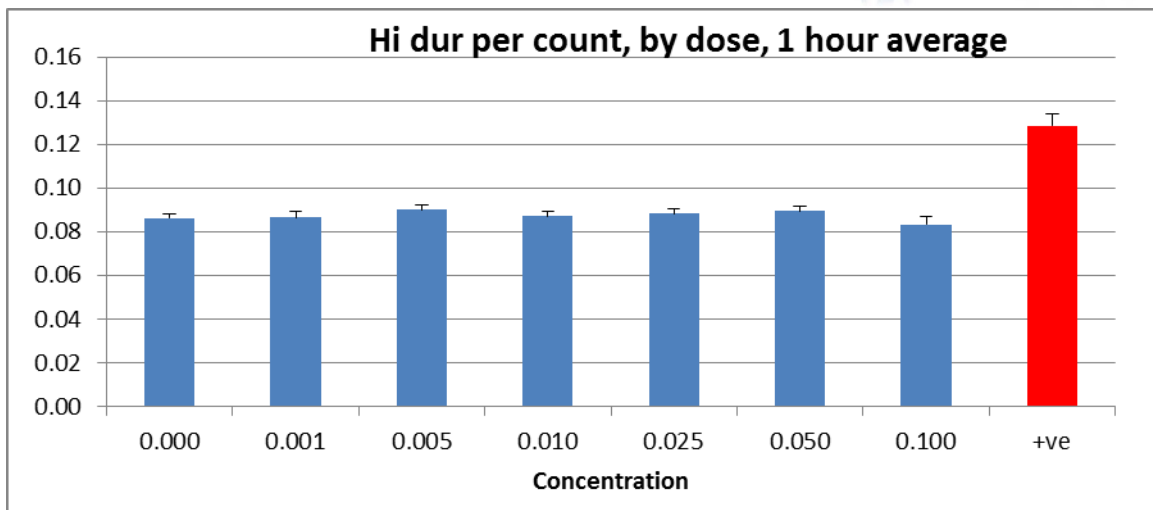


Figure 35. Average counts of ‘high duration activities’ of zebrafish movement categorised by the tracking software of n=12 zebrafish over 1 hour for increasing concentrations of Ag NM 300k 0 = negative control, +ve = PTZ positive control, 0.001 represents $10 \mu\text{g L}^{-1}$ with the concentration increasing $50 \mu\text{g L}^{-1}$ (0.005), $100 \mu\text{g L}^{-1}$ (0.01), $250 \mu\text{g L}^{-1}$ (0.025), $500 \mu\text{g L}^{-1}$ (0.05) up to $1000 \mu\text{g L}^{-1}$ (0.1)

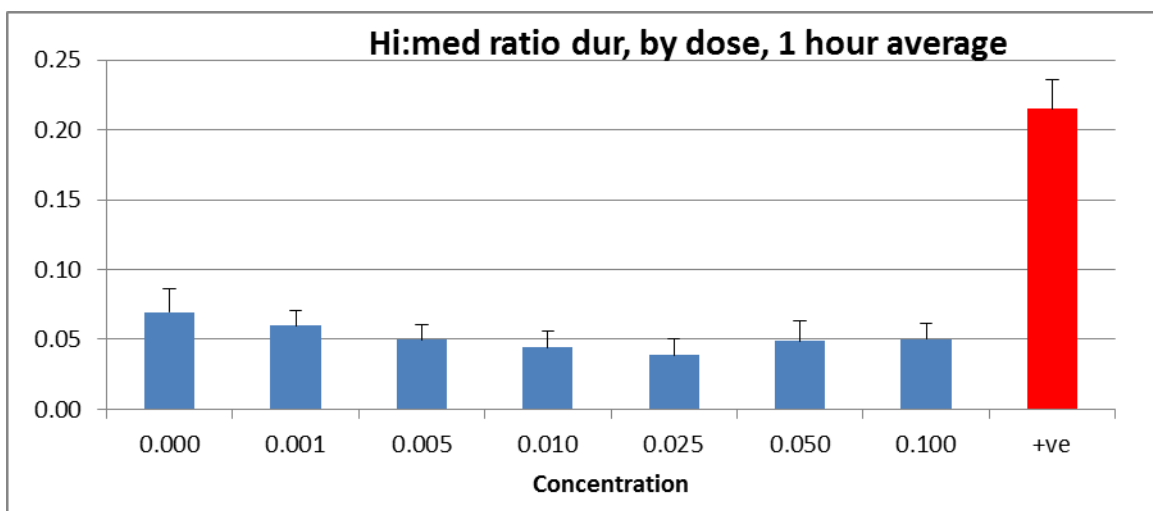


Figure 36. Average ratios of ‘high: medium duration activities’ of zebrafish movement categorised by the tracking software of n=12 zebrafish over 1 hour for increasing concentrations of Ag NM 300k 0 = negative control, +ve = PTZ positive control, 0.001 represents $10 \mu\text{g L}^{-1}$ with the concentration increasing $50 \mu\text{g L}^{-1}$ (0.005), $100 \mu\text{g L}^{-1}$ (0.01), $250 \mu\text{g L}^{-1}$ (0.025), $500 \mu\text{g L}^{-1}$ (0.05) up to $1000 \mu\text{g L}^{-1}$ (0.1)

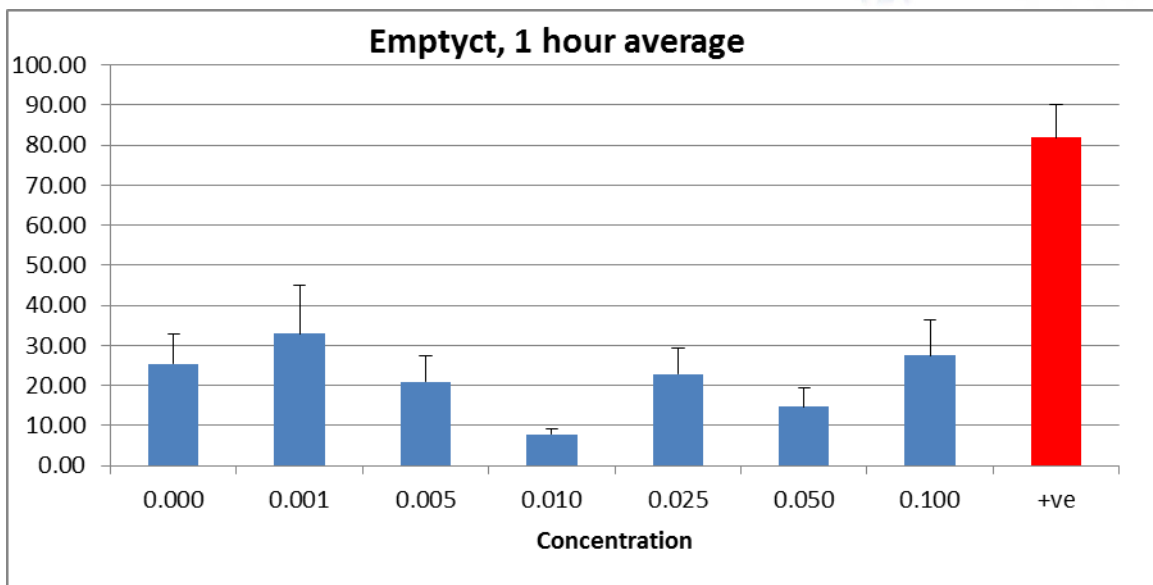


Figure 37. Average number of times during which no object/animal is detected in the screening location by the video capture program software for n=12 zebrafish over 1 hour for increasing concentrations of Ag NM 300k 0 = negative control, +ve = PTZ positive control, 0.001 represents $10 \mu\text{g L}^{-1}$ with the concentration increasing $50 \mu\text{g L}^{-1}$ (0.005), $100 \mu\text{g L}^{-1}$ (0.01), $250 \mu\text{g L}^{-1}$ (0.025), $500 \mu\text{g L}^{-1}$ (0.05) up to $1000 \mu\text{g L}^{-1}$ (0.1)

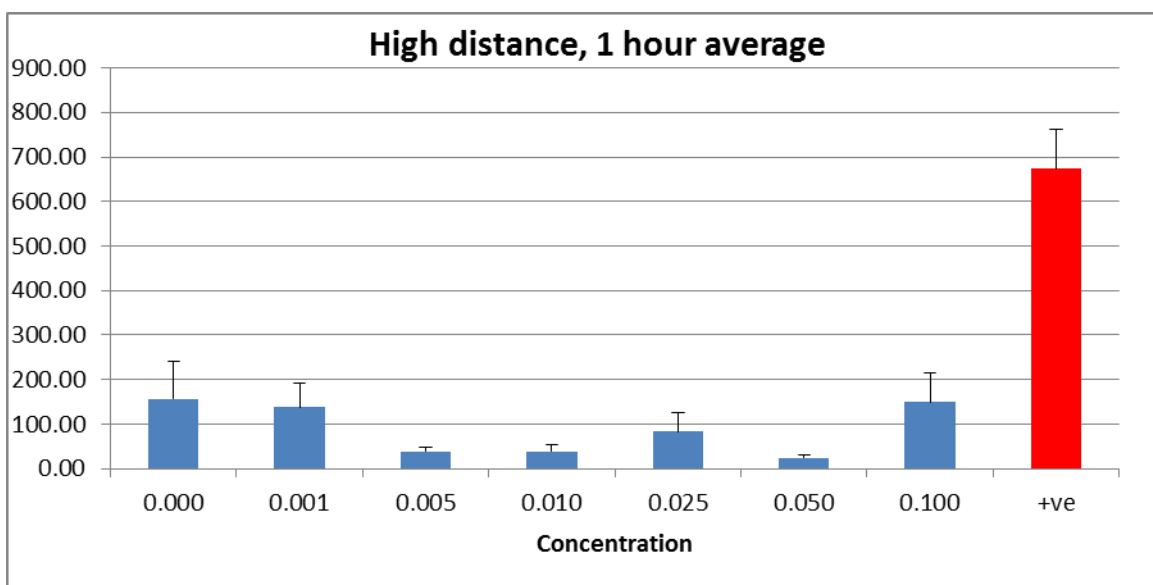


Figure 38. Average 'high distance' events as categorised by the video tracking software for n=12 zebrafish over 1 hour for increasing concentrations of Ag NM 300k 0 = negative control, +ve = PTZ positive control, 0.001 represents $10 \mu\text{g L}^{-1}$ with the concentration increasing $50 \mu\text{g L}^{-1}$ (0.005), $100 \mu\text{g L}^{-1}$ (0.01), $250 \mu\text{g L}^{-1}$ (0.025), $500 \mu\text{g L}^{-1}$ (0.05) up to $1000 \mu\text{g L}^{-1}$ (0.1)

There were 3 treatment specific mortality events across the assay at $1000 \mu\text{g L}^{-1}$ for AgNO_3 , AgCit (7nm) and AgPVP. For these 3 treatments there was 100% mortality at the highest concentration after 16 hours of exposure. These studies were then re-run with lower concentrations.

48 hour acute toxicity test: None of the parameters measured were significantly modified by exposure to any of the tested NPs. The toxic concentrations of AgPVP and AgCit (7nm) at 5 dpf were not toxic for 24 and 48 hour embryos. The only toxicity that occurred was for AgNO_3 (see Figure 39).

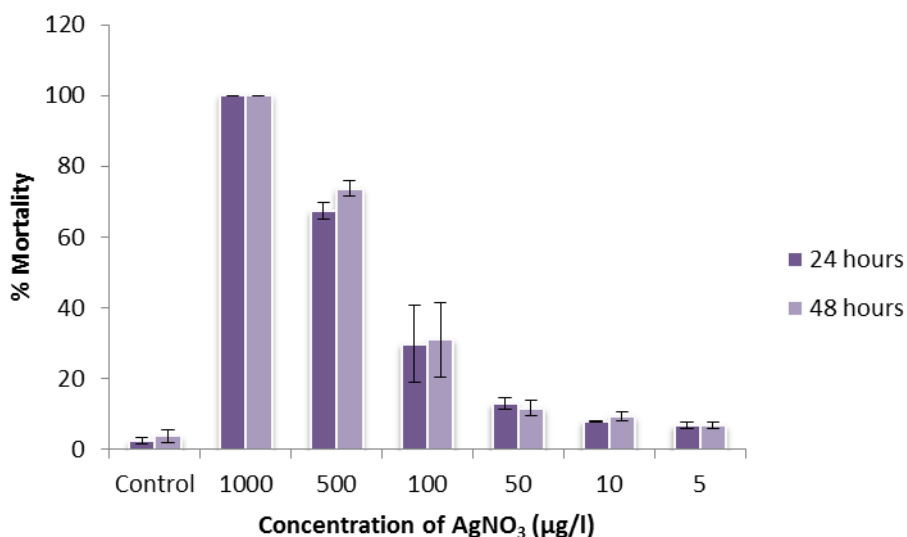


Figure 39. Percentage mortality of zebrafish embryos at 24 and 48 hpf for various concentrations of silver nitrate.

Discussion

Overt toxicity was seen in both assays for AgNO₃ and in the 5 day assessment for AgCit (7nm) and AgPVP, all at a concentration of 1000 µg L⁻¹. Although the toxicity of AgNO₃ is not surprising, the difference in toxicity at 24 and 48 hours compared to the toxicity at 5 days for the smaller coated silver particles indicates that availability of these particles to the developing embryo or larvae plays a significant role in their toxicological profiles. Furthermore, it suggests a more stable Ag NP suspension with a coating/capping agent that doesn't dissolve rapidly to a free ionic form.

The only sub-lethal effect detected by the behavioural assay was for the ZnO NP treatment (Figure S6) where the 500 µg L⁻¹ treatment appeared to mimic the positive control in a number of measured behavioural parameters including, an increase towards in number of rotations, the ratio of high to medium movement events and an elevated amount of high distance of movement at the beginning of the assay. Zinc plays a key role in synaptic transmission and has been associated with epilepsy and traumatic brain injury. At extreme concentrations excess zinc leads to ecotoxicity, oxidative stress, and impairment of neuronal energy production, all of which can not only damage neurons but also lead to neuronal death (Morris and Levenson 2012; Lavoie *et al.* 2007). It is likely however that such subtle markers of toxicity would not be picked up in 24 or 48 hpf toxicity testing when the nervous system is not fully developed.

Some of the measured parameters of the behavioural assay were highly variable, and there were no discernible trends between certain treatment groups, these include the number of times during which no object/animal is detected in the screening location by the video capture software (Figure 30) and the inactivity measurement (Figure 24). These measured parameters are likely to signal for the same endpoint, i.e. level of activity/inactivity of the animal within the well. It should be recognised that the assay has been designed to detect seizure-like specific effects and whilst zinc and potentially silver may have interactions or roles within the nervous system, many other types of NP, might have no effect on

those types of behaviour. It is possible however that some NMs might have effects on other features of behaviour not captured by this assay in its current form.

The 48 h developmental assay also did not detect any subtle changes in morphology when challenged with various NP. Despite the particles tested not presenting any phenotypic responses at the dosed concentrations, the capacity to identify a wide range of early stage, overt and indiscriminate or specific and localised, responses from the embryo is significant.

Exposures with terrestrial invertebrates

P. scaber (titanium dioxide, cerium oxide and silver nanomaterials)

Materials and Methods

Exposure particles: Terrestrial isopods *P. scaber* (Isopoda, Crustacea) were exposed to silver (Silver(JRC)-NM300K), titanium dioxide nanoparticles and titanium dioxide nanoparticles coated with PVP (NNM PROM-TiO₂un-10nm-121113c and NNM PROM-TiO₂PVP-10nm-121113c) and ceria nanomaterials (NNM JRC-CeO₂-NM212-2420b).

Animals and Exposure Conditions: The isopods were collected from uncontaminated locations in Slovenia and kept in a terrarium filled with a layer of moistened soil and a thick layer of partly decomposed hazelnut tree leaves (*Corylus avellana*), at a temperature of 20 ± 2°C and a 16:8-h light:dark photoperiod.

In the feeding experiments the animals consumed the NPs applied in a suspension on the dried hazelnut leaf (*Corylus avellana*). Adult animals of both sexes or females with marsupia (weighing more than 30 mg) were used in the experiments. A suspension of particles or distilled water was brushed onto the lower leaf surface to give final nominal concentrations of NPs on the leaves and left until dry. Each individual animal was placed in a Petri dish and one hazelnut leaf was the animal's only food source. Humidity in the Petri dish was maintained by spraying tap water on the internal side of the lid every day. All Petri dishes are kept in a large glass container under controlled conditions in terms of air humidity (2:80%), temperature (21 ± 1°C), and light regimen (16:8h light:dark photoperiod).

Animals in each individual experiment were exposed to different concentrations of NPs (TiO₂, Ag or CeO₂) for 14 days or for different periods in the case of females with marsupia. Animals were fed with leaves dosed with TiO₂, Ag or CeO₂ NPs suspension, providing nominal concentrations of 1000 (for all three NPs) and 5000 (only for CeO₂ NPs) µg NPs/g on a leaf.

Analyses and endpoints measured: Feeding parameters (feeding rate, food assimilation efficiency, faecal production rate) and survival were assessed. The initial number of animals tested was selected on the basis of the type of analyses that was to be conducted after exposure. After the exposure, the animals were anesthetized at a low temperature and then decapitated and their digestive glands and gut isolated for NP analysis.

After the exposure, the faecal pellets and leaves were removed from the Petri dishes, dried at room temperature for 24 h, and weighed separately. The feeding rate of isopods was then calculated as the mass of consumed leaves per animal's wet weight per day. The food assimilation efficiency is

calculated as the difference between the mass of consumed leaves and the mass of faecal pellets divided by the mass of consumed leaf. The amount of NPs consumed is then calculated on the basis of the quantity of leaf consumed and the amount of NPs applied on the leaf, with the assumption that the suspension is applied evenly on the leaf surface.

After feeding experiments animals were anesthetized at a low temperature and then decapitated and their digestive glands and gut isolated for analysis of NP/metal content. Samples of glands, gut and rest of the animal's body were lyophilized, weighed, and completely digested in an acid, as described previously. We conducted the digestion using microwave acid digestion or with the traditional "hot plate". After digestion of samples, residue were taken up in HNO_3 and total element concentrations in the tissue were determined by atomic absorption spectrometry (AAS). Reagent blanks and standard solutions were used to ensure accuracy and precision in the analysis.

Cell membrane stability in NP exposure animals was measured as an index of animal stress (Valant et al. 2009). A single isolated hepatopancreatic tube was obtained from each animal from individual feeding experiments. This was incubated for 5 min in a mixture of the fluorescent dyes, acridine orange and ethidium bromide, and then put on a microscope slide. Fresh samples were photographed and examined by an Axioimager.Z1 fluorescent microscope (Zeiss) with two different sets of filters. The excitation filter 450 to 490 nm and the emission filter 515 nm (filter set 09) were used to visualize acridine orange- and ethidium bromide-stained nuclei, and the excitation filter 365 nm and the emission filter 397 nm (filter set 01) were used to visualize nuclei stained with ethidium bromide only. Cell membrane integrity was assessed by examination of micrographs. Photographs of intact digestive glands were examined by the same observer twice at intervals of at least 24 h. Cell membrane integrity was assessed visually and classified from 0 to 9 according to a predefined scale. On the basis of preliminary experiments, we concluded that non treated (control) animals showed less than 5% of nuclei stained by ethidium bromide, whereas severely stressed animals had up to 100% of ethidium bromide-stained nuclei.

Results and Discussion

Feeding parameters and mortality after TiO_2 , Ag or CeO_2 NPs ingestion: Feeding parameters (feeding rate, food assimilation efficiency, faecal production rate) and survival were not affected below a nominal exposure concentration of 1000 μg TiO_2 , Ag or CeO_2 NPs/g dry weight of leaf or 5000 μg CeO_2 NPs/g dry weight of leaf.

Accumulation of Ag in digestive tissue after NPs ingestion: Results of elemental analyses of different body fractions (digestive glands, gut and the rest of the body) with atomic absorption spectroscopy after exposing animals to Ag NPs (JRC) showed that Ag accumulated in the hepatopancreas and not in gut or the rest of body of animals. In contrast Ag accumulated in the hepatopancreas, gut and rest of the body of animals in case of exposure of animals to AgNO_3 .

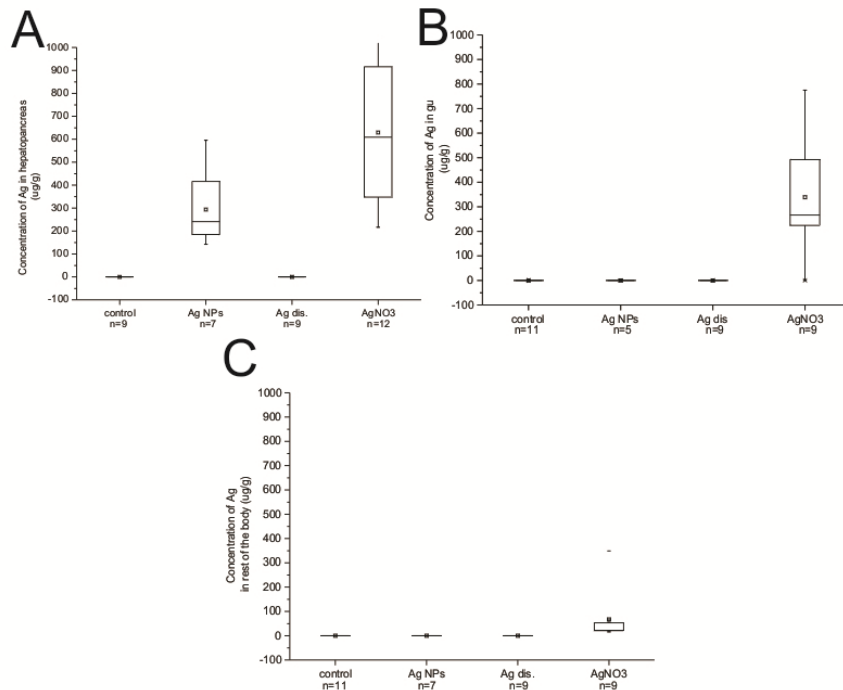


Figure 40: (A) Concentration of Ag in hepatopancreas of animals exposed to Ag NPs, Ag dispersant or AgNO₃, (B) Concentration of Ag in gut of animals exposed to Ag NPs, Ag dispersant or AgNO₃, (C) Concentration of Ag in rest of the body of animals exposed to Ag NPs, Ag dispersant or AgNO₃. Symbols on the box plot represent minimum and maximum data values (whiskers), mean value (□), 75th percentile (upper edge of box), 25th percentile (lower edge of box), median (line in box) and max and min value (-).

Digestive gland cell membrane stability after CeO₂ NPs ingestion: We have previously published that the digestive gland cell membrane stability value was higher than 2 (on a scale from 0 to 9) in only 5% of animals from a stock culture of animals that were in good physiological condition. The cell membranes are considered destabilised when this value is higher than an index of 2. The digestive gland cell membrane stability of controls or animals exposed to 1000 or 5000 µg CeO₂ NPs/g dry weight of leaf was not affected.

Eisenia fetida, *Folsomia candida*, *Hypoaspis aculeifer*

Materials and Methods

Selected particles

Table 8: Selected nanomaterials for the exposures

Particle composition & source	NanoMILE code
PROM Cerium(IV)oxide nanoparticle Particle size: 20 nm Formulation type: dispersion Concentration: 3.1% w/w, nominal	PROM-CeO ₂ -20nm-230114a
Bulk CeO ₂ Particel size: 5 µm Formulation type: none (powder) Purity: 100%, nominal	SIGMA-CeO ₂ Bulk – 5 microns.230114a

Exposures

***Eisenia fetida*:** Test vessels for the tests with *Eisenia fetida* were Bellaplast containers consisting of inert (non-toxic) plastic (Polystyrene). The test vessels have a bottom area of 11 x 15.5 cm (= 170.5 cm²) and a height of 6 cm and were covered by a transparent lid. The earthworms were tested in an artificial soil. The composition of this artificial soil was based on OECD Guideline No. 222 (2006). The percentages refer to the dry weight: 10 / 5 % Sphagnum peat (no visible plant remains; finely ground and air-dried); 20 % Kaolin-Clay (kaolinite content > 30%); 70 / 75 % Quartz sand (fine sand content with particles between 50 and 200 µm higher than 50%); 0.4 % Calcium carbonate (CaCO₃)

The air dried peat was shredded in a chaff-cutter. Afterwards, all parts of the artificial soil were mixed homogeneously. The pH value was adjusted to 6 ± 0.5 using calcium carbonate. The moisture content was adjusted to 40 – 60% of WHC_{max} using deionised water.

The following test conditions were maintained: Temperature: 20 ± 2 °C. Light/dark cycle was 16 : 8 h with a constant light intensity at the substrate surface of 400 – 800 lx.

The adult worms were fed with finely ground cow manure (free of growth promoters, nematicides or similar veterinary pharmaceuticals). Before starting the experiment an amount of 5 g food per 500 g soil dry weight was mixed into the artificial soil to be used in the test. After the start of the experiment food was first provided one day after application of the test item and introduction of the adult worms.

Thereafter, the adult worms were fed weekly during the first 4 weeks of the test. An amount of 4 g cow manure moistened with 4 g de-ionised water was spread on the soil surface of each test container. If



food remained uneaten the ration was reduced accordingly. After removing of the adults on day 28 further 4 g of food was mixed with the artificial soil of each test vessel.

Application of Ceria nanoparticles and reference material and test concentrations: Ceria nanoparticles (PROM-CeO₂-20nm-230114a) were used as a water- miscible substance. The Ceria nanoparticles were dissolved in an amount of deionised water sufficient to prepare the respective test solutions. The concentrations to be tested were based on the purity of the Ceria nanoparticles (3.1 % nominal). An appropriate amount of the test solutions served to prepare the different concentrations of the test item in the artificial soil.

The test item solutions were incorporated into the soil by thoroughly mixing in the respective test item solution for approx. 5 minutes. The reference material (SIGMA-CeO₂-Bulk-5microns-230114a) was poorly soluble in water; therefore, a mixture of finely ground quartz sand and the reference material was produced for each concentration. The concentrations to be tested were based on the purity of the reference material (100 % nominal). The test item was mixed in an amount of quartz sand sufficient to prepare a mixture for each test item concentration separately. An appropriate amount of these test item/quartz sand mixtures served to prepare the different concentrations of the test item in the artificial soil. The test item was incorporated into the remainder of the artificial soil by thoroughly mixing in the respective test item/quartz sand mixtures for at least 5 minutes.

Finally, the contaminated artificial soil was filled into the test vessels. Per test vessel an amount corresponding to 500 g dw was used. The test item and the reference item were applied at 100 and 1000 mg/kg soil dry weight, respectively. An untreated control group was also tested.

The tests were carried out as described in the OECD guideline 222. Each test item group included four replicates containing 10 adult earthworms each. The control group included eight replicates containing 10 adult earthworms each. After day 28, the adult earthworms were removed and weighed, and after 56 days, the number of juveniles in each replicate was counted. The test was considered to be valid if the following criteria are met for the control group at the end of the test: Mean adult mortality: ≤ 10 %; Mean number of juveniles per vessel: ≥ 30; CV (Coefficient of variation) for the number of juveniles: ≤ 30 %

Folsomia candida: Test vessels for the tests with *Folsomia candida* were glass containers (able to be closed tightly) of about 250 mL capacity and with a diameter of about 6.5 cm. The collembolans were tested in an artificial soil as described in chapter 3.1.1 with an organic matter content of 5 % peat. The composition of this artificial soil is based on OECD Guideline No. 232 (2009). The test conditions were maintained as described above for *Eisenia fetida*. The collembolans were fed with a sufficient amount of granulated dry yeast per test vessel at the beginning of the test and after 14 days *ad libidum*.

Application of Ceria nanoparticles and reference material and test concentrations: Ceria nanoparticles and reference material were applied to the test substrate as described for *Eisenia fetida*. Per test vessel an amount corresponding to 30 g dw was applied. The test item and the reference item were applied at 100 and 1000 mg/kg soil dry weight, respectively. An untreated control group was also tested.

The tests were carried out as described in OECD guideline 232. Each test item group included four replicates containing 10 juvenile springtails each. The control group included eight replicates containing 10 juvenile springtails each. The springtails were fed with granulated yeast at test start and after 14 days. After 28 days of exposure, the numbers of adult and juvenile springtails were determined.



The test is considered to be valid if the following criteria are met for the control group at the end of the test: Mean adult mortality: $\leq 20\%$; mean number of juveniles per vessel: ≥ 100 ; CV (Coefficient of variation) for the number of juveniles: $\leq 30\%$.

The level of significance for all statistical procedures was set to $\alpha = 0.05$. Differences in mortality between the control group and the test item groups were analysed using pairwise Fisher's exact binomial tests (one-sided greater). Data on reproduction were analysed for normal distribution and variance homogeneity using Shapiro-Wilk test and Levene's test. As both criteria were met, Student test (one-sided smaller) was used to detect differences between the test item groups and the control group.

Hypoaspis aculeifer: Test vessels for the tests with *Hypoaspis aculeifer* were glass containers (able to be closed tightly) of about 100 mL capacity and with a diameter of about 5.5 cm. The mites were tested in an artificial soil as described for *Eisenia fetida*, with an organic matter content of 5% peat. The composition of this artificial soil is based on OECD Guideline No. 226 (2008). The test conditions were maintained as described for *Eisenia fetida*. The mites were fed with cheese mites (*Tyrophagus putrescentiae*) *ad libitum* 2-3 times a week.

Application of ceria nanoparticles and reference material and test concentrations: Ceria nanoparticles and reference material were applied to the test substrate as described for *Eisenia fetida*. Per test vessel an amount corresponding to 20 g dw was used. The test item and the reference item were applied at 100 and 1000 mg/kg soil dry weight, respectively. An untreated control group was also tested.

The tests were carried out as described in OECD guideline 226. Each test item group included four replicates containing 10 adult females each. The control group included eight replicates containing 10 adult females each. The mites were fed with cheese mites (*Tyrophagus putrescentiae*) *ad libitum* 2-3 times a week. After 14 days of exposure, the surviving adult females and juveniles were extracted from the soil using a high temperature gradient extractor (McFadyen, 1961). The test is considered to be valid if the following criteria are met for the control group at the end of the test: Mean adult mortality: $\leq 20\%$; Mean number of juveniles per vessel: ≥ 50 ; CV (Coefficient of variation) for the number of juveniles: $\leq 30\%$.

The level of significance for all statistical procedures was set to $\alpha = 0.05$. Differences in mortality between the control group and the test item groups were analysed using pairwise Fisher's exact binomial tests (one-sided greater). Data on reproduction were analysed for normal distribution and variance homogeneity using Shapiro-Wilk test and Levene's test. As both criteria were met, Student test (one-sided smaller) was used to detect differences between the test item groups and the control group.

Results and Discussion

Eisenia fetida: Tests need to be repeated due to invalidity of the first tests (Results will be available in April 2015).

Folsomia candida

Mortality of introduced springtails

Table 9: Mortality rates for expose to nanomaterials in springtails

Treatment group	Concentration [mg/kg sdw]	Total number of adult females introduced	Total number of not recovered adult females	Mean mortality [%]
Control (n=8)	0	80	6	7.5
PROM-CeO ₂ -20nm (n=4)	100	40	1	2.5
	1000	40	4	10.0
SIGMA-CeO ₂ Bulk-5microns (n=4)	100	40	0	0.0
	1000	40	2	5.0

n: Number of replicates

sdw: Soil dry weight

The mortality observed in the control group was 7.5 % and 2.5 % and 10.0 % in the test group with ceria nanoparticles, and 0.0 % and 5.0 % in the test group with the reference item. No statistically significant difference was seen between the control group and the PROM-CeO₂-20nm and the reference item groups (Fisher's Exact Binomial Test, one-sided greater, $\alpha = 0.05$) was determined for the mortality of the springtails.

Reproduction

Table 10: Impacts on nanomaterial exposure on reproduction in springtails

Treatment group	Concentration [mg/kg sdw]	Mean number of juveniles per replicate	\pm SD	CV	Reduction in reproduction ¹⁾ [%]
Control (n=8)	0	778.6	107.0	13.7	--
PROM-CeO ₂ -20nm (n=4)	100	775.3	67.6	8.7	0.4
	1000	725.6	102.7	14.2	6.8
SIGMA-CeO ₂ Bulk-5microns (n=4)	100	787.7	114.0	14.5	-1.2
	1000	777.1	146.6	18.9	0.2

¹⁾ Negative values indicate higher reproduction compared to control

CV: Coefficient of Variation, \pm SD: Standard Deviation, n: Number of replicates, sdw: Soil dry weight

The mean number of juveniles in the control group was determined as 778.6 juveniles per replicate. In the treatment groups the mean number of juveniles ranged from 725.6 to 787.7 juveniles per replicate. No statistically significant difference between the control group and the PROM-CeO₂-20nm and the reference item groups (Student's t-Test, one-sided smaller, $\alpha = 0.05$) was determined for the reproduction of the springtails.

Hypoaspis aculeifer

Mortality of introduced adult females

Table 11: Mortality rates for exposure to nanomaterials in *Hypoaspis*

Treatment group	Concentration [mg/kg sdw]	Total number of adult females introduced	Total number of not recovered adult females	Mean mortality [%]
Control (n=8)	0	80	8	10.0
PROM-CeO ₂ -20nm (n=4)	100	40	7	17.5
	1000	40	5	12.5
SIGMA-CeO ₂ Bulk-5microns (n=4)	100	40	2	5.0
	1000	40	3	7.5

n: Number of replicates

sdw: Soil dry weight

The mortality observed in the control group was 10.0 % and 17.5 % and 10.0 % in the test group with Ceria nanoparticles, and 5.0 % and 7.5 % in the test group with the reference item. No statistically significant difference between the control group and the PROM-CeO₂-20nm and the reference item groups (Fisher's Exact Binomial Test, one-sided greater, $\alpha = 0.05$) was determined for the mortality of the mites.

Reproduction

Table 12: Impacts of nanomaterial exposure on reproduction in *Hypoaspis*

Treatment group	Concentration [mg/kg sdw]	Mean number of juveniles per replicate	\pm SD	CV	Reduction in reproduction ¹⁾ [%]
Control (n=8)	0	234.4	30.6	13.1	--
PROM-CeO ₂ -20nm (n=4)	100	263.5	44.9	17.0	-12.4
	1000	236.8	31.5	13.3	-1.0
SIGMA-CeO ₂ Bulk-5microns (n=4)	100	307.5	26.5	8.6	-31.2
	1000	301.3	26.5	8.8	-28.5

¹⁾ Negative values indicate higher reproduction compared to control

CV: Coefficient of Variation, \pm SD: Standard Deviation, n: Number of replicates, sdw: Soil dry weight

The mean number of juveniles in the control group was determined as 234.4 juveniles per replicate. In the treatment groups the mean number of juveniles ranged from 236.8 to 307.5 juveniles per replicate.

No statistically significant difference between the control group and the PROM-CeO₂-20nm and the reference item groups (Student's t-Test, one-sided smaller, $\alpha = 0.05$) was determined for the reproduction of the springtails.

C. elegans

Materials and Methods

Selected particles: Ag NM300K, ZnO NM110, CeO₂ NM212 or CeO₂ NM211 NPs were selected as study particles. These were obtained from the European Commission Joint Research Centre (JRC) and underwent characterisation by dynamic light scattering before the experiments (DLS; **Table 13**).

Table 13. Particle characterization by dynamic light scattering (DLS) analysis

Particle	Diameter [nm]	Zeta Potential, ζ [mV]
Ag NM300K	58.02	-6.91
ZnO NM110	3165	-10.7
CeO ₂ NM 212	1326	-18.6
CeO ₂ NM211	2422	-20.2

Particle suspensions were prepared as follows: CeO₂ NM212 (powder), CeO₂ NM211 (powder), ZnO NM110 (powder), Ag NM300K (solution) NPs as well as the dispersant of Ag NM300K NPs (NM300KDIS) were obtained from the European Commission Joint Research Centre (JRC). The stock suspensions of uncoated CeO₂ NM212 and NM211 or ZnO NM110 NPs were produced by suspension of 1.6 mg mL⁻¹ powder in ultrapure water and sonication in a cup horn sonicator (Cuphorn Branson) at 200W for 2 minutes to disrupt particles and obtain homogeneous suspensions. The Ag NM300K NPs (100 mg mL⁻¹) were further diluted to 1 mg mL⁻¹ and sonicated as described above. All particle dispersions were serially diluted in ultrapure water. Solutions of zinc and silver ions were prepared by dissolving ZnCl₂ or AgNO₃ in ultrapure water. Particles were characterized for particle size (nm) and zeta potential (ξ , mV) in ultrapure water by dynamic light scattering (DLS) with a Zetasizer Nano-ZS (Malvern Instruments Ltd.).

Exposure studies.

Adult *C. elegans* (wild type, N2) were chronically exposed with increasing concentrations of Ag, ZnO or CeO₂ NPs and subjected to life span analyses (Figure 41) and age-resolved observation of locomotion phenotypes (Figure 42). All NPs were additionally analysed in 24 hour exposures by quantitative observation of the reproductive phenotype internal hatch, e.g. neuromuscular defects of the egg laying system (Figure 43).

Life span assays were performed as described previously (Petrascheck et al., 2007). Briefly, life span was assessed in liquid medium (S-medium with 50 $\mu\text{g mL}^{-1}$ carbenicillin and 0.1 $\mu\text{g mL}^{-1}$ fungizone) in 96-well plates at 20°C. 10-15 age-synchronized *C. elegans* were seeded per well as L1 larvae and co-incubated together with *Escherichia coli* OP50 as food source. Liquid medium contained antibiotics to



keep the *Escherichia coli* at a constant number, *e.g.* inhibit bacterial proliferation. To prevent self-fertilization of the hermaphrodite worms, 5-fluoro-29-deoxyuridine was added 42–45 hours after seeding (0.12 mM final concentration). Where indicated, NPs were added to the liquid culture approximately 68 hours after seeding, which corresponded to both, day 1 of adulthood and of the life span assay. The fraction of animals alive was quantified by scoring / detection of body movement. The mortality data were subjected to Kaplan–Meier survival analysis, to prepare survival curves. Statistical comparisons of mean life span values between the control and NP-treated worms were analyzed by Peto’s log-rank test. All *C. elegans* strains, *e.g.* Bristol strain N2 (wild type), DR1572 *daf-2* (e1368) III and CF1038 *daf-16* (mu86) I, were provided by the *Caenorhabditis* Genetics Center (CGC, University of Minnesota, MN, USA).

Quantitative observation of locomotion phenotypes was conducted in an age-resolved manner, *e.g.* during the life span assays described above. Movement of adult *C. elegans* in liquid medium was classified into three categories, namely (1) swimming, (2) uncoordinated or (3) exclusive head and/ or tail movement (*Herndon et al., 2002*).

Quantitative observation of the egg laying defect internal hatch, *e.g.* bag of worms (BOW), age-synchronized nematodes were grown on NGM plates until day 1 of adulthood. Worms were then transferred to 96-well plates containing liquid medium with 12 mg mL⁻¹ *E.coli* OP50 as food source in a 150 µl total volume per well. The tested concentrations were 160, 80, 20 µg mL⁻¹ for CeO₂, ZnO NPs and ZnCl₂ or 100, 50, 25, 10 and 1 µg mL⁻¹ for Ag NPs and AgNO₃. After 24 hours the fraction of nematodes with internal hatched larvae was scored on 5% agarose pads containing 10 µM NaN₃.

Statistical differences between control and exposed *C. elegans* worms were determined by Student’s t test (Microsoft Excel) or one way ANOVA with Tukey’s post-hoc test (Origin 8.5). All data reported were based on at least three independent experiments.

Results and Discussion

Life span experiments were carried out in liquid medium in multi-well plates at 20°C which replicates environmental conditions in the fluid phase of soil. These conditions turned out to be favourable, since untreated wild type N2 worms survived for up to 36 days (Figure 41, A-D). Each experiment included senescence genes mutants *daf-2* or *daf-16* as additional life span controls that define a time window of survival expectancy. An important regulator of *C. elegans* life span is the insulin-like signalling pathway. Life span extensions are caused by mutations in upstream signalling pathway genes such as the *daf-2* insulin-like growth factor (IGF) receptor gene, whereas loss-of function mutations of the downstream *daf-16* forkhead transcription factor gene reduce life span. Accordingly, *daf-2* controls live for up to 44 days in the life span assays, while *daf-16* control worms maximally reach an age of 30 days (Figure 41, A-D).

Addition of a variety of NPs to the life span assays resulted in different worm survival. Addition of 1 µg/ml Ag NM300K did not alter the life span in comparison to untreated control *C. elegans* (Figure 41A). However, incubation with 10 µg/ml Ag NM300K had already reduced worm survival significantly between days 22 and 32 compared to untreated controls. This outcome was even more dramatic when worms were exposed to 100 µg/ml Ag NM300K. Here, all *C. elegans* were dead after 8 days. Notably, the concentration of 10 µg/ml Ag NM300K reduced life span, but NP-exposed worms still survived the short-lived *daf-16* mutants (Figure 41A). In contrast, the highest concentration of 100 µg/ml Ag NM300K

clearly falls below the survival curve of *daf-16* animals. Next ZnO NM110, CeO₂ NM212 or CeO₂ NM211 NPs were tested in the life span assays. All ZnO and CeO₂ NPs applied in concentrations between 20 and 160 µg/ml did not reduce the life span of adult *C. elegans*. As for their untreated counterparts, ZnO or CeO₂ NP-exposed *C. elegans* survived for up to 36 days and the respective survival curves show no significant differences (Figure 41B-D). These results are further validated by the observation that survival curves of untreated controls as well as ZnO or CeO₂ NP-treated worms run between the ones of short-lived *daf-16* and long-lived *daf-2* mutants, respectively. Taken together we show that Ag NM300K NPs reduce the life span of *C. elegans* in a concentration-dependent manner, whereas ZnO NM110, CeO₂ NM212 or CeO₂ NM211 NPs do not alter worm survival in concentrations between 20 and 160 µg/ml.

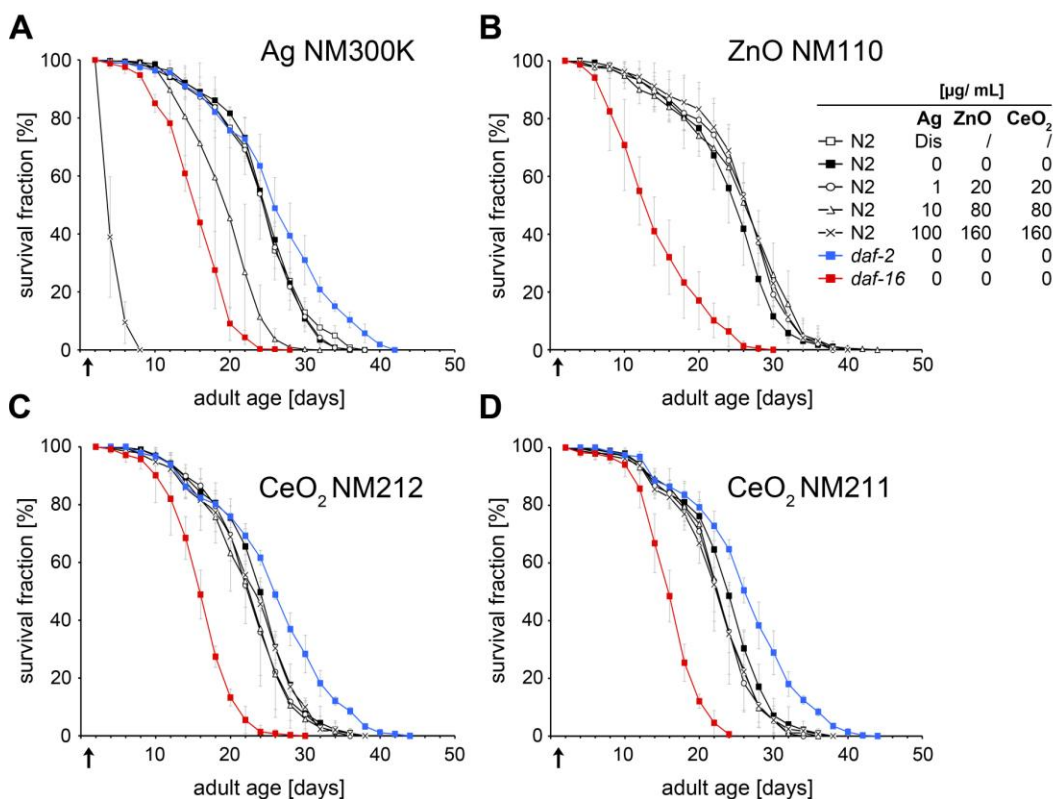


Figure 41. Life span of *C. elegans* exposed to different NPs. (A) Adult *C. elegans* that were exposed to 10 or 100 µg mL⁻¹ Ag NPs show a significant decrease ($p < 0.01$) of survival in comparison to untreated worms (filled squares). In contrast, the life span of nematodes exposed to 1 µg mL⁻¹ Ag NPs or dispersant only is similar compared to untreated controls. Worms exposed to 160, 80 or 20 µg mL⁻¹ of (B) ZnO NPs, (C) CeO₂ NM212 NPs or (D) CeO₂ NM211 NPs have similar survival curves compared with untreated control worms. Long-lived *daf-2* mutants (blue) and short-lived *daf-16* mutants (red) show extended or shortened survival curves that define the window of expected survival in *C. elegans*. Arrows, days of particle addition; dis, dispersant only.

As it was shown previously that certain NPs accelerate age-related amyloid protein aggregation and behavioural phenotypes in adult *C. elegans* (Scharf et al., 2013) we next analysed if worm survival is correlated with locomotion phenotypes. Typically, wild-type worms show an age-related decline of forward movement (Huang et al., 2004). To record all movements, animals were scored according to three modes of locomotion in liquid medium, namely (1) swimming, (2) uncoordinated or (3) head/tail only during their entire life span (Figure 42). Untreated wild-type *C. elegans* show an age-related decline of swimming movements, whereas uncoordinated and head/tail restricted movements increase with age. Worms exposed to 20, 80 and 160 µg/ml ZnO NM110, CeO₂ NM212 or CeO₂ NM211 NPs display similar locomotion phenotypes in comparison to untreated controls (Figure 42B-D). In contrast,

C. elegans treated with 10 $\mu\text{g}/\text{ml}$ Ag NM300K NPs show significantly altered locomotion, e.g. significantly reduced swimming on day 8 of the observations (**Figure 42A**; asterisks). The swimming phenotype is likewise significantly reduced in worms exposed to 100 $\mu\text{g}/\text{ml}$ Ag NM300K NPs between days 2 and 6. Simultaneously these worms show a significant premature acceleration of uncoordinated movements and movements that are restricted to the head and the tail (**Figure 42A**; asterisks). The results of quantitative locomotion scoring suggest that worm survival and locomotion behaviour is closely linked in response to NPs. Ag NM300K NPs that significantly reduce worm survival also accelerate age-related impairment of forward movement, whereas ZnO NM110, CeO₂ NM212 or CeO₂ NM211 NPs neither reduce *C. elegans* life span nor alter locomotion phenotypes in comparison to untreated control worms.

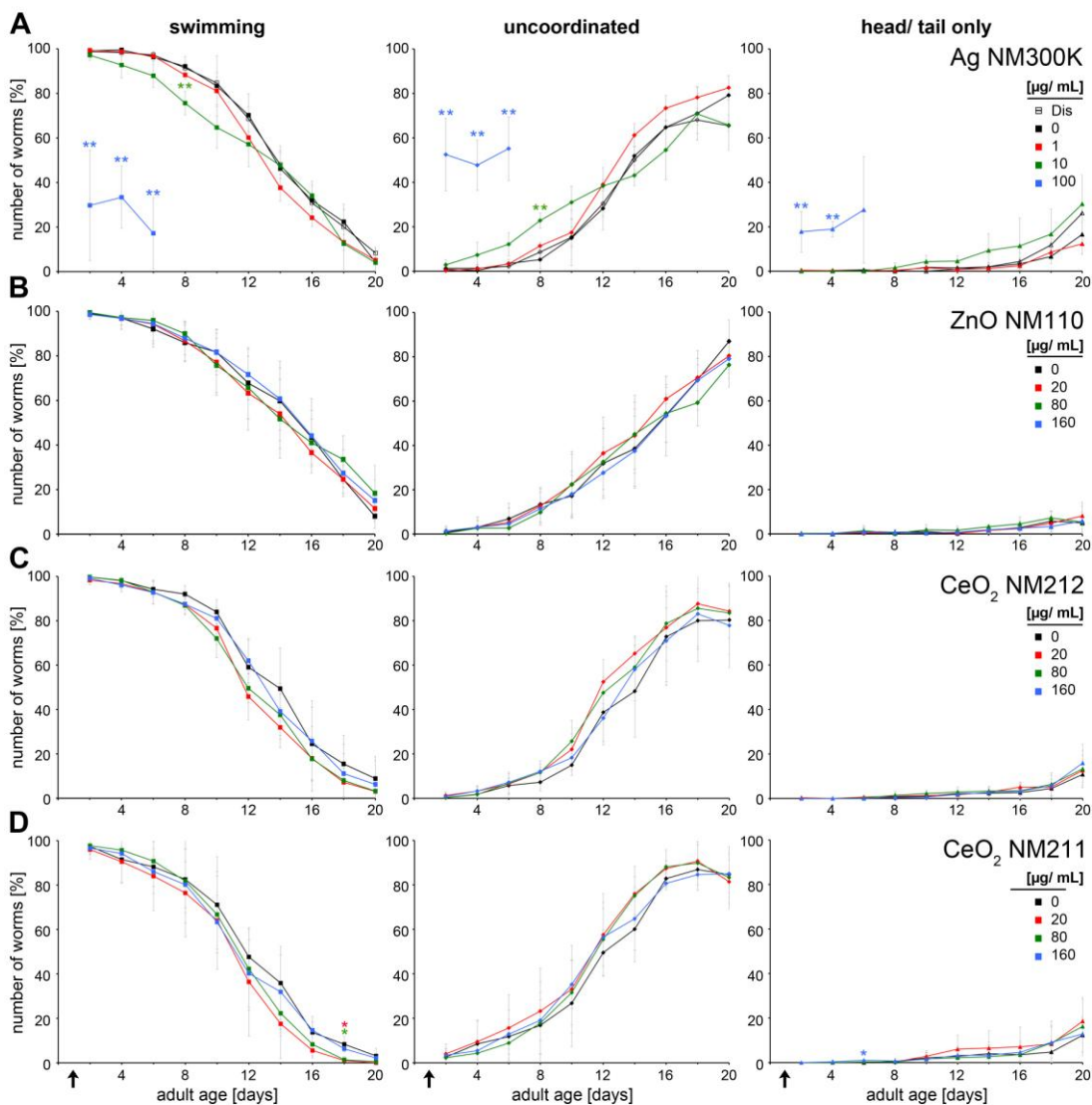


Figure 42. Quantitative observation of locomotion behaviors in NP-exposed *C. elegans*. Locomotion phenotypes of nematodes were classified according to the three categories swimming, uncoordinated or head/ tail only and plotted against adult worm age. All graphs show an age-related decline of swimming nematodes and simultaneous increase of uncoordinated and head/ tail only movements. Phenotypes were scored in nematodes exposed to (A) Ag NPs or the dispersant only control, (B) ZnO NPs, (C) CeO₂ NM212 NPs and (D) CeO₂ NM211 NPs in comparison to untreated controls (black). *, $p < 0.05$; **, $p < 0.01$; arrows, days of particle addition; dis, dispersant only.

Next we analysed another behavioural phenotype that was previously reported to occur after exposition of adult *C. elegans* to silica nanoparticles (Pluskota et al., 2009). The bag of worms (BOW) represents a neural phenotype that is normally age-related and results from neuromuscular defects of the vulva. Hence, egg-laying through the vulva is impaired and eggs hatch within the body of the parent worm (internal hatch). Wild type N2 worms were left untreated or exposed to Ag NM300K, ZnO NM110, CeO₂ NM212 or CeO₂ NM211 NPs and their salts in different concentrations (Figure 3). As early as after 24 hours 37% of worms treated with 100 µg/ml Ag NM300K NPs show the BOW phenotype which represents a significant increase in comparison to untreated controls and animals that were treated with lower concentrations of the nanomaterial (Figure 43A; asterisks). Scoring of the BOW phenotype in *C. elegans* exposed to concentrations between 1 – 100 µg/ml of the corresponding salt AgNO₃ revealed that already the lowest concentration of 1 µg/ml significantly induced the internal hatch phenotype after 24 hours suggesting a role of Ag-ions in dissolution. In contrast, neither ZnO and CeO₂ NPs nor ZnCl₂ induced a significant increase of the BOW phenotype indicating that the neuromuscular function of the vulva is not a target for all nanoparticles or their metal ions (Figure 43B, C). Again, the results of the BOW analyses correspond well with both, life span analyses and locomotion scoring in that only the Ag NM300K NPs show significant effects. Detailed studies of the role of Ag-ion dissolution are required due to the result that AgNO₃ salts likewise significantly induce the BOW phenotype.

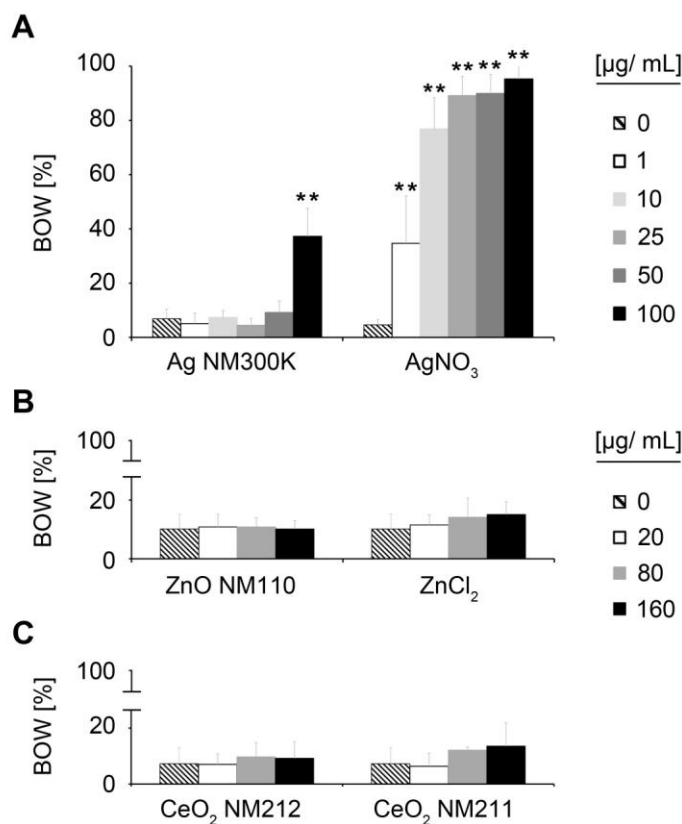


Figure 43. Quantification of the internal hatch (BOW) phenotype in *C. elegans* exposed to different NPs. Nematodes with internally hatched larvae were scored 24 hours after addition of NPs or respective salts. (A) Worms treated with increasing concentrations of AgNO₃ showed a significant increase of the BOW phenotype in comparison to untreated controls. The BOW phenotype was likewise significantly increased in nematodes exposed to 100 µg mL⁻¹ Ag NPs, but remained unchanged after addition of lower Ag NP-concentrations between 1 - 50 µg mL⁻¹. No increase of the BOW phenotype was observed in *C. elegans* treated with ZnO NPs, ZnCl₂ (B) or CeO₂ NM212 and NM211 NPs (C). **, p<0.01; BOW, bag of worms.

Comparing multiple endpoints such as life span and age-related behaviour phenotypes we show that Ag NPs induce significant toxicity in a concentration-dependent manner. Such toxicity was confirmed by the other endpoints. Nano-Ag likewise reduced life span, accelerated age-related reduction of locomotion and induced the reproductive defect internal hatch. The results are in good agreement with the literature as Ag NPs are generally reported to be toxic in *C. elegans* and across species, e.g. in bacteria, algae, crustaceans, and fish. In contrast, we did not observe any adverse effects of CeO₂ or ZnO NPs in our chronic exposure studies, indicating that the particles used do not confer toxicity in adult *C. elegans*.

6. Conclusions and Recommendations

Relating to the particles:

AgNP:

- Silver nanomaterials were found to show toxicity and they did so across the wide range of study organisms we tested.
- Dissolution of AgNP occurred in the exposure medium at a low rate, however, the results overall indicate that the release of Ag⁺ and its uptake into the cell is the main cause of AgNP toxicity.
- No adverse effects on the organisms studied are expected for AgNP concentration modelled for surface waters in Europe or that occur in surface soils (although under exceptional circumstances this may occur for heavily contaminated land etc.)
- At non-toxic concentrations an adverse effect of Ag⁺ on metal homeostasis cannot be ruled out and this warrants further investigation.

ZnONP:

- Dissolution of ZnO NP in the exposure medium was rapid and it can be reasonably assumed that the predominant mode of toxicity of ZnO NP would be due to zinc ions.
- Elevated Zn⁺ concentration in the aquatic environment, that may result from accidental spills of ZnO NP, could potentially adversely affect aquatic organisms.
- In the current studies no adverse effects were found for exposures across a wide range of terrestrial and aquatic organisms for concentrations of ZnONP with relevance for most environmental compartments.

CeO₂:

- No effects of CeO₂ were seen for any dosing level, albeit the focus was on apical endpoints for most study organisms and the main mode of action reported for CeO₂ (via oxidative stress) was not measured in these studies.

TiO₂:

- No effects of TiO₂ were seen on feeding activity in isopoda (the only organism on which this material was tested)

Relating to Study Organisms:

- None of the test organisms studied was found to be significantly more sensitive to AgNP exposure (the only toxic material at environmentally relevant concentrations) and therefore, of the diverse animals studied we have not identified one species that is more suitable than others for NP testing/screening (based on sensitivity alone).
- Microscopy-based toxicity screening of embryogenesis in zebrafish offers the potential for medium throughput screening for toxicity assessments of NPs
- Microscopy-based toxicity screening, combined with approaches for measuring particle uptake, distribution and localization would provide a highly integrative approach for effects analysis associated with NP exposure (see deliverable also deliverable 6.4: Identification of body target tissues accumulating NPs).
- Zebrafish early life stages are suitable for *in vivo* nanoparticle toxicity screening based on behaviour effects, through harnessing of the 'seizure assay' which can be operated in a semi-automated analysis system (albeit none of the particle we tested induced adverse behaviour phenotypes)
- Bioavailability of the materials in the different ecotoxicity tests will likely differ due differences in NP behaviour in the different test media, that will include agglomeration and dissolution (for some metal NPs). Thus, characterisation of the NPs in the exposure systems is crucial for interpretation on any resulting biological effects.
- Isopoda offer an excellent model for assessing NP accumulation in a terrestrial animal (accumulation occurs in a specific tissue - the digestive gland cells)
- *C. elegans* offers significant potential as a model for the development of a medium throughput method to screen NPs in a liquid media.
- *C. elegans* also provides an integrated system for chronic exposure effects assessments of NPs (the life span model).
- Neuromuscular effects of NPs can also be assessed in *C. elegans* via observation of neural behaviour phenotypes (such as the process of egg-laying).

7. References

Chlamydomonas

- Adam N, Schmitt C, Galceran J, Companys E, Vakurov A, Wallace R, Knapen D, Blust R. 2014. The chronic toxicity of ZnO nanoparticles and ZnCl₂ to *Daphnia magna* and the use of different methods to assess nanoparticle aggregation and dissolution. *Nanotoxicology* 8(7):709-717.
- Bacelo J, Poschenrieder C. 2004. Struktural and ultrastruktural changes in heavy metal exposed plants. In: Prasad M, editor. *Heavy metal stress in plants, from biomolecules to ecosystems*. Berlin Heidelberg: Springer-Verlag
- Behra R, Sigg L, Clift MJD, Herzog F, Minghetti M, Johnston B, Petri-Fink A, Rothen-Rutishauser B. 2013. Bioavailability of silver nanoparticles and ions: from a chemical and biochemical perspective. *Journal of the Royal Society Interface* 10(87).
- Benetti F, Bregoli L, Olivato I, Sabbioni E. 2014. Effects of metal(loid)-based nanomaterials on essential element homeostasis: The central role of nanometallomics for nanotoxicology. *Metallomics* 6(4):729-747.
- Brooks SA, Carter TM. 2001. N-acetylgalactosamine, N-acetylglucosamine and sialic acid expression in primary breast cancers. *Acta Histochemica* 103(1):37-51.
- Burchardt AD, Carvalho RN, Valente A, Nativo P, Gilliland D, Garcia CP, Passarella R, Pedroni V, Rossi F, Lettieri T. 2012. Effects of silver nanoparticles in diatom *Thalassiosira pseudonana* and cyanobacterium *Synechococcus* sp. *Environ Sci Technol* 46(20):11336-44.
- Dewez D, Oukarroum A. 2012. Silver nanoparticles toxicity effect on photosystem II photochemistry of the green alga *Chlamydomonas reinhardtii* treated in light and dark conditions. *Toxicological and Environmental Chemistry* 94(8):1536-1546.
- Domingos RF, Rafiei Z, Monteiro CE, Khan MAK, Wilkinson KJ. 2013. Agglomeration and dissolution of zinc oxide nanoparticles: role of pH, ionic strength and fulvic acid. *Environmental Chemistry* 10(4):306-312.
- Fortin C, Campbell PGC. 2000. Silver uptake by the green alga *Chlamydomonas reinhardtii* in relation to chemical speciation: Influence of chloride. *Environmental Toxicology and Chemistry* 19(11):2769-2778.
- Franklin NM, Adams MS, Stauber JL, Lim RP. 2001. Development of an improved rapid enzyme inhibition bioassay with marine and freshwater microalgae using flow cytometry. *Archives of Environmental Contamination and Toxicology* 40(4):469-480.
- Franklin NM, Rogers NJ, Apte SC, Batley GE, Gadd GE, Casey PS. 2007. Comparative toxicity of nanoparticulate ZnO, bulk ZnO, and ZnCl₂ to a freshwater microalga (*Pseudokirchneriella subcapitata*): The importance of particle solubility. *Environmental Science & Technology* 41(24):8484-8490.
- Gottschalk F, Sun TY, Nowack B. 2013. Environmental concentrations of engineered nanomaterials: Review of modeling and analytical studies. *Environmental Pollution* 181:287-300.
- Gunawan C, Sirimanoonphan A, Teoh WY, Marquis CP, Amal R. 2013. Submicron and nano formulations of titanium dioxide and zinc oxide stimulate unique cellular toxicological responses in the green microalga *Chlamydomonas reinhardtii*. *Journal of Hazardous Materials* 260:984-992.
- Harris EH, Stern DB, Witman G. 2009. *Introduction to Chlamydomonas and its laboratory use* Harris. London:: Elsevier.
- Heinlaan M, Ivask A, Blinova I, Dubourguier HC, Kahru A. 2008. Toxicity of nanosized and bulk ZnO, CuO and TiO₂ to bacteria *Vibrio fischeri* and crustaceans *Daphnia magna* and *Thamnocephalus platyurus*. *Chemosphere* 71(7):1308-1316.
- Hessen DO, De Lange HJ, Van Donk E. 1997. UV-induced changes in phytoplankton cells and its effects on grazers. *Freshwater Biology* 38(3):513-524.
- Howe G, Merchant S. 1992. Heavy Metal-Activated Synthesis of Peptides in *Chlamydomonas-Reinhardtii*. *Plant Physiology* 98(1):127-136.
- Ivask A, Elbadawy A, Kaweeteerawat C, Boren D, Fischer H, Ji Z, Chang CH, Liu R, Tolaymat T, Telesca D and others. 2014a. Toxicity Mechanisms in *Escherichia coli* Vary for Silver Nanoparticles and Differ from Ionic Silver. *ACS Nano* 8(1):374-86.
- Ivask A, Kurvet I, Kasemets K, Blinova I, Aruoja V, Suppi S, Vija H, Kakinen A, Titma T, Heinlaan M and others. 2014b. Size-dependent toxicity of silver nanoparticles to bacteria, yeast, algae, crustaceans and Mammalian cells in vitro. *PLoS One* 9(7):e102108.
- Klein CL, Comero S, Stahlmecke B, Romazanov J, Kuhlbusch TAJ, Van Doren E, De Temmerman P-J, Mast J, Wick P, Krug H and others. 2011. NM-Series of Representative Manufactured Nanomaterials, NM-300 Silver Characterisation, Stability, Homogeneity. Ispra, Italy: European Commission Joint Research Centre

- Laban G, Nies LF, Turco RF, Bickham JW, Sepulveda MS. 2010. The effects of silver nanoparticles on fathead minnow (*Pimephales promelas*) embryos. *Ecotoxicology* 19(1):185-195.
- Leclerc S, Wilkinson KJ. 2014. Bioaccumulation of Nanosilver by *Chlamydomonas reinhardtii*-Nanoparticle or the Free Ion? *Environmental Science & Technology* 48(1):358-364.
- Li M, Lin D, Zhu L. 2013. Effects of water chemistry on the dissolution of ZnO nanoparticles and their toxicity to *Escherichia coli*. *Environ Pollut* 173:97-102.
- Lv JT, Zhang SZ, Luo L, Han W, Zhang J, Yang K, Christie P. 2012. Dissolution and Microstructural Transformation of ZnO Nanoparticles under the Influence of Phosphate. *Environmental Science & Technology* 46(13):7215-7221.
- Ma R, Levard C, Marinakos SM, Cheng YW, Liu J, Michel FM, Brown GE, Lowry GV. 2012. Size-Controlled Dissolution of Organic-Coated Silver Nanoparticles. *Environmental Science & Technology* 46(2):752-759.
- McTeer J, Dean AP, White KN, Pittman JK. 2014. Bioaccumulation of silver nanoparticles into *Daphnia magna* from a freshwater algal diet and the impact of phosphate availability. *Nanotoxicology* 8(3):305-316.
- Merdzan V, Domingos RF, Monteiro CE, Hadioui M, Wilkinson KJ. 2014. The effects of different coatings on zinc oxide nanoparticles and their influence on dissolution and bioaccumulation by the green alga, *C. reinhardtii*. *Science of the Total Environment* 488:316-324.
- Miao AJ, Luo Z, Chen CS, Chin WC, Santschi PH, Quigg A. 2010. Intracellular uptake: a possible mechanism for silver engineered nanoparticle toxicity to a freshwater alga *Ochromonas danica*. *PLoS One* 5(12):e15196.
- Miao AJ, Schwehr KA, Xu C, Zhang SJ, Luo ZP, Quigg A, Santschi PH. 2009. The algal toxicity of silver engineered nanoparticles and detoxification by exopolymeric substances. *Environmental Pollution* 157(11):3034-3041.
- Miller RJ, Lenihan HS, Muller EB, Tseng N, Hanna SK, Keller AA. 2010. Impacts of Metal Oxide Nanoparticles on Marine Phytoplankton. *Environmental Science & Technology* 44(19):7329-7334.
- Muysen BTA, Janssen CR. 2001. Zinc acclimation and its effect on the zinc tolerance of *Raphidocelis subcapitata* and *Chlorella vulgaris* in laboratory experiments. *Chemosphere* 45(4-5):507-514.
- Navarro E, Piccapietra F, Wagner B, Marconi F, Kaegi R, Odzak N, Sigg L, Behra R. 2008. Toxicity of silver nanoparticles to *Chlamydomonas reinhardtii*. *Environ Sci Technol* 42(23):8959-64.
- Piccapietra F, Allue CG, Sigg L, Behra R. 2012. Intracellular Silver Accumulation in *Chlamydomonas reinhardtii* upon Exposure to Carbonate Coated Silver Nanoparticles and Silver Nitrate. *Environmental Science & Technology* 46(13):7390-7397.
- Pillai S, Behra R, Nestler H, Suter MJF, Sigg L, Schirmer K. 2014. Linking toxicity and adaptive responses across the transcriptome, proteome, and phenotype of *Chlamydomonas reinhardtii* exposed to silver. *Proceedings of the National Academy of Sciences of the United States of America* 111(9):3490-3495.
- Pletikapic G, Zutic V, Vrcek IV, Svetlicic V. 2012. Atomic force microscopy characterization of silver nanoparticles interactions with marine diatom cells and extracellular polymeric substance. *Journal of Molecular Recognition* 25(5):309-317.
- Quigg A, Chin W-C, Chen C-S, Zhang S, Jiang Y, Miao A-J, Schwehr KA, Xu C, Santschi PH. 2013. Direct and Indirect Toxic Effects of Engineered Nanoparticles on Algae: Role of Natural Organic Matter. *Sustainable Chem. Eng.*, 1(7):686-702.
- Ribeiro F, Gallego-Urrea JA, Jurkschat K, Crossley A, Hasselov M, Taylor C, Soares AM, Loureiro S. 2014. Silver nanoparticles and silver nitrate induce high toxicity to *Pseudokirchneriella subcapitata*, *Daphnia magna* and *Danio rerio*. *Sci Total Environ* 466-467:232-41.
- Soliz M, Odermatt A. 1995. Copper and silver transport by CopB-ATPase in membrane vesicles of *Enterococcus hirae*. *J Biol Chem* 270(16):9217-21.
- Sorensen SN, Baun A. 2014. Controlling silver nanoparticle exposure in algal toxicity testing - A matter of timing. *Nanotoxicology*:1-9.
- Stevenson LM, Dickson H, Klanjscek T, Keller AA, McCauley E, Nisbet RM. 2013. Environmental Feedbacks and Engineered Nanoparticles: Mitigation of Silver Nanoparticle Toxicity to *Chlamydomonas reinhardtii* by Algal-Produced Organic Compounds. *Plos One* 8(9).
- Thio BJR, Montes MO, Mahmoud MA, Lee DW, Zhou DX, Keller AA. 2012. Mobility of Capped Silver Nanoparticles under Environmentally Relevant Conditions. *Environmental Science & Technology* 46(13):6985-6991.
- Tierbach A. 2014. Mechanistic and systematic understanding of the toxicity of CeO₂ nanoparticles in the algae *Chlamydomonas reinhardtii*. Duebendorf, Switzerland: Eawag, Swiss Federal Institute of Aquatic Science and Technology.
- Turner A, Brice D, Brown MT. 2012. Interactions of silver nanoparticles with the marine macroalga, *Ulva lactuca*. *Ecotoxicology* 21(1):148-154.
- Vandonk E, Hessen DO. 1995. Reduced Digestibility of Uv-B Stressed and Nutrient-Limited Algae by *Daphnia-Magna*. *Hydrobiologia* 307(1-3):147-151.



- Waalewijn-Kool PL, Diez Ortiz M, van Straalen NM, van Gestel CA. 2013. Sorption, dissolution and pH determine the long-term equilibration and toxicity of coated and uncoated ZnO nanoparticles in soil. *Environ Pollut* 178:59-64.
- Wang Z, Chen JW, Li XH, Shao JP, Peijnenburg WJGM. 2012. Aquatic toxicity of nanosilver colloids to different trophic organisms: Contributions of particles and free silver ion. *Environmental Toxicology and Chemistry* 31(10):2408-2413.

Zebrafish

- Asharani, P. V., L. Yi, Z. Gong and S. Valiyaveetil (2011). "Comparison of the toxicity of silver, gold and platinum nanoparticles in developing zebrafish embryos." *Nanotoxicology* 5(1): 43-54.
- Asharani, P. V., Y. L. Wu, Z. Y. Gong and S. Valiyaveetil (2008). "Toxicity of silver nanoparticles in zebrafish models." *Nanotechnology* 19(25).
- Alshut R, Legradi J, Liebel U, Yang L, Wezel J, Strähle U, Mikut R, Reischl M (2010) Methods for Automated High-Throughput Toxicity Testing Using Zebrafish Embryos. In: *KI 2010: Advances in Artificial Intelligence*, vol. 6359 (Dillmann, R. et al., eds), pp 219-226: Springer Berlin Heidelberg.
- Baraban, S.C., Taylor, M.R., Castro, P.A., Baier, H., 2005. Pentylentetrazole induced changes in zebrafish behavior, neural activity and c-fos expression. *Neuroscience* 131, 759-768.
- Bilberg, K., M. B. Hovgaard, F. Besenbacher and E. Baatrup (2012). "In Vivo Toxicity of Silver Nanoparticles and Silver Ions in Zebrafish (*Danio rerio*)." *Journal of Toxicology* 2012.
- Browning, L. M., K. J. Lee, T. Huang, P. D. Nallathamby, J. E. Lowman and X. H. N. Xu (2009). "Random walk of single gold nanoparticles in zebrafish embryos leading to stochastic toxic effects on embryonic developments." *Nanoscale* 1(1): 138-152.
- Choi, J. E., S. Kim, J. H. Ahn, P. Youn, J. S. Kang, K. Park, J. Yi and D.-Y. Ryu (2010). "Induction of oxidative stress and apoptosis by silver nanoparticles in the liver of adult zebrafish." *Aquatic Toxicology* 100(2): 151-159.
- Cunningham S, Brennan-Fournet ME, Ledwith D, Byrnes L, Joshi L (2013) Effect of nanoparticle stabilization and physicochemical properties on exposure outcome: acute toxicity of silver nanoparticle preparations in zebrafish (*Danio rerio*). *Environ Sci Technol* 47:3883-3892.
- Hagedorn, M., F. W. Kleinhans, D. Artemov and U. Pilatus (1998). "Characterization of a major permeability barrier in the zebrafish embryo." *Biol Reprod* 59(5): 1240-1250.
- Hagedorn, M., F. W. Kleinhans, R. Freitas, J. Liu, E. W. Hsu, D. E. Wildt and W. F. Rall (1997). "Water distribution and permeability of zebrafish embryos, *Brachydanio rerio*." *J Exp Zool* 278(6): 356-371.
- Harper SL, Carriere JL, Miller JM, Hutchison JE, Maddux BL, Tanguay RL (2011) Systematic evaluation of nanomaterial toxicity: utility of standardized materials and rapid assays. *ACS Nano* 5:4688-4697.
- Jemec A, Djinovic P, Crnivec IG, Pintar A (2015) The hazard assessment of nanostructured CeO₂-based mixed oxides on the zebrafish *Danio rerio* under environmentally relevant UV-A exposure. *Sci Total Environ* 506-507:272-278.
- Jemec A, Djinovic P, Tisler T, Pintar A (2012) Effects of four CeO₂ nanocrystalline catalysts on early-life stages of zebrafish *Danio rerio* and crustacean *Daphnia magna*. *J Hazard Mater* 219-220:213-220.
- Kim, D.-H., Y. Sun, Y. Seok, S. Ho Lee and B. Kim "Investigating chorion softening of zebrafish embryos with a microrobotic force sensing system." *Journal of Biomechanics* 38(6): 1359-1363
- Kimmel CB, Ballard WW, Kimmel SR, Ullmann B, Schilling TF (1995) Stages of embryonic development of the zebrafish. *Dev Dyn* 203:253-310.



- Lavoie, N., M. R. Peralta, M. Chiasson, K. Lafortune, L. Pellegrini, L. Seress and K. Tóth (2007). "Extracellular chelation of zinc does not affect hippocampal excitability and seizure-induced cell death in rats." *The Journal of Physiology* 578(1): 275-289.
- Lee, K. J., P. D. Nallathamby, L. M. Browning, C. J. Osgood and X.-H. N. Xu (2007). "In vivo imaging of transport and biocompatibility of single silver nanoparticles in early development of zebrafish embryos." *ACS Nano* 1(2): 133-143.
- Lin S, Zhao Y, Ji Z, Ear J, Chang CH, Zhang H, Low-Kam C, Yamada K, Meng H, Wang X, Liu R, Pokhrel S, Madler L, Damoiseaux R, Xia T, Godwin HA, Nel AE (2013) Zebrafish high-throughput screening to study the impact of dissolvable metal oxide nanoparticles on the hatching enzyme, ZHE1. *Small* 9:1776-1785.
- Mikut R, Dickmeis T, Driever W, Geurts P, Hamprecht FA, Kausler BX, Ledesma-Carbayo MJ, Maree R, Mikula K, Pantazis P, Ronneberger O, Santos A, Stotzka R, Strahle U, Peyrieras N (2013) Automated Processing of Zebrafish Imaging Data: A Survey. *Zebrafish*.
- Morris, D. R. and C. W. Levenson (2012). "Ion channels and zinc: mechanisms of neurotoxicity and neurodegeneration." *J Toxicol* 2012: 785647.
- Osborne, O. J., B. D. Johnston, J. Moger, M. Balousha, J. R. Lead, T. Kudoh and C. R. Tyler (2013). "Effects of particle size and coating on nanoscale Ag and TiO₂ exposure in zebrafish (*Danio rerio*) embryos." *Nanotoxicology* 7(8): 1315-1324.
- Shaw BJ, Handy RD (2011) Physiological effects of nanoparticles on fish: a comparison of nanometals versus metal ions. *Environ Int* 37:1083-1097.
- van Aerle, R., A. Lange, A. Moorhouse, K. Paszkiewicz, K. Ball, B. D. Johnston, E. de-Bastos, T. Booth, C. R. Tyler and E. M. Santos (2013). "Molecular Mechanisms of Toxicity of Silver Nanoparticles in Zebrafish Embryos." *Environmental Science & Technology* 47(14): 8005-8014.
- Van Hoecke K, Quik JT, Mankiewicz-Boczek J, De Schamphelaere KA, Elsaesser A, Van der Meeren P, Barnes C, McKerr G, Howard CV, Van de Meent D, Ryzdzynski K, Dawson KA, Salvati A, Lesniak A, Lynch I, Silversmit G, De Samber B, Vincze L, Janssen CR (2009) Fate and effects of CeO₂ nanoparticles in aquatic ecotoxicity tests. *Environ Sci Technol* 43:4537-4546.
- Westerfield M (1995) *The Zebrafish Book*. Eugene, OR: University of Oregon Press.
- Yang L, Ho NY, Alshut R, Legradi J, Weiss C, Reischl M, Mikut R, Liebel U, Muller F, Strahle U (2009) Zebrafish embryos as models for embryotoxic and teratological effects of chemicals. *Reprod Toxicol* 28:245-253.
- Winter, M.J., Redfern, W.S., Hayfield, A.J., Owen, S.F., Valentin, J.-P., Hutchinson, T.H., 2008. Validation of a larval zebrafish locomotor assay for assessing the seizure liability of early-stage development drugs. *Journal of Pharmacological and Toxicological Methods* 57, 176-187.
- Zhu, X. S., L. Zhu, Z. H. Duan, R. Q. Qi, Y. Li and Y. P. Lang (2008). "Comparative toxicity of several metal oxide nanoparticle aqueous suspensions to Zebrafish (*Danio rerio*) early developmental stage." *Journal of Environmental Science and Health Part a-Toxic/Hazardous Substances & Environmental Engineering* 43(3): 278-284.
- Zhu, X. S., L. Zhu, Y. Li, Z. H. Duan, W. Chen and P. J. J. Alvarez (2007). "Developmental toxicity in zebrafish (*Danio rerio*) embryos after exposure to manufactured nanomaterials: Buckminsterfullerene aggregates (nC(60)) and fullerol." *Environmental Toxicology and Chemistry* 26(5): 976-979.

Soil Invertebrates

CEB Method 230: Method for Evaluation of the Impact of Plant Protection Products on Honeybees, 2012

DECOURTYE A, DEVILLERS J, GENECQUE E, LE MENACH K, BUDZINSKI H, CLUZEAU S AND PHAM-DELEGUE MH (2005). Comparative sublethal toxicity of nine pesticides on olfactory learning performances of the honeybee *Apis mellifera*. *Archives of Environmental Contamination and Toxicology* 2005; 48: 242-250



- DUNGER, W. (1964). Regenwürmer, Lumbriciden. In Tiere im Boden. A. Ziemsen Verlag, Wittenberg, Germany. pp. 70–83.
- HOPKIN SP (1997). Biology of the Springtails (Insecta : Collembola). Oxford University Press. 330pp (ISBN 0-19-854084-1).
- KARG, W. (1993): Acari (Acarina), Milben Parasitiformes (Anactinochaeta), Cohors Gamasina Leach, Raubmilben, Die Tierwelt Deutschlands, 59. Teil; Gustav Fischer Verlag: Jena, Germany: 1993; pp 11-51.
- LEE, K.E. (1985). Earthworms — Their ecology and relationships with soils and land use. Academic Press, Sydney, Australia. pp. 411.
- McFadyen, A. Improved Funnel-Type Extractors for Soil Arthropods. J. Anim. Ecol. 1961; 30: 171-184
- OECD Guideline for the testing of chemicals No. 213; Honey bees; acute oral toxicity test. 1998
- OECD Guideline for the testing of chemicals No. 214; Honey bees; acute contact toxicity test. 1998
- OEPP/EPPO Guideline for the efficacy evaluation of plant protection products – Side effects on honeybees. OEPP/EPPO, PP 1/170 (4) update 2000, 19 - 23.
- OECD Guideline for the testing of chemicals No. 222 'Earthworm Reproduction Test (*Eisenia fetida/andrei*)'. Adopted: 13. April 2004.
- OECD Guideline for the testing of chemicals No. 226 "Predatory mite (*Hypoaspis (Geolaelaps) aculeifer*) reproduction test in soil"; Adopted: 3 October 2008.
- OECD Guideline for the testing of chemicals No. 232'Collembolan Reproduction Test in Soil'; Adopted: 7 September 2009.
- PONGE, J.F., AND DELHAYE, L. (1995). The heterogeneity of humus profiles and earthworm communities in a virgin beech forest. Biol. Fertil. Soils, 20: 24–32.
- RONDE, G. (1960). Regenwürmer süddeutscher Waldböden. Allg. Forstztg. 15: 265–269.
- RUF, A. (1991): Do females eat males?: Laboratory studies on the population development of *Hypoaspis aculeifer* (Acari: Parasitiformes). In: F. Dusbabek & V. Bukva (eds.): Modern Acarology. Academia Prague & SPD Academic Publishing, The Hague, Vol. 2, 487-492.
- RUF, A. (1995): Sex ratio and clutch size control in the soil inhabiting predatory mite *Hypoaspis aculeifer* (Canestrini 1883) (Mesostigmata, Dermanyssidae). Proc. 2nd Symp. EURAAC: p 241-249.
- RUF, A. (1996): Life-history patterns in soil-inhabiting mesostigmatid mites. Proc. IXth Internat. Congr. Acarol. 1994, Columbus, Ohio: p 621-628.
- SAS SOFTWARE, VERSION 9.1 OF THE SAS SYSTEM FOR WINDOWS. COPYRIGHT © 2002-2003 SAS INSTITUTE INC. SAS AND ALL OTHER SAS INSTITUTE INC. PRODUCT OR SERVICE NAMES ARE REGISTERED TRADEMARKS OF SAS INSTITUTE INC., CARY, NC, USA.
- SATCHELL, J.E. (1983). Earthworm ecology in forest soil. In Earthworm ecology — from Darwin to vermiculture. Edited by J.E. Satchell. Chapman and Hall, London, UK. pp. 161–170.
- Schneider-Orelli, O. Entomologisches Praktikum. H.R. Sauerländer & Co., Aarau, 2. Auflage 1947; [Schneider-Orelli, O. Entomological Practical Course. H.R. Sauerländer & Co., Aarau, 2nd Edition 1947].
- ToxRat Solutions GmbH, ToxRat Professional 2.10.
- ULBER B (1983). Einfluss von *Onychiurus fimatus* Gisin (Collembola, Onychiuridae) und *Folsomia fimetaria* L. (Collembola, Isotomidae) auf *Pythium ultimum* Trow. einen Erreger des Wurzelbrandes der Zuckerrübe. In New trends in soil Biology (Lebrun Ph, André HM, De Medts A, Grégoire-Wibo, Wauthy G (Eds), Proceedings of the VI. international colloquium on soil zoology, Louvain-la-neuve (Belgium), 30 August-2 September 1982, I Dieu-Brichart, Ottignies-Louvain-la-Neuve, pp. 261-268.



Van der Steen, J. (): Review of the methods to determine the hazard and toxicity of pesticides to bumble bees. *Apidologie* 2001; 32: 399-406.

WILCKE, D.E. (1953). Über die vertikale Verteilung der Lumbriciden im Boden. *Z. Morph. Ökol. Tiere*, 41: 372–385.

Zicsi, A. (1968). Ein zusammenfassendes Verbreitungsbild der Regenwürmer auf Grund der Boden- und Vegetationsverhältnisse Ungarns. *Opusc. Zool. (Budap)*. 8: 99–164.

Isopods

Drobne D. 1997. Terrestrial isopods - A good choice for toxicity testing of pollutants in the terrestrial environment. *Environmental Toxicology and Chemistry* 16: 1159-1164

Drobne D., Blazic M., Van Gestel C. A. M., Leser V., Zidar P., Jemec A. and Trebse P. 2008. Toxicity of imidacloprid to the terrestrial isopod *Porcellio scaber* (Isopoda, Crustacea). *Chemosphere* 71: 1326-1334

Drobne D. and Hopkin S. P. 1994. Ecotoxicological Laboratory Test for Assessing the Effects of Chemicals on Terrestrial Isopods. *Bulletin of Environmental Contamination and Toxicology* 53: 390-397

Drobne D. and Hopkin S. P. 1995. The Toxicity of Zinc to Terrestrial Isopods in a Standard Laboratory Test. *Ecotoxicology and Environmental Safety* 31: 1-6

Hames C. A. C. and Hopkin S. P. 1989. The Structure and Function of the Digestive-System of Terrestrial Isopods. *Journal of Zoology* 217: 599-627

Jemec A., Drobne D., Remskar M., Sepcic K. and Tisler T. 2008. Effects of ingested nano-sized titanium dioxide on terrestrial isopods (*Porcellio scaber*). *Environmental Toxicology and Chemistry* 27: 1904-1914

Jereb V., Horvat M., Drobne D. and Pihlar B. 2003. Transformations of mercury in the terrestrial isopod *Porcellio scaber* (Crustacea). *Science of the Total Environment* 304: 269-284

Pipan-Tkalec Z., Drobne D., Jemec A., Romih T., Zidar P. and Bele M. 2010. Zinc bioaccumulation in a terrestrial invertebrate fed a diet treated with particulate ZnO or ZnCl₂ solution. *Toxicology* 269: 198-203

Pipan Tkalec Ž., Drobne D., Vogel-Mikuš K., Pongrac P., Regvar M., Štrus J., Pelicon P., Vavpetič P., Grlj N. and Remškar M. 2011. Micro-PIXE study of Ag in digestive glands of a nano-Ag fed arthropod (*Porcellio scaber*, Isopoda, Crustacea). *Nuclear Instruments and Methods in Physics Research Section B: Beam Interactions with Materials and Atoms* -: -

Valant J., Drobne D., Sepcic K., Jemec A., Kogej K. and Kostanjsek R. 2009. Hazardous potential of manufactured nanoparticles identified by in vivo assay. *Journal of Hazardous Materials* 171: 160-165

C. elegans

Herndon LA, Schmeissner PJ, Dudaronek JM, Brown PA, Listner KM, Sakano Y, Paupard MC, Hall DH, Driscoll M. Stochastic and genetic factors influence tissue-specific decline in ageing *C. elegans*. *Nature* 2002; 419: 808-814.

Huang C, Xiong C, Kornfeld K. Measurements of age-related changes of physiological processes that predict lifespan of *Caenorhabditis elegans*. *Proc Natl Acad Sci USA* 2004; 101: 8084–8089.

Kaletta T, Hengartner MO. Finding function in novel targets: *C. elegans* as a model organism. *Nat Rev Drug Discov*. 2006; 5: 387-398.

Kiontke K, Sudhaus W. Ecology of *Caenorhabditis* species. *WormBook*. 2006; 9: 1-14.



Meyer D, Williams PL. Toxicity testing of neurotoxic pesticides in *Caenorhabditis elegans*. J Toxicol Environ Health B Crit Rev 17: 284-306.

Petraschek M, Ye X, Buck L. An antidepressant that extends lifespan in adult *Caenorhabditis elegans*. Nature 2007; 450: 553-557.

Pluskota A, Horzowski E, Bossinger O, von Mikecz A. In *Caenorhabditis elegans* Nanoparticle-Bio-Interactions Become Transparent: Silica-Nanoparticles Induce Reproductive Senescence. PLoS One 2009; 4: e6622.

Roh JY, Sim SJ, Yi J, Park K, Chung KH, Ryu DY, Choi J. Ecotoxicity of silver nanoparticles on the soil nematode *Caenorhabditis elegans* using functional ecotoxicogenomics. Environ. Sci. Technol. 2009; 43: 3933–3940.

Sakaue Y, Kim J, Miyamoto Y. Effects of TAT-conjugated nanoparticles on lifespan of mitochondrial electron transport complex-1 deficient *Caenorhabditis elegans* nuo-1. Int J Nanomedicine 2010; 5: 687-695.

Schafer WR. Deciphering the neural and molecular mechanisms of *C. elegans* behavior. Current Biology 2005; 15: R723-729.

Scharf A, Piechulek A, von Mikecz A. Effect of nanoparticles on the biochemical and behavioral aging phenotype of the nematode *Caenorhabditis elegans*. ACS Nano. 2013; 7: 10695-106703.

Vidal-Gadea A, Topper S, Young L, Crisp A, Kressin L, Elbel E, Maples T, Brauner M, Erbguth K, Axelrod A, Gottschalk A, Siegel D, Pierce-Shimomura JT. *Caenorhabditis elegans* selects distinct crawling and swimming gaits via dopamine and serotonin. Proc Natl Acad Sci U S A. 2011; 108: 17504-17509.

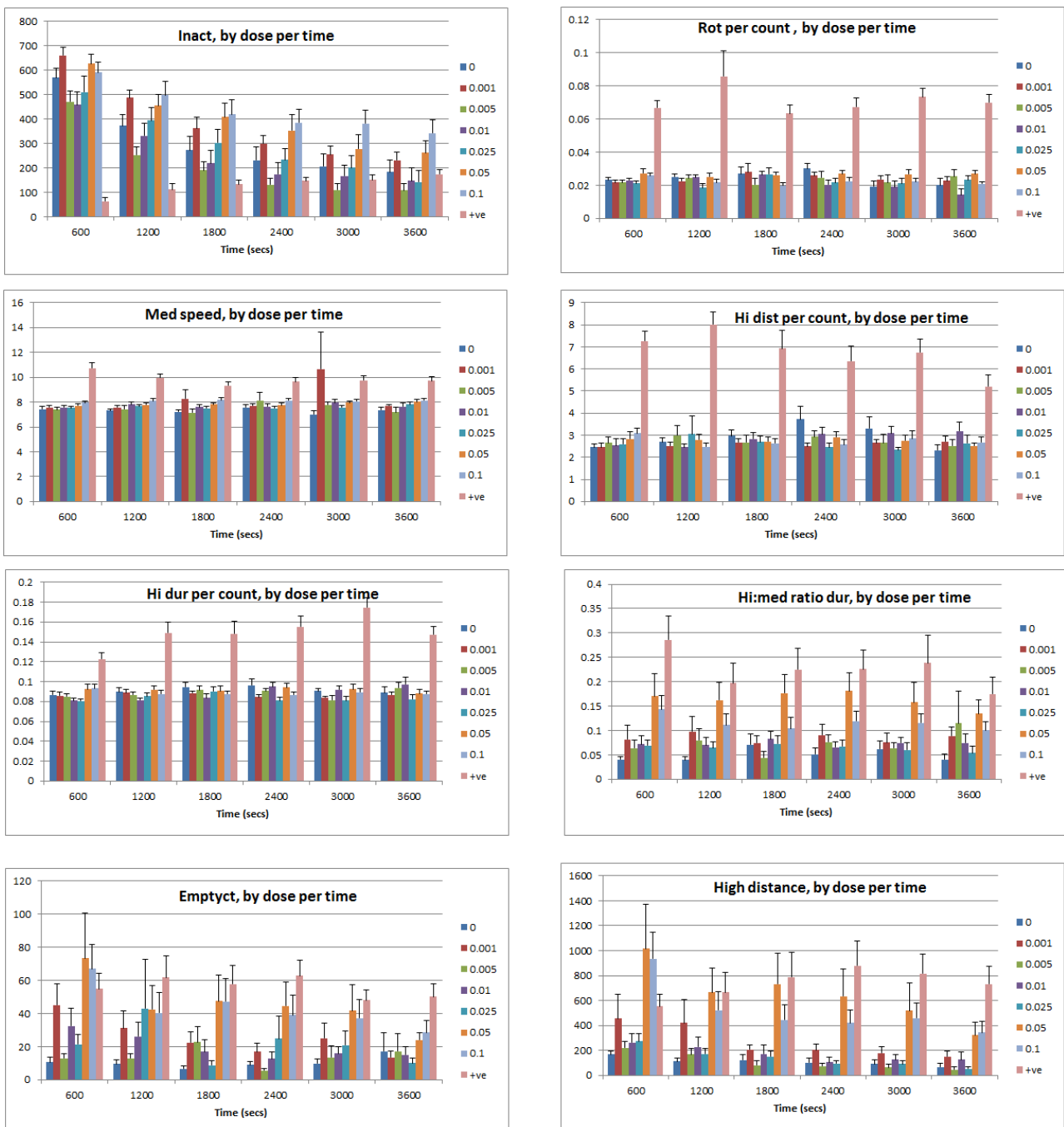
Zhang H, He X, Zhang Z, Zhang P, Li Y, Ma Y, Kuang Y, Zhao Y, Chai Z. Nano-CeO₂ exhibits adverse effects at environmental relevant concentrations. Environ Sci Technol. 2011; 45: 3725-3730.

8. Appendix I

Zebrafish Behaviour (Seizure) Assay

Figure S1. Silver nitrate a) activity graphs showing concentration response curves during each time interval, across the 1 hour recording period. b) activity graphs showing concentration response curves averaged across all time points by animal. 0 = negative control, +ve = PTZ positive control, 0.001 represents $10 \mu\text{g L}^{-1}$ with the concentration increasing $50 \mu\text{g L}^{-1}$ (0.005), $100 \mu\text{g L}^{-1}$ (0.01), $250 \mu\text{g L}^{-1}$ (0.025), $500 \mu\text{g L}^{-1}$ (0.05) up to $1000 \mu\text{g L}^{-1}$ (0.1)

a)



b)

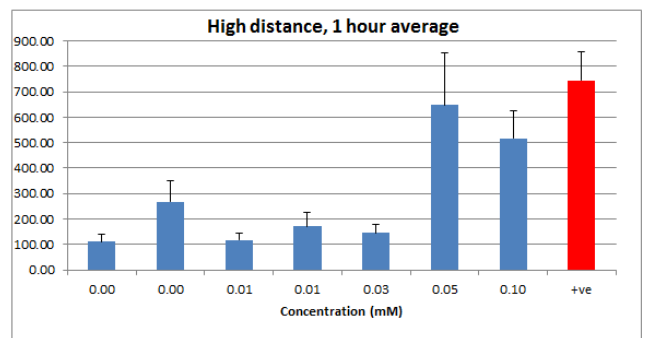
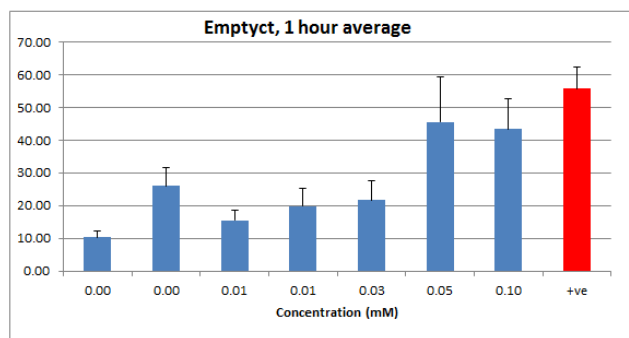
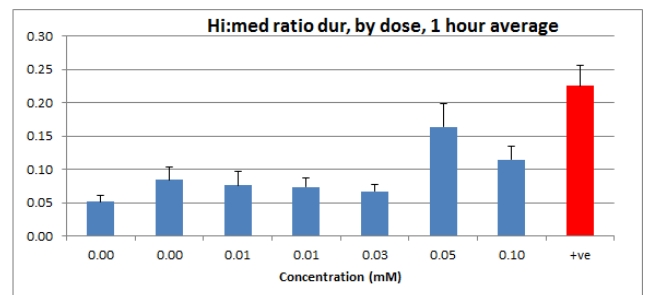
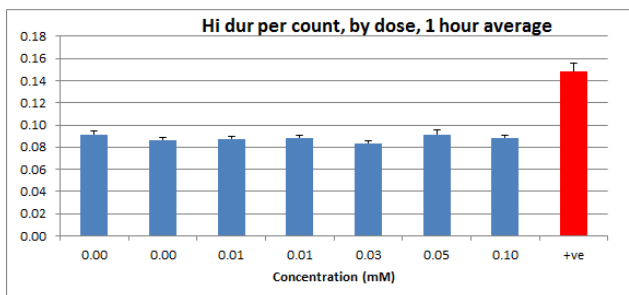
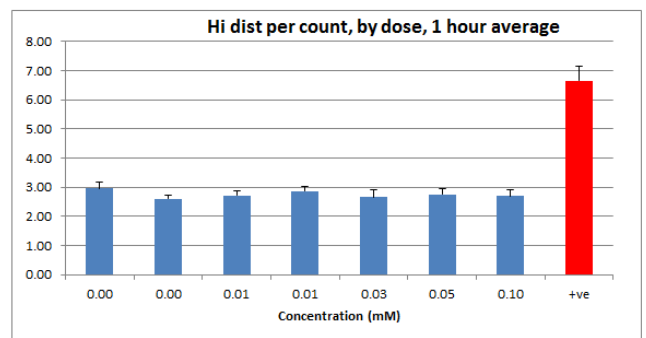
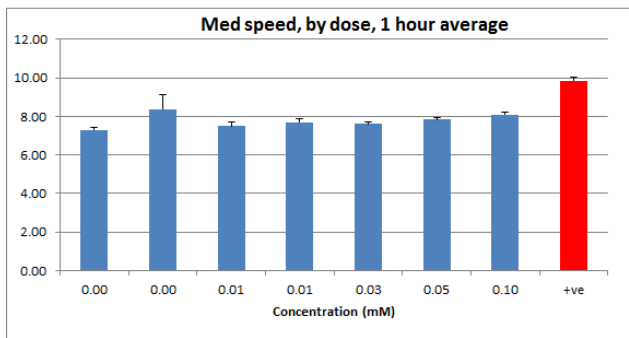
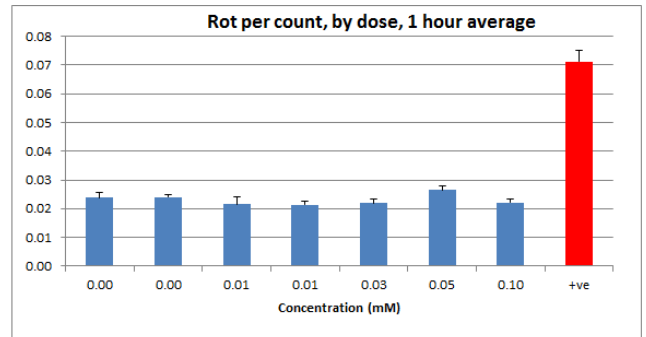
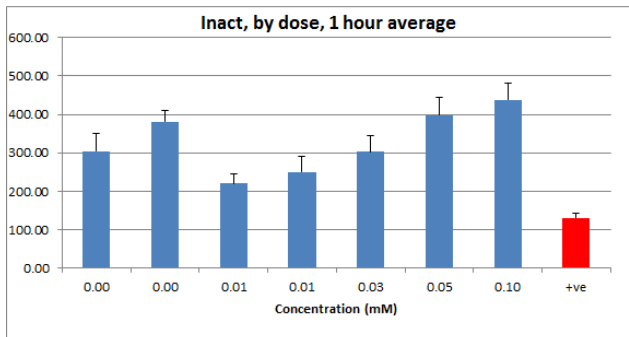


Figure S2. Ag NM300k activity graphs showing concentration response curves during each time interval, across the 1 hour recording period. Activity graphs showing concentration response curves averaged across all time points by animal are presented in the main deliverable report. 0 = negative control, +ve = PTZ positive control, 0.001 represents $10 \mu\text{g L}^{-1}$ with the concentration increasing $50 \mu\text{g L}^{-1}$ (0.005), $100 \mu\text{g L}^{-1}$ (0.01), $250 \mu\text{g L}^{-1}$ (0.025), $500 \mu\text{g L}^{-1}$ (0.05) up to $1000 \mu\text{g L}^{-1}$ (0.1)

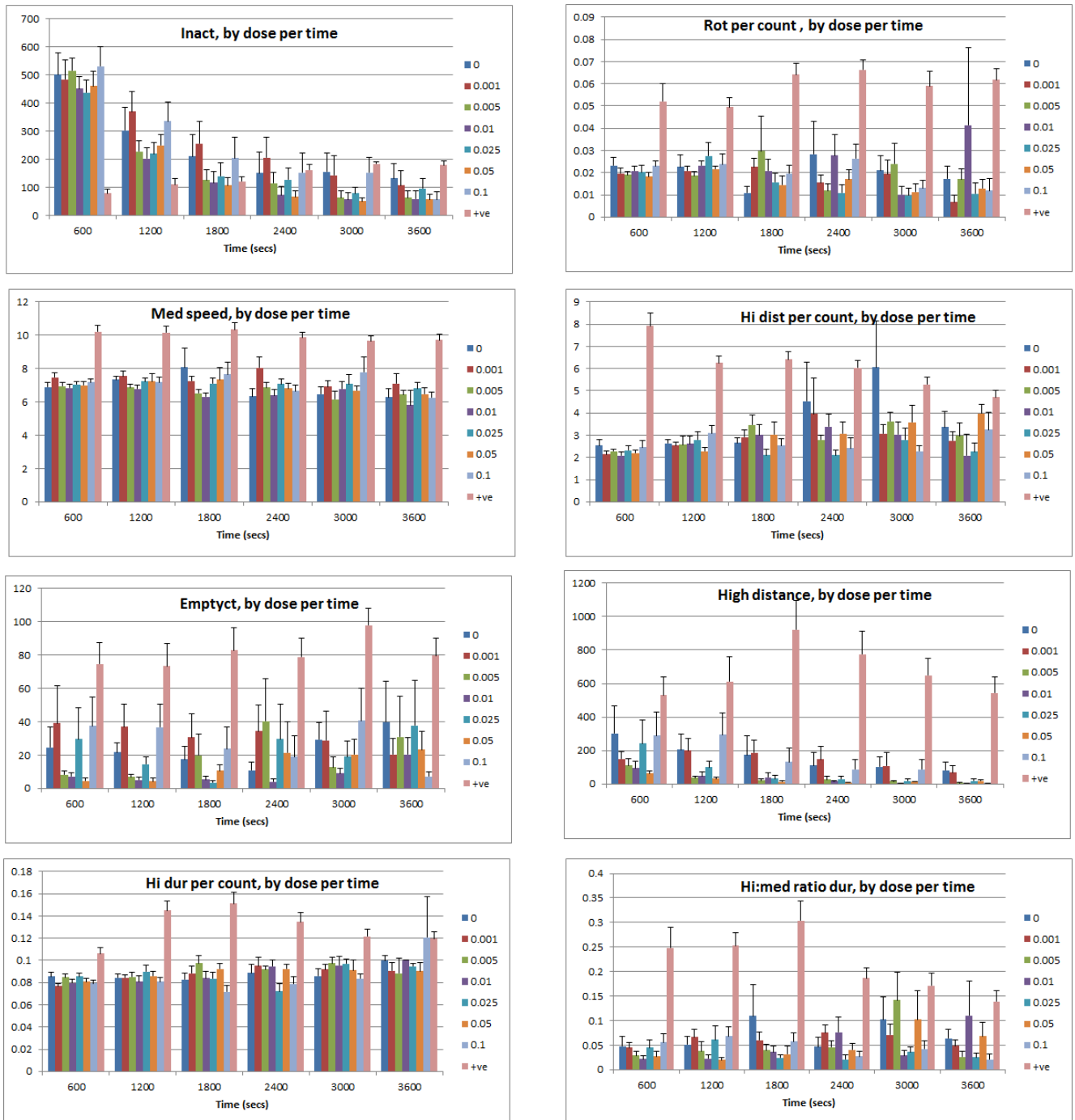
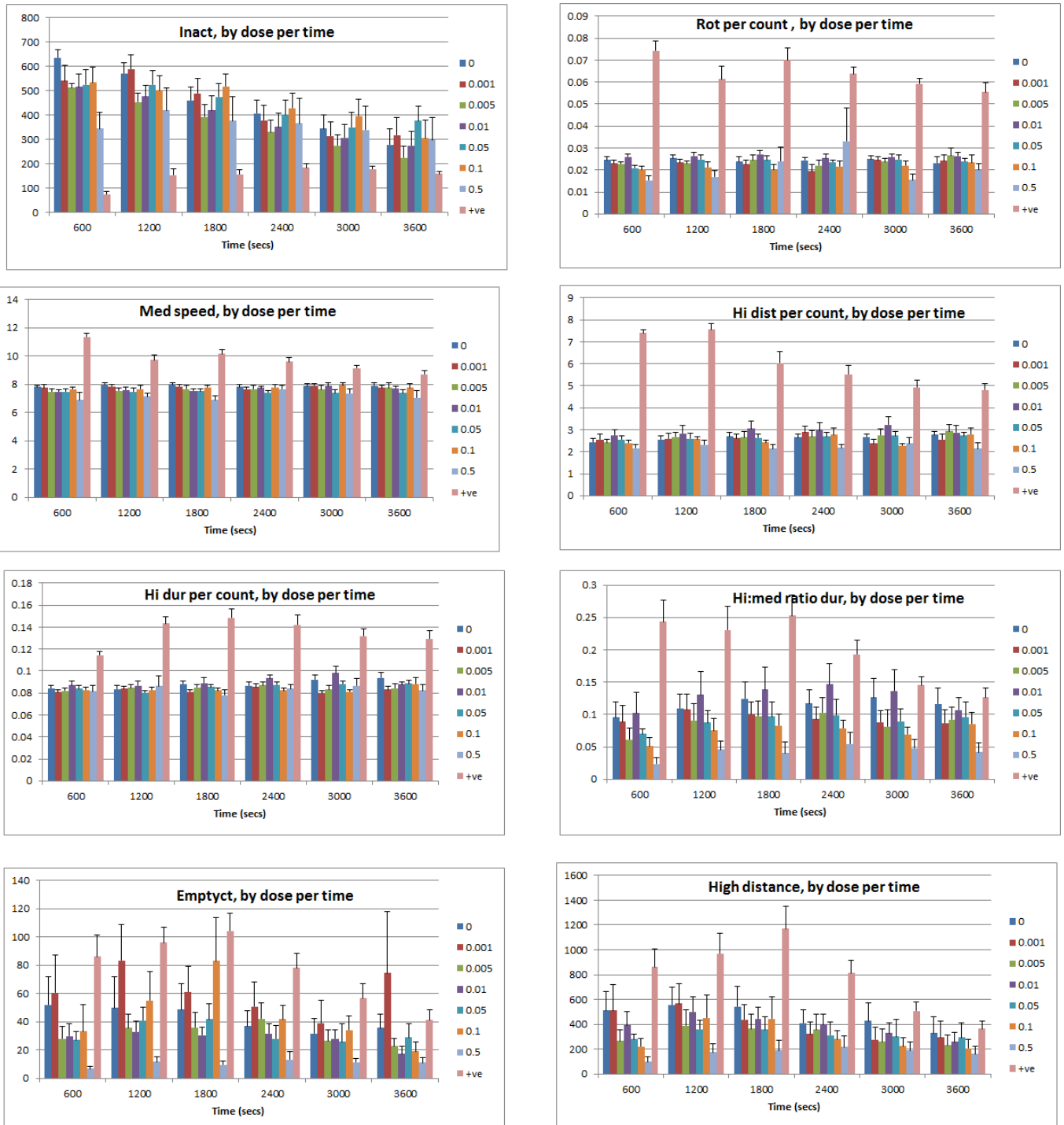


Figure S3. 7 nm citrate coated Ag NP (AgCit-7nm), a) activity graphs showing concentration response curves during each time interval, across the 1 hour recording period. b) activity graphs showing concentration response curves averaged across all time points by animal. 0 = negative control, +ve = PTZ positive control, 0.001 represents $1 \mu\text{g L}^{-1}$ with the concentration increasing $5 \mu\text{g L}^{-1}$ (0.005), $10 \mu\text{g L}^{-1}$ (0.01), $50 \mu\text{g L}^{-1}$ (0.05), $100 \mu\text{g L}^{-1}$ (0.1) up to $500 \mu\text{g L}^{-1}$ (0.5)

a)



b)

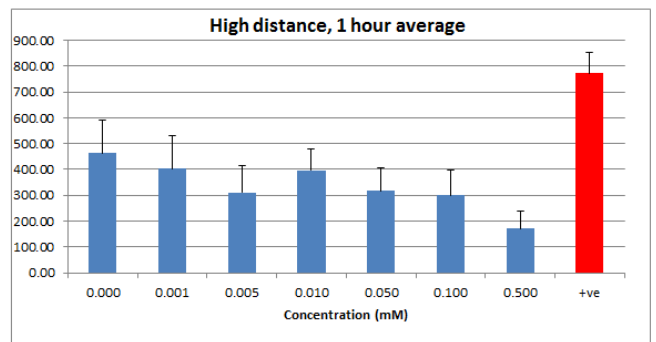
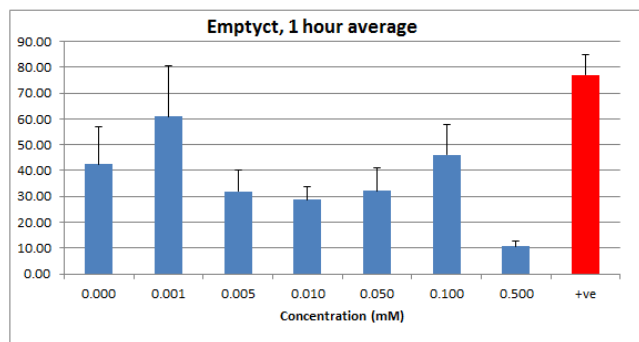
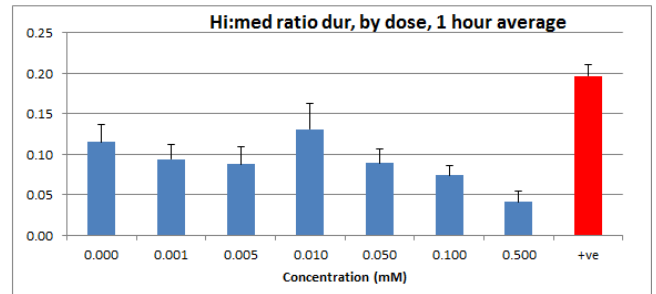
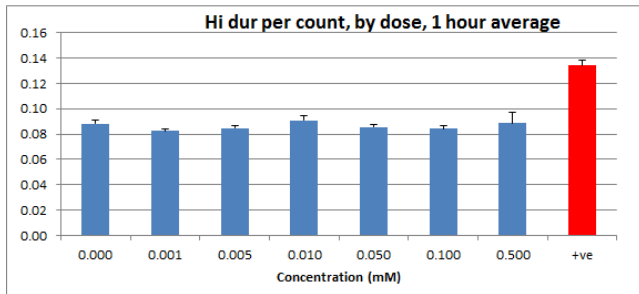
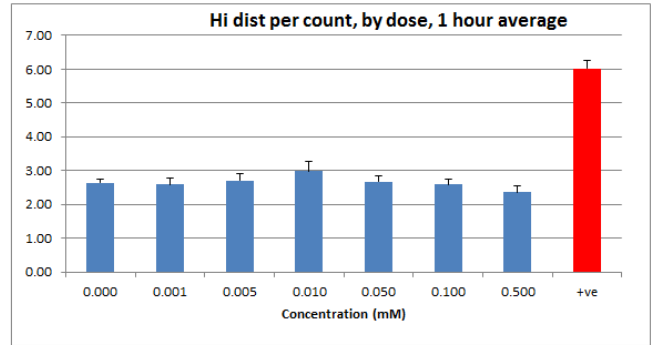
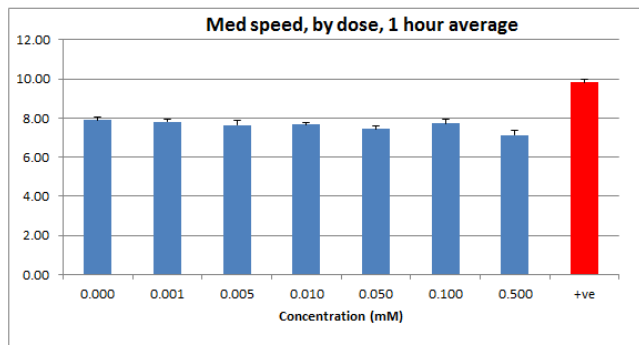
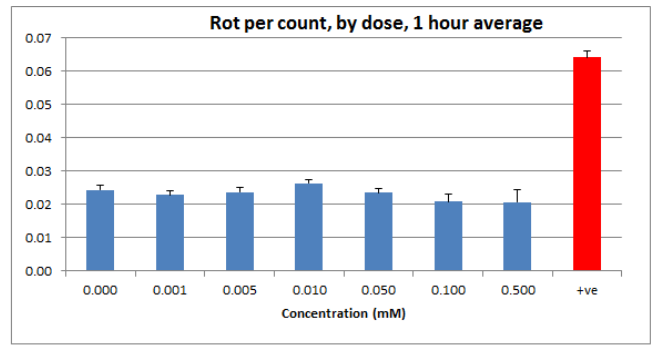
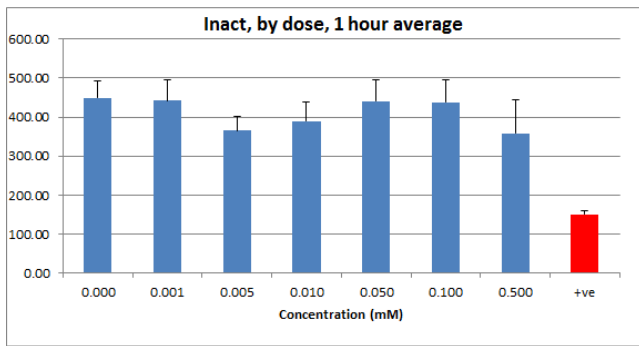
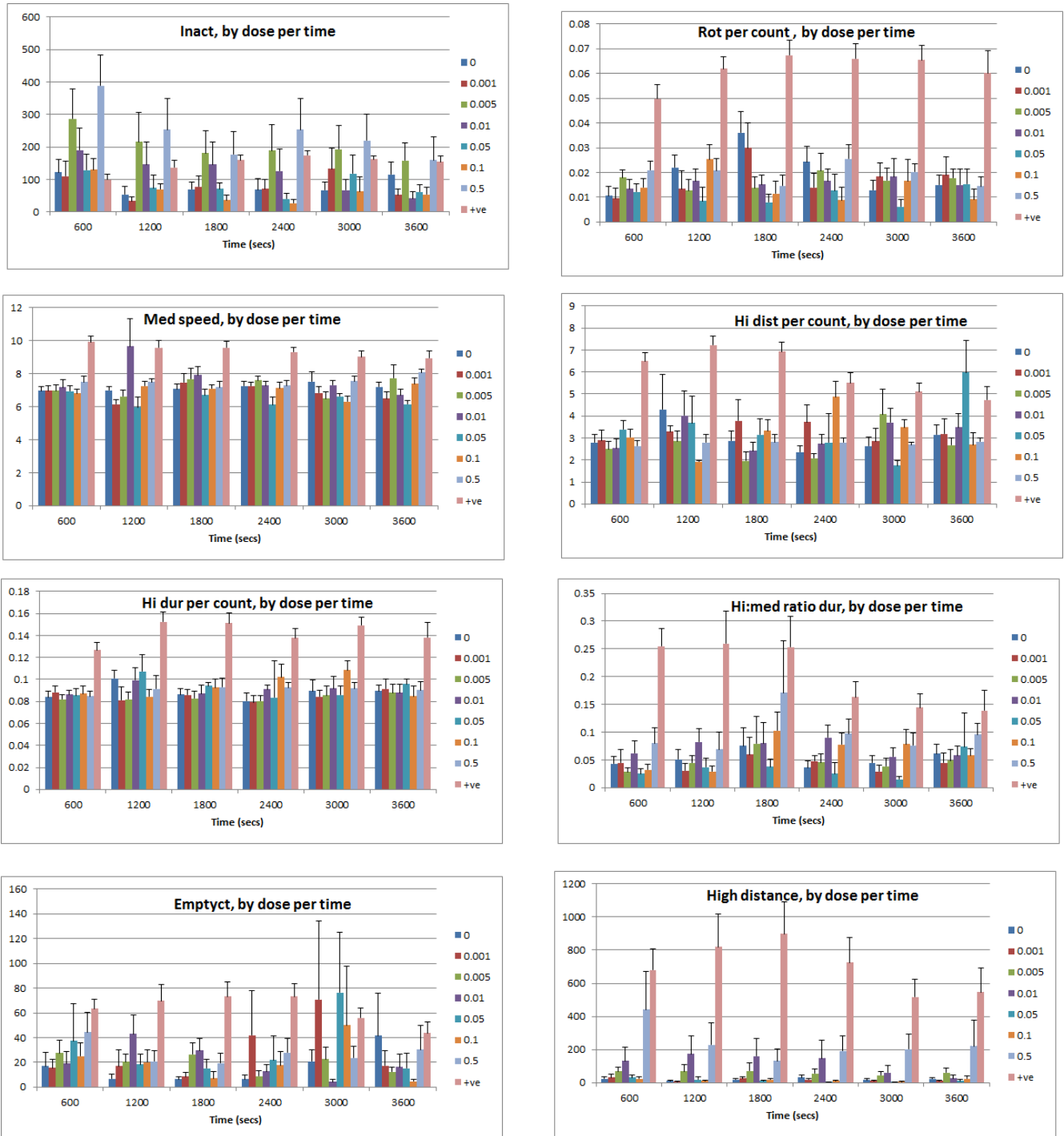


Figure S4. citrate coated Ag bulk particles(AgCit), a) activity graphs showing concentration response curves during each time interval, across the 1 hour recording period. b) activity graphs showing concentration response curves averaged across all time points by animal. 0 = negative control, +ve = PTZ positive control, 0.001 represents $1 \mu\text{g L}^{-1}$ with the concentration increasing $5 \mu\text{g L}^{-1}$ (0.005), $10 \mu\text{g L}^{-1}$ (0.01), $50 \mu\text{g L}^{-1}$ (0.05), $100 \mu\text{g L}^{-1}$ (0.1) up to $500 \mu\text{g L}^{-1}$ (0.5)

a)



b)

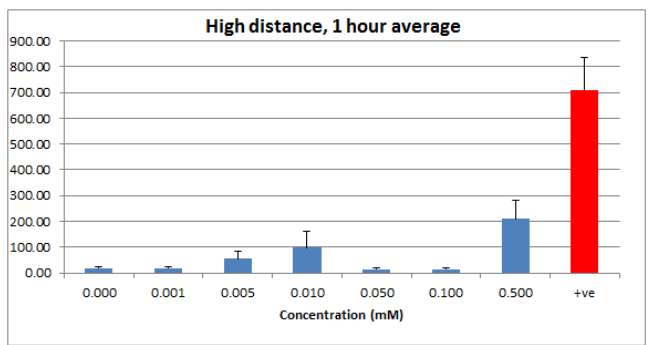
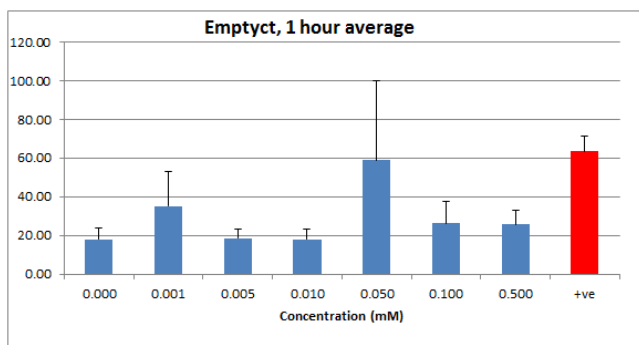
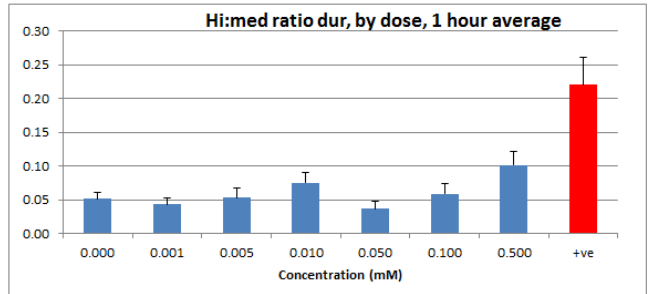
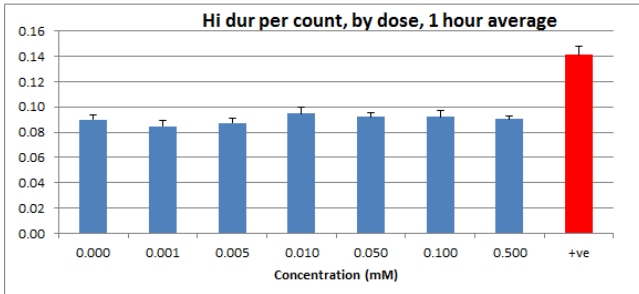
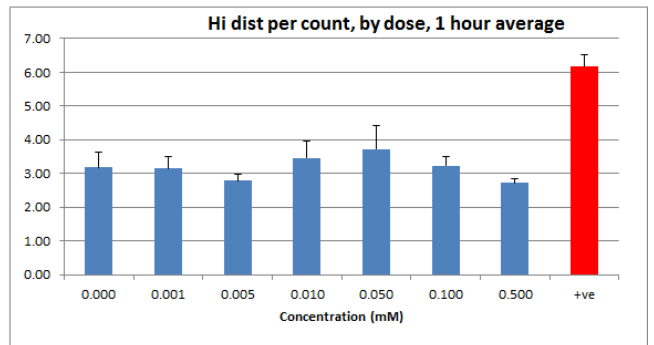
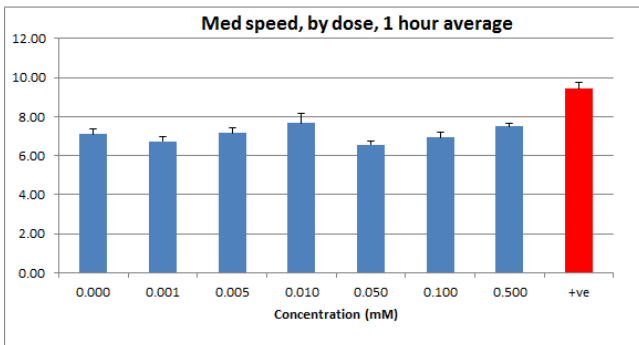
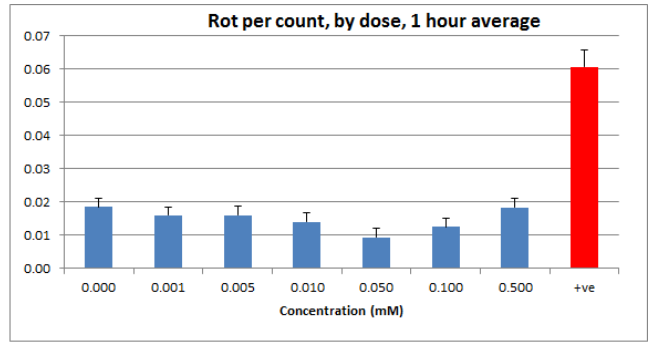
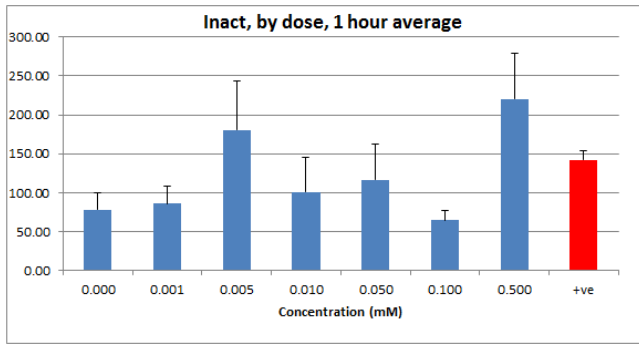
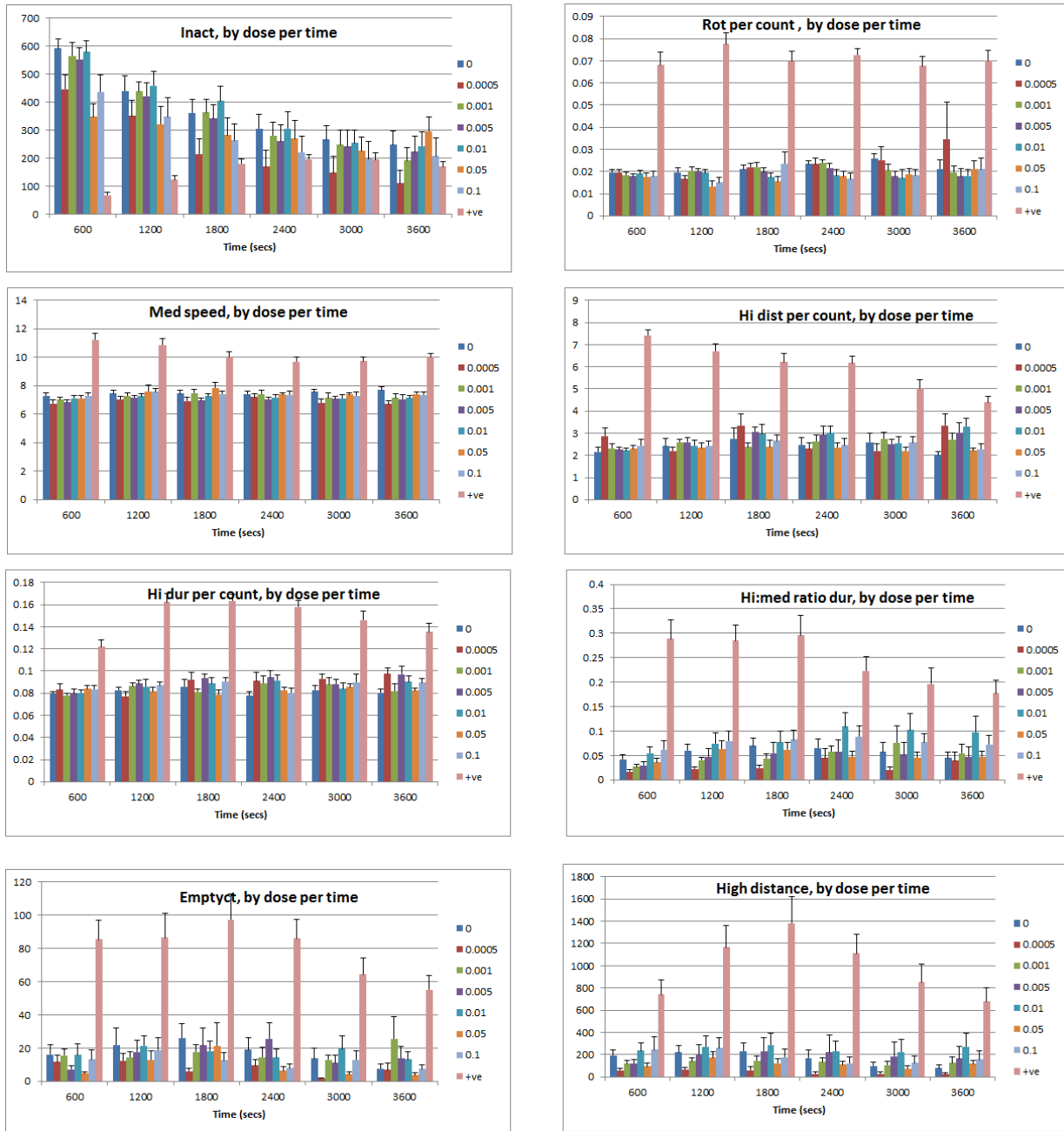


Figure S5. PVP coated Ag NP (AgPVP), a) activity graphs showing concentration response curves during each time interval, across the 1 hour recording period. b) activity graphs showing concentration response curves averaged across all time points by animal. 0 = negative control, +ve = PTZ positive control, 0.0005 represents $0.5 \mu\text{g L}^{-1}$ with the concentration increasing $1 \mu\text{g L}^{-1}$ (0.001), $5 \mu\text{g L}^{-1}$ (0.005), $10 \mu\text{g L}^{-1}$ (0.01), $50 \mu\text{g L}^{-1}$ (0.05), up to $100 \mu\text{g L}^{-1}$ (0.1).

a)



b)

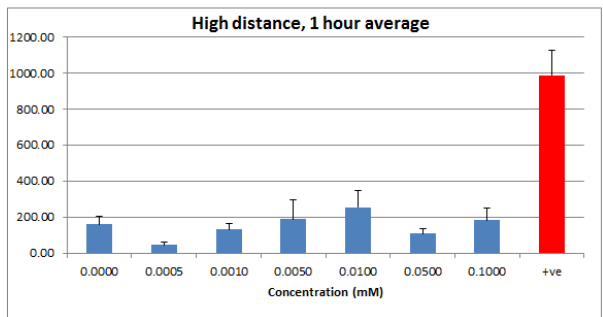
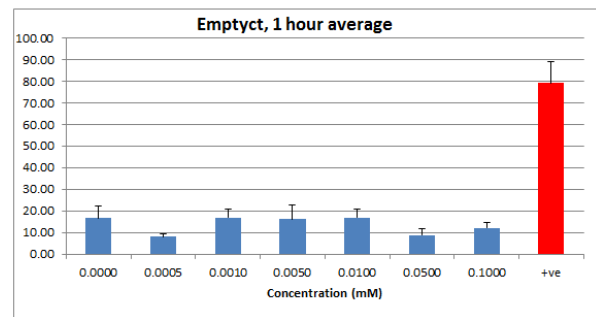
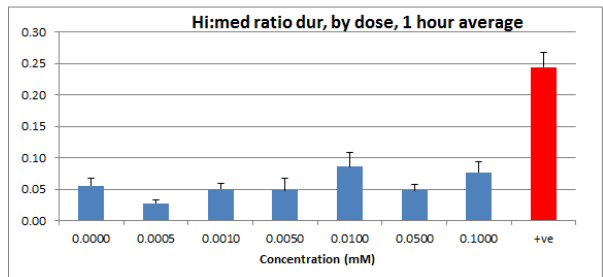
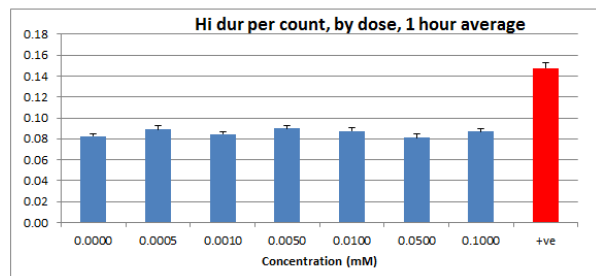
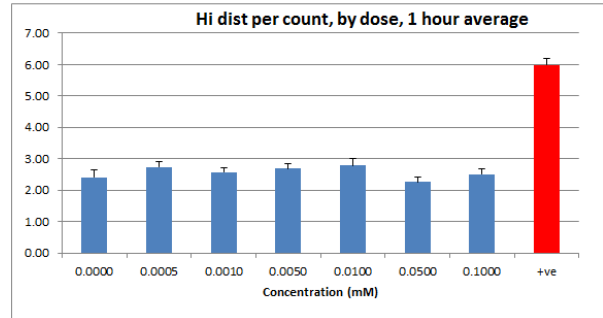
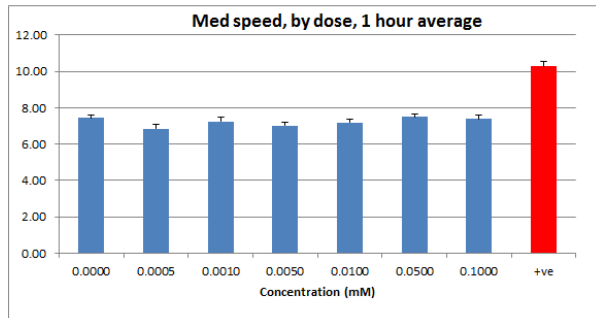
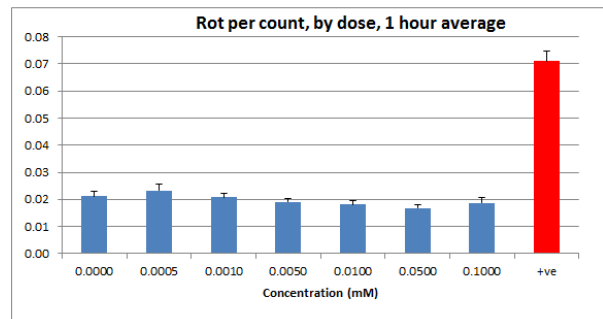
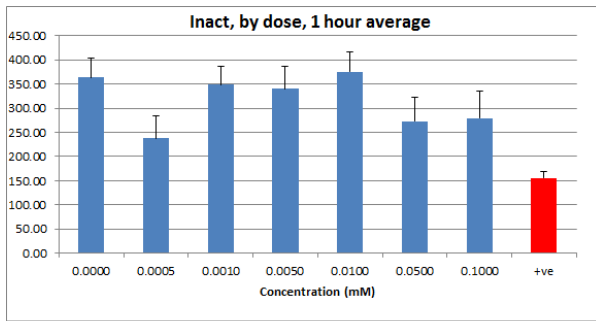
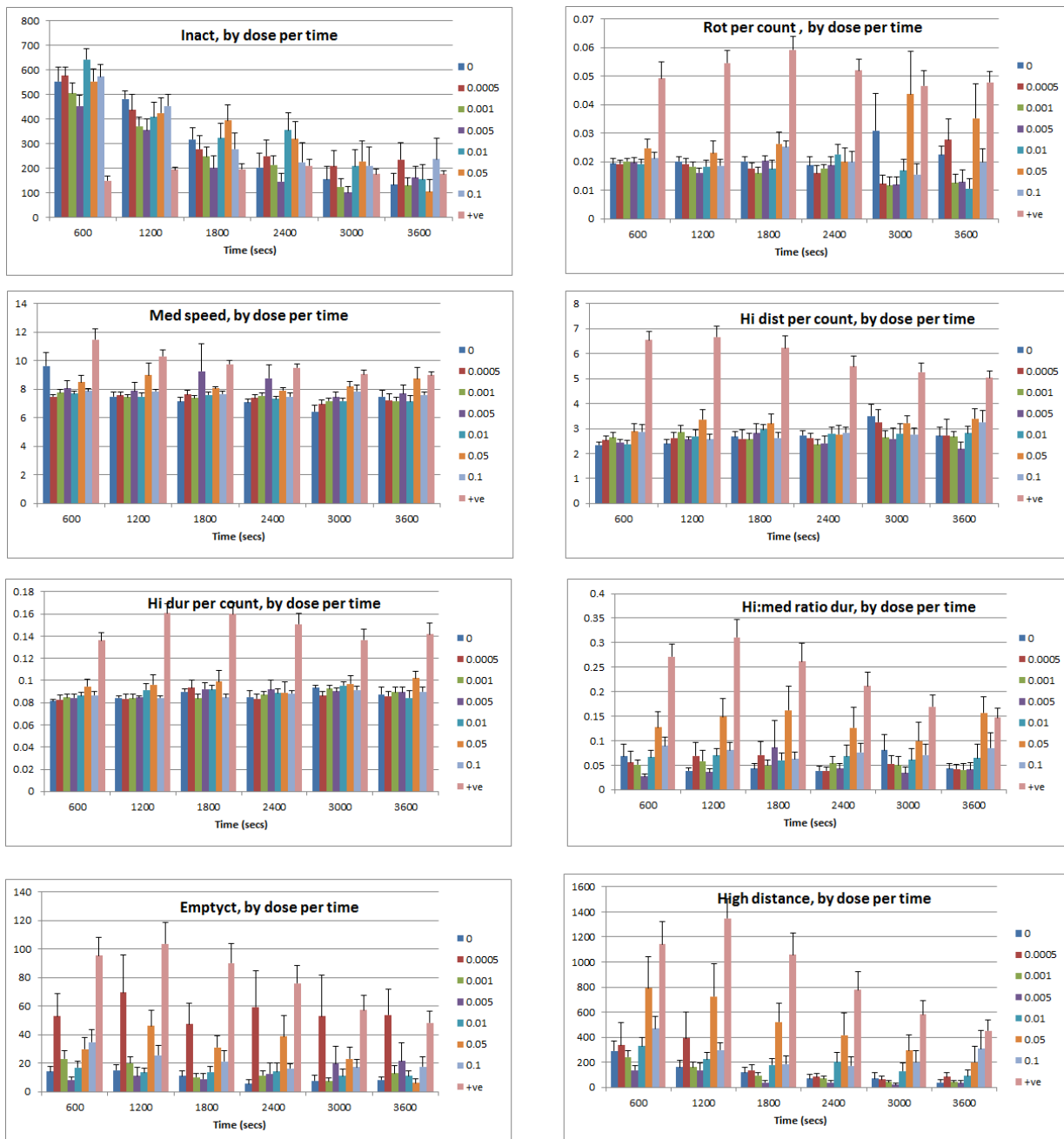


Figure S6. ZnO NP a) activity graphs showing concentration response curves during each time interval, across the 1 hour recording period. b) activity graphs showing concentration response curves averaged across all time points by animal. 0 = negative control, +ve = PTZ positive control, 0.0005 represents $5 \mu\text{g L}^{-1}$ with the concentration increasing $10 \mu\text{g L}^{-1}$ (0.001), $50 \mu\text{g L}^{-1}$ (0.005), $100 \mu\text{g L}^{-1}$ (0.01), $500 \mu\text{g L}^{-1}$ (0.05), up to $1000 \mu\text{g L}^{-1}$ (0.1).

a)



b)

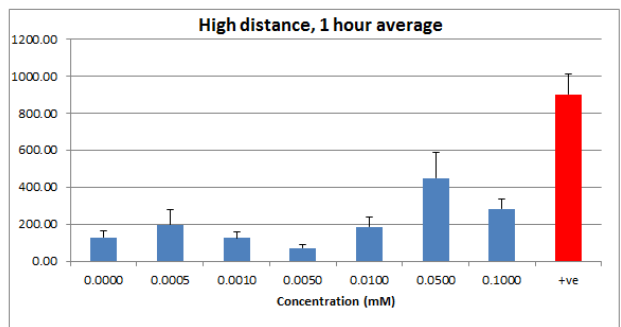
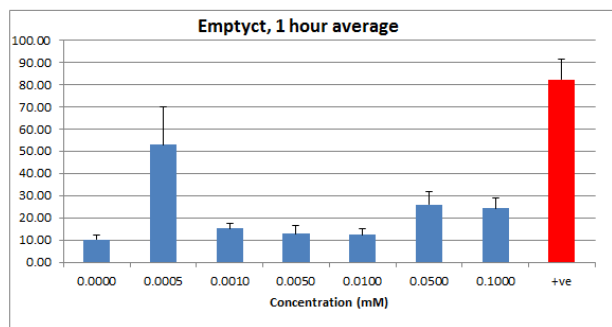
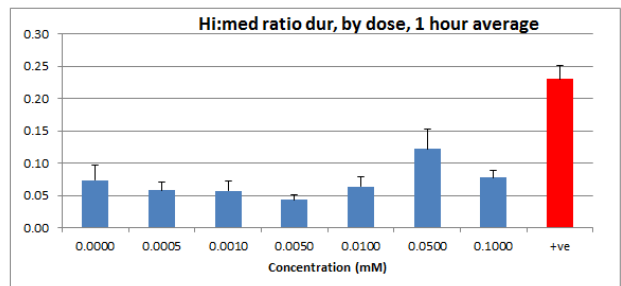
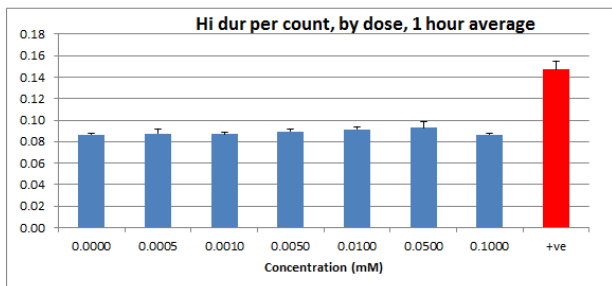
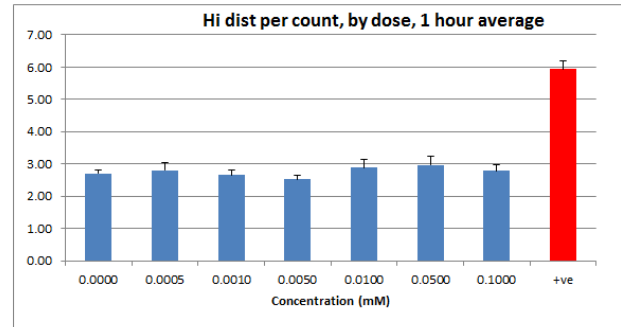
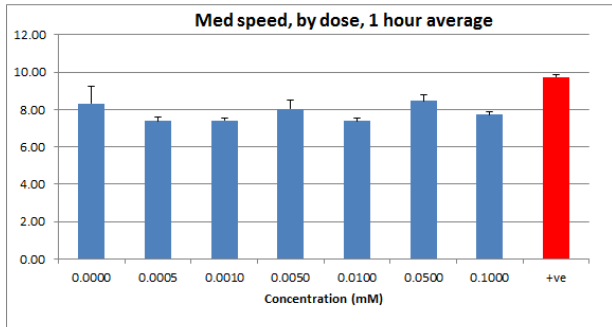
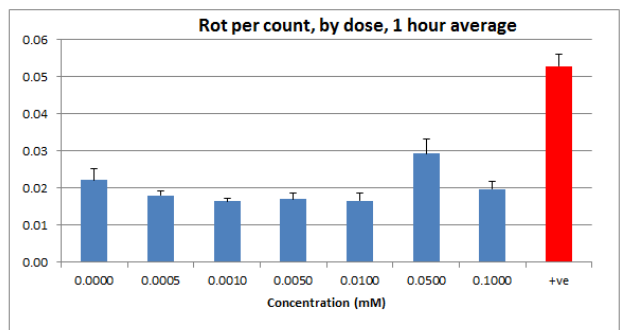
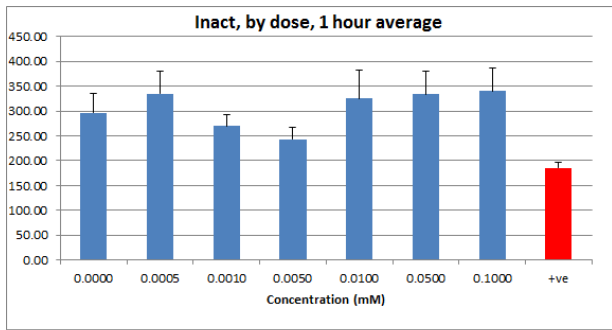
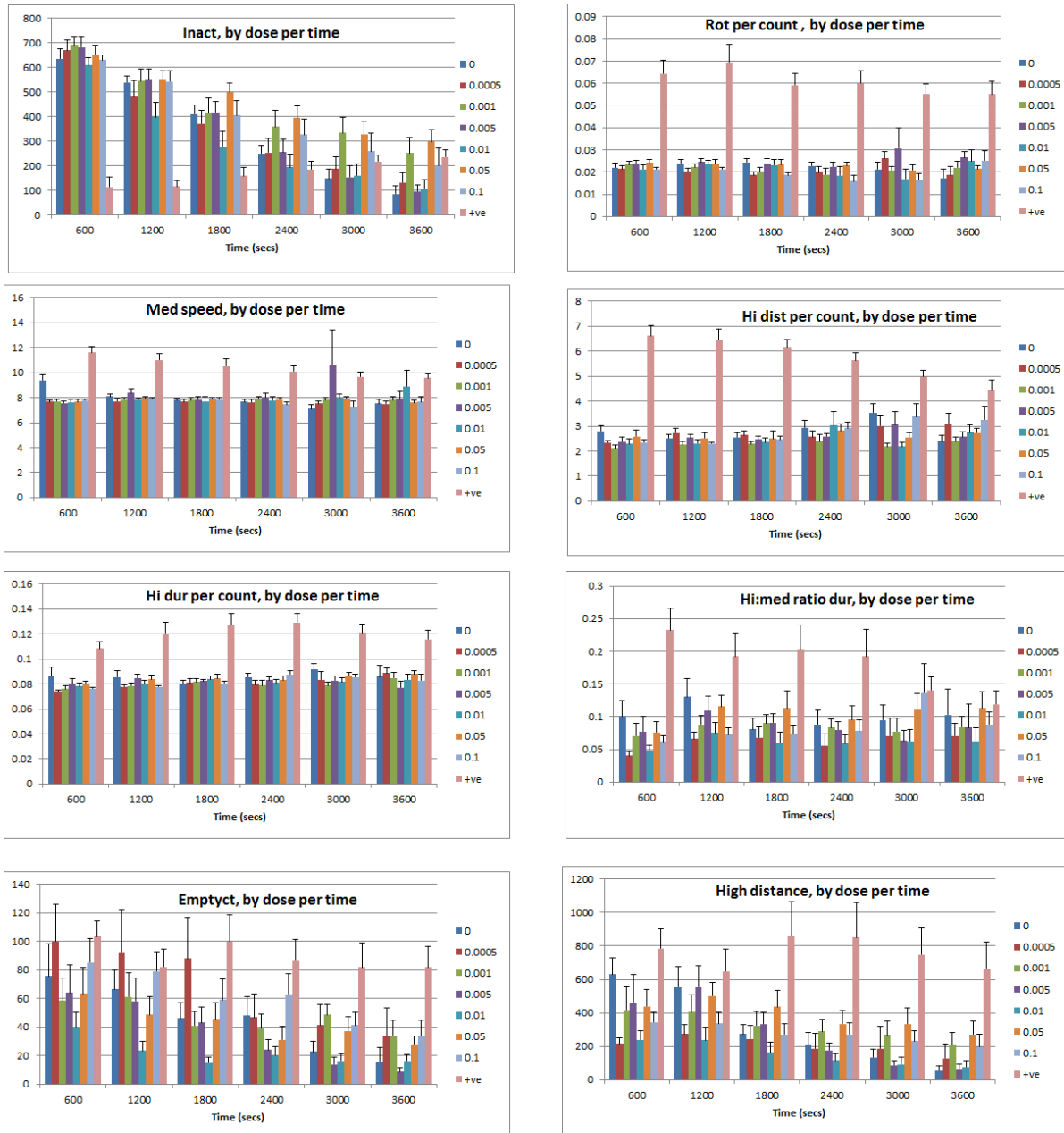


Figure S6. ZnCl₂ NP a) activity graphs showing concentration response curves during each time interval, across the 1 hour recording period. b) activity graphs showing concentration response curves averaged across all time points by animal. 0 = negative control, +ve = PTZ positive control, 0.0005 represents 5 $\mu\text{g L}^{-1}$ with the concentration increasing 10 $\mu\text{g L}^{-1}$ (0.001), 50 $\mu\text{g L}^{-1}$ (0.005), 100 $\mu\text{g L}^{-1}$ (0.01), 500 $\mu\text{g L}^{-1}$ (0.05), up to 1000 $\mu\text{g L}^{-1}$ (0.1).

a)



b)

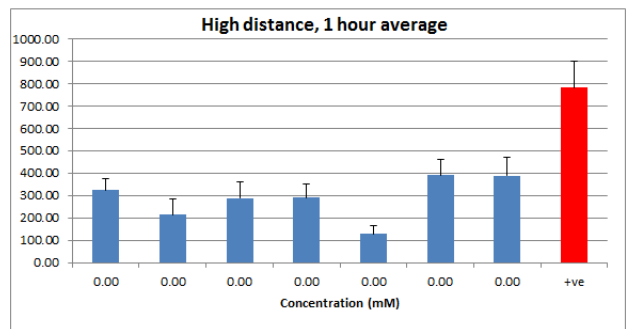
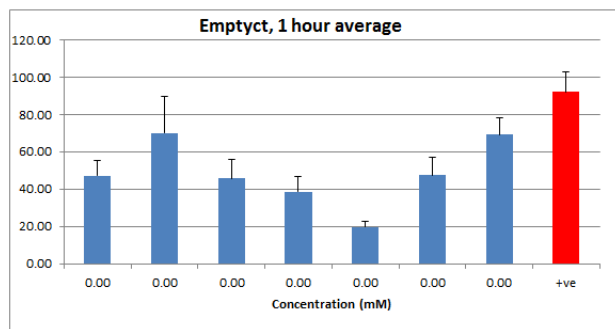
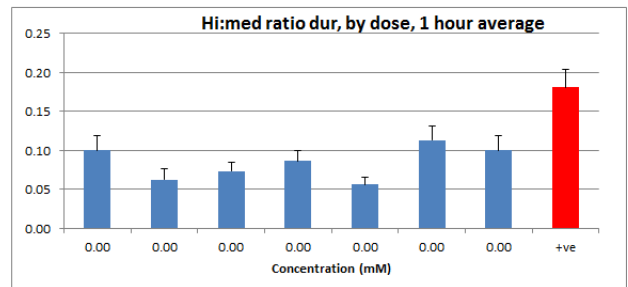
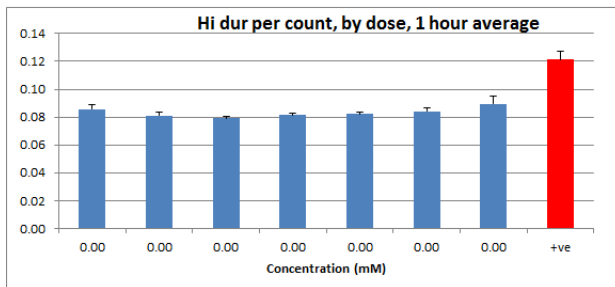
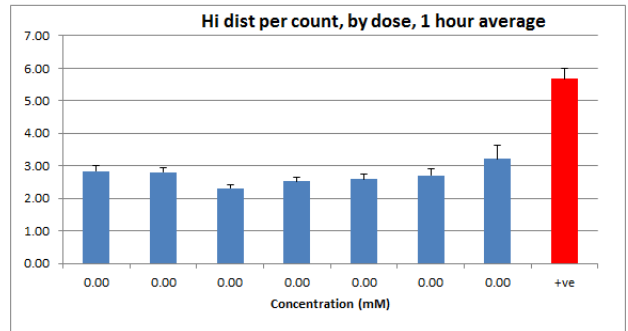
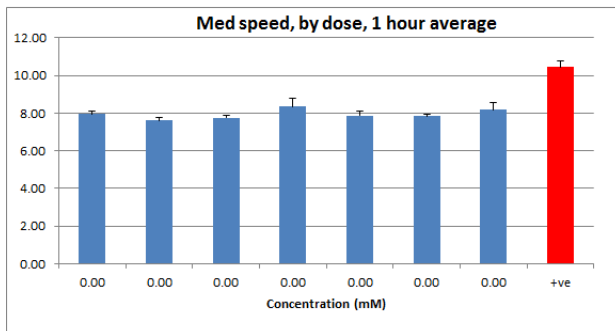
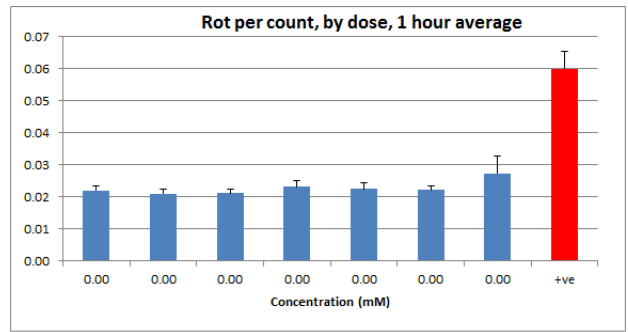
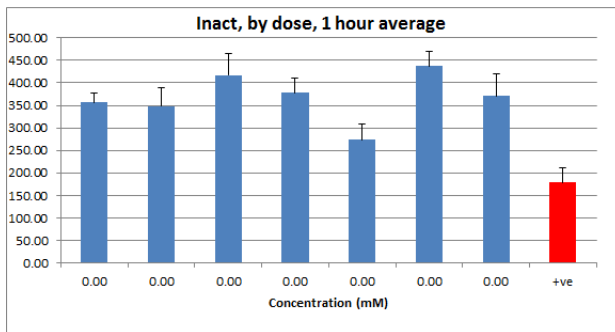
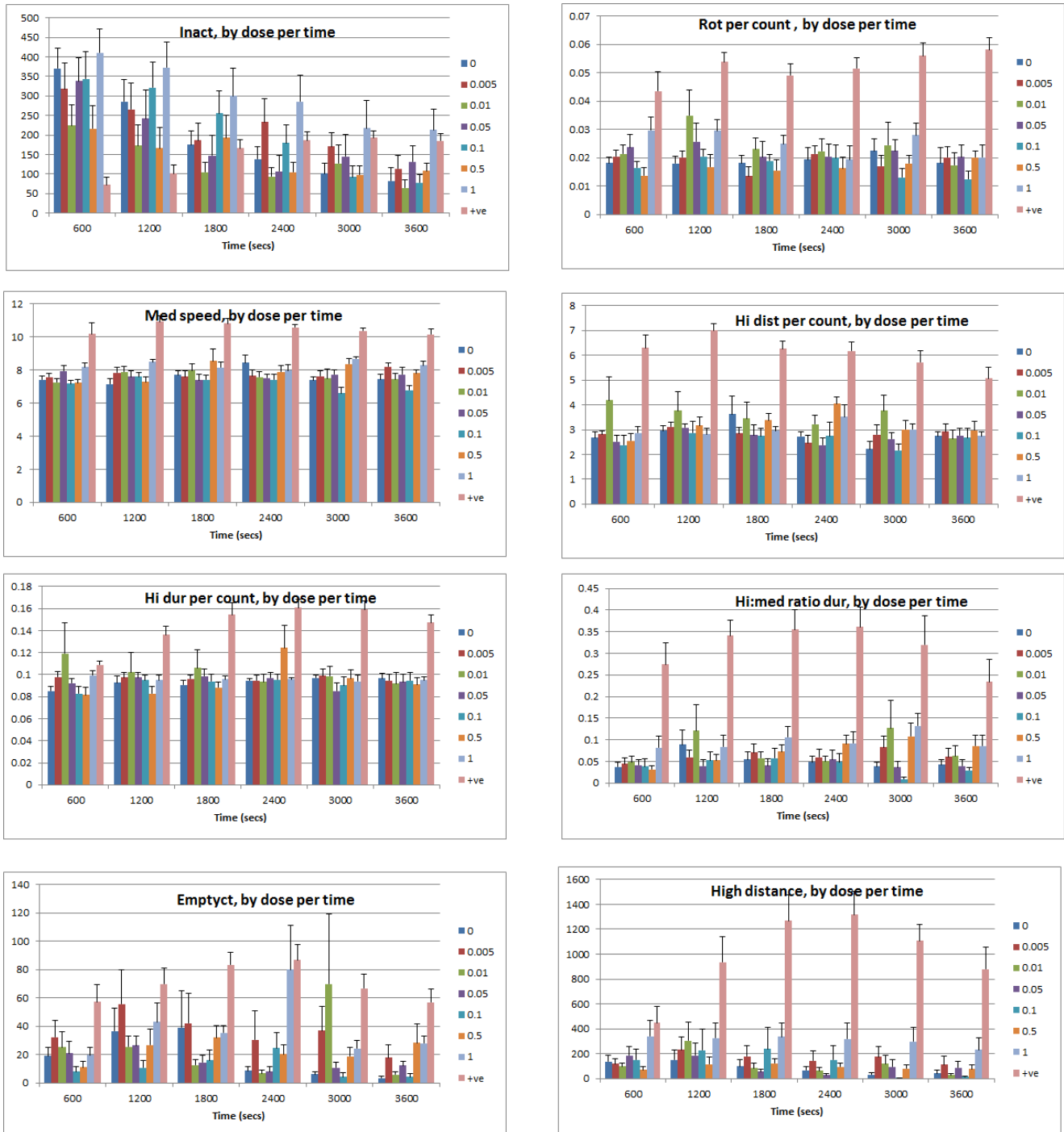


Figure S7. CeO₂ NP a) activity graphs showing concentration response curves during each time interval, across the 1 hour recording period. b) activity graphs showing concentration response curves averaged across all time points by animal. 0 = negative control, +ve = PTZ positive control, 0.005 represents 5 μg L⁻¹ with the concentration increasing 10 μg L⁻¹ (0.01), 50 μg L⁻¹ (0.05), 100 μg L⁻¹ (0.1), 500 μg L⁻¹ (0.5), up to 1000 μg L⁻¹ (1).

a)



b)

